AN ANALYSIS ON THE POTENTIAL APPLICATION OF LOW TEMPERATURE PLASMAS TO LAUNDER ASTRONAUT CLOTHING

A Thesis

By

ABISMAEL DIAZ

Submitted to the Office of Graduate and Professional Studies of
Texas A&M University
in partial fulfillment of the requirements for the degree of

MASTER OF SCIENCE

Chair of Committee,	David Staack
Committee Members,	Suresh Pillai Kentaro Hara
Head of Department,	Andreas A. Polycarpou

May 2018

Major Subject: Mechanical Engineering

ABSTRACT

Space laundry is non-existent onboard the ISS. Astronauts are forced to wear the same clothing for up to 3-5 days. After the clothing becomes soiled, it is discarded in resupply cargo ships. The discardment of soiled clothing requires periodic resupply ships to the ISS. According to 2008 NASA contract prices with SpaceX, the launch cost per lb of mass is approximately $18,000. A crew of 6 astronauts needs approximately 900 lbs of clothing per year. With planned 3-year long missions to Mars, this equates to a total cost of 48.6 million dollars. A space laundry system is needed to make interplanetary travel sustainable. Plasmas are a gaseous mixture of ions, electrons, neutrals, radicals, and photons, and have well documented successes in bacterial disinfection and odor control. Non-equilibrium plasmas are suitable candidates for the laundering of soiled astronaut clothing in space since they occupy minimal space, use zero water, and only need two resources: 10W of power and atmospheric pressure. These two resources are readily available on the ISS. Our research has shown that DBD plasmas and low pressure plasmas are potentially capable of laundering clothing in space. Results show that a 10-min, 1.27 W/cm^2 DBD plasma can provide an *E.coli* CFU log reduction of 2.7, can reduce the concentration of an actual body odor molecule (isovaleric acid) by 92%, and can do this while causing minimal visible damage to the fabric. In addition, a 4-5 min 0.016 W/cm^2 LPPR plasma can provide an *E.coli* CFU log reduction of up to 1.03, and can do so without negatively affecting either the tensile strength or ductility of the treated merino wool or causing any changes to their microstructure. These results are evidence that a plasma-based laundering system is a working concept. Following proper design and development

processes, these plasma technologies could have tremendous cost-savings potential for deep space exploration missions. By simply doubling the wearability of clothing, the cost of launching to Mars could decrease by millions of dollars.

ACKNOWLEDGEMENTS

I would like to thank Dr. David Staack for giving me the opportunity to join his lab and work on this very exciting research project. I would also like to thank Dr. Pillai and his graduate student, Sohini Bhatia, for their incredible help in the biological study of this research project. Special thanks to Dr. Tanil Ozkan for providing guidance and assistance in the mechanical study of plasma treated textiles. I also want to thank my lab mates, Nick, Matt, Xin, Kunpeng, Chris, John, and Josef for their help and support. Finally, special thanks to NASA Johnson Space Center (Evelyne Orndoff, Darwin H. Porowitz, Henry H. Tang) for their support and guidance.

CONTRIBUTORS AND FUNDING SOURCES

Contributors

This work was supervised by a thesis committee consisting of Professor David Staack (advisor) of the Department of Mechanical Engineering, Professor Suresh Pillai of the Department of Poultry Science, and Professor Kentaro Hara of the Department of Aerospace Engineering.

The *E. coli* disinfection data in Table 3 were counted and tabulated by Sohini Bhatia. The rotary scissors, ABS template, and ABS jaws shown in Figure 39 and 49 were provided by Dr. Tanil Ozkan of the Department of Mechanical Engineering. The scanning electron microscopy images of Figures 54, 55, 59, and 60 were taken by PhD candidate Matthew Burnette of the Department of Mechanical Engineering. Black merino wool, green modacrylic, and white cotton T-shirts were provided by NASA Johnson Space Center.

All other work conducted for the thesis was completed by the student independently, under advisement of Dr. David Staack and Dr. Suresh Pillai of Texas A&M University, and Evelyne Orndoff, Darwin H. Poritz, and Henry H. Tang of NASA Johnson Space Center under the NASA-JSC & Texas A&M University Space Act Umbrella Agreement No. SAA-AD-14-14316 (Annex Number 02).

Funding Sources

This work was partially funded by a 3M non-tenured faculty grant program and internal institutional resources.

TABLE OF CONTENTS

Page

1. INTRODUCTION 1

2. BACKGROUND 9
2.1 Body Odor Generation And Its Transfer To Textiles 9
2.2 Common Textiles 12
2.2.1 Merino Wool 12
2.2.2 Cotton 17
2.2.3 Modacrylic 20
2.3 Plasma Science 21
2.4 Electron Beam Science 27

3. EXPERIMENTAL METHODS AND PROCEDURES 32
3.1 Direct Dielectric Barrier Discharge Reactor Setup and Operation 32
3.2 Indirect Dielectric Barrier Discharge Setup and Operation 35
3.3 Low Pressure Plasma Reactor Setup and Operation 38
3.4. Electron Beam Setup and Operation 39
3.5 Fabric Sample Holder Setup and Operation 40

4. RESULTS 42
4.1 Plasma-Induced Wettability Changes 42
4.1.1 DBD Plasma 43
4.1.2 Low Pressure Plasma 44
4.1.3 Electron Beam 45
4.1.4 Wettability Lifetime 47
4.1.5. Effect of Contaminants (Dirt and Oil) 50
4.2. Plasma Penetration of Fabric 53
4.2.1 DBD Plasma Penetration of Fabric 53
4.2.2 LPPR Plasma Penetration of Fabric 57
4.3. Plasma-Assisted Disinfection of Bacteria Inoculated Fabric 59
4.3.1 DBD Treatment without Fabric 59
4.3.2 DBD Treatment with Blue Merino Wool 61
4.3.3 LPPR Treatment with Blue Merino Wool 64
4.4. Plasma's Effect on Fabric's Tensile Strength 68
4.4.1 Blue Merino Wool 71
4.4.2 Black Merino Wool 74
4.4.3 Green Modacrylic 76
4.4.4 White Cotton 79

4.5 Plasma-Induced Morphological Changes in Various Fabrics 83
4.5.1 Two Minute DBD Treatment at 1.27 W/cm^2 83
4.5.2 Fifteen Minute DBD Treatment at 1.27 W/cm^2 86
4.5.3 Ten Minute DBD Treatment at 0.85 W/cm^2 92
4.5.4 Twenty Minute DBD Treatment at 0.85 W/cm^2 97
4.5.5 Fifteen Minute LPPR Treatment at 0.016 W/cm^2 102
4.5.6 Electron Beam Treatment at 50 kGy 103
4.6 Plasma-Assisted Deodorization of Isovaleric Acid 104
4.6.1 Indirect DBD Treatment of IVA in Water 104
4.6.2 Direct DBD Treatment of IVA-Bathed Merino Wool 106
4.6.3 Direct DBD Treatment of IVA-Spot-Wetted Merino Wool 121

5. DISCUSSION 127

6. CONCLUSION 134

7. FUTURE WORK 135

8. REFERENCES 137

8. APPENDIX 140

LIST OF TABLES

Page

Table 1 Wettability Lifetime Study. 48

Table 2 Wettability Lifetime Study for Stained Merino Wool... 52

Table 3 CFU Log Reduction of E. Coli 67

Table 4 Sample Composition and Treatment Time 108

LIST OF FIGURES

Page

Figure 1 Chemical structure of typical laundry detergent surfactant and corresponding micelle structure 3

Figure 2 Carboxylic acids responsible for body odor 10

Figure 3 SEM image of a human hair and a merino wool hair 12

Figure 4 Versions of merino wool fibers. 13

Figure 5 The structure of a merino wool fiber 14

Figure 6 Example of merino wool fibers after alkali or acidic attack 17

Figure 7 The blooming process of cotton 18

Figure 8 SEM Images of cotton fibers 18

Figure 9 Monomers of modacrylic fibers 20

Figure 10 Electron avalanche mechanism 22

Figure 11 Dielectric Barrier Discharge and a Low Pressure Plasma Reactor 23

Figure 12 Tungsten Cathode Configurations 28

Figure 13 Electron Beam Electron Lens 29

Figure 14 Electron Beam Magnetic Lens 30

Figure 15 Drawing of DBD Reactor's Acrylic Housing 32

Figure 16 Drawing of Copper Electrode Disc for DBD Reactor 33

Figure 17 Assembly of Atmospheric Pressure DBD Reactor 34

Figure 18 Cross-sectional View of an Indirect DBD Reactor 36

Figure 19 Indirect DBD Reactor Showing Plasma Filaments and Teflon-made liquid sample holder 37

Figure 20 Experimental Setup of an Indirect DBD Reactor 37

Page

Figure 21 Low Pressure Plasma Reactor in off and on position 39

Figure 22 Electron Beam Treatment Setup Diagram 40

Figure 23 Fabric Holder Dimensions and Setup 40

Figure 24 Initial Water Contact Angle on Untreated Merino Wool 43

Figure 25 Wettability vs DBD Exposure Time Study. 44

Figure 26 E-Beam Treatment of Blue Merino Wool at 52.2 kGy with Different Configurations 45

Figure 27 Return of Low Wettability Contact Angle. 49

Figure 28 Water contact angles on untreated oil stained and dirt stained blue merino wool samples. 51

Figure 29 Backside Contact Angle Test Procedure 53

Figure 30 Backside Contact Angle Test Results 54

Figure 31 DBD treatment of multi-layered fabric 55

Figure 32 DBD treatment of stretched and unstretched fabrics 56

Figure 33 DBD treatment of fabrics at various gap distances 56

Figure 34 Stapled stack of 1" x 1" blue merino wool samples in LPPR 57

Figure 35 Results of LPPR penetration test 58

Figure 36 Baclight analysis of DBD treated and untreated E.coli samples 61

Figure 37 CFU count differences between plasma treated and untreated E.coli samples 62

Figure 38 Comparison of the disinfection capabilities of the DBD reactor vs LPPR reactor 68

Figure 39 Effect of cutting mechanism on fabric sample quality 69

Figure 40 Materials and samples for tensile test 70

Page

Figure 41 Force vs Elongation plot of LPPR and E-Beam Treated Blue Merino Wool 72

Figure 42 Box plot of maximum observed loads during each tensile test of treated blue merino wool. 73

Figure 43 Tensile Test of Treated Black Merino Wool 74

Figure 44 Boxplot for maximum load observed during each tensile test of treated black merino wool 75

Figure 45 Curling behavior of black merino wool during LPPR treatment. 76

Figure 46 Tensile test of treated green modacrylic 77

Figure 47 Boxplot for maximum load observed during each tensile test of treated green modacrylic 78

Figure 48 Example of DBD treated cotton strip before and after tensile test. 79

Figure 49 Side experiment to examine the correlation between hole placement and fabric failure point 80

Figure 50 Force vs elongation plot for tension tested cotton samples after separate DBD, LPPR, and E-Beam treatments 81

Figure 51 Box plot for maximum load observed during each tensile test of treated white cotton fabric strips 82

Figure 52 Box plot for maximum elongation in treated cotton fabric strips 83

Figure 53 Optical micrographs of DBD treated blue merino wool 84

Figure 54 SEM images of untreated blue merino wool sample. 85

Figure 55 SEM images of blue merino wool after 2-min 1.27 W/cm^2 DBD treatments 86

Figure 56 Blue merino wool after a 15 min exposure to the DBD Reactor at 1.27 W/cm^2 at 1 mm gap distance 87

Page

Figure 57 Photographs of untreated and DBD treated blue merino wool....88

Figure 58 DBD treatment visual effect on other fabrics....89

Figure 59 SEM images of blue merino wool after a 15-min 1.27 W/cm^2 DBD treatment....91

Figure 60 SEM images of another location of the blue merino wool sample that was also exposed to 15 min of a 1.27 W/cm^2 DBD plasma....92

Figure 61 SEM image of blue merino wool fibers after a 10-min 0.85 W/cm^2 DBD treatment....93

Figure 62 SEM image of a black merino wool fiber bundle....94

Figure 63 SEM image of a cotton fabric sample after a 10-min 0.85 W/cm^2 DBD plasma treatment....95

Figure 64 SEM image of green modacrylic after a 10-min 0.85 W/cm^2 DBD plasma treatment....96

Figure 65 SEM image of blue merino wool after being exposed to a 20-min 0.85 W/cm^2 DBD treatment....98

Figure 66 SEM image of black merino wool after exposure to a 20-min 0.85 W/cm^2 DBD plasma treatment....99

Figure 67 SEM image of white cotton fabric after being exposed to a 20-min 0.85 W/cm^2 DBD treatment....100

Figure 68 SEM image of green modacrylic after exposure to a 20-min 0.85 W/cm^2 DBD plasma treatment....101

Figure 69 SEM images of blue merino wool after a 15-min 0.016 W/cm^2 LPPR treatment....102

Figure 70 SEM images of blue merino wool after a 50 kGy electron beam treatment....103

Figure 71 GC-FID chromatogram of isovaleric acid after indirect exposure to a 4-min DBD plasma....105

Page

Figure 72 IVA-wetted blue merino wool sample preparation 107

Figure 73 IVA-bathed blue merino wool samples in 10 mL of DCM post DBD treatment. 108

Figure 74 Filtrate from DBD treated blue merino wool after a 24-hour IVA-H2O bath 109

Figure 75 GC-FID chromatogram for DBD treated IVA-stained blue merino wool..... 110

Figure 76 GC-FID chromatogram of duplicated experiment from Figure 75..... 113

Figure 77 GC-FID chromatogram comparison from both deodorization experiments. 115

Figure 78 GC-MS Chromatograms of DBD-treated IVA samples..... 116

Figure 79 Mass spectrograms of untreated and 32-min, 0.85 W/cm^2 DBD treated IVA. 117

Figure 80 Entire mass spectrogram of untreated and 32-min 0.85 W/cm^2 DBD treated IVA 119

Figure 81 Overlaid mass spectrograms of selected DBD treatment times 120

Figure 82 GC-FID chromatogram of IVA spot wetted cotton fabrics..... 123

Figure 83 Single GC-FID chromatogram of 4.6 mg/mL IVA treated with a 20-min 0.85 W/cm^2 DBD plasma treatment..... 124

Figure 84 DBD-Isovaleric Acid Reaction Rate Data 126

1. INTRODUCTION

The International Space Station (ISS) is a remarkable technological achievement. Several technical engineering challenges had to be overcome to bring this low-earth-orbit laboratory to life. However, space laundering continues to be an issue for astronauts in the ISS. Traditional laundering requires large amounts of water, and the ISS has a limited supply of water (so much so, that astronaut's sweat and urine are continually recycled and distilled to aid supply levels). This alone makes our current, water-based laundry system completely incompatible in space.

The absence of an onboard laundromat not only forces ISS astronauts to wear the same clothing for up to 3-5 days, but also demands new clothing during costly resupply missions to the ISS [1, 2]. This problem is even more pronounced for future manned missions to Mars, which will not have the convenience of resupply missions. According to NASA estimates, a manned space mission to Mars could take as long as three years [3]. Without an onboard laundry device, the Mars spacecraft would have to use limited storage space to carry approximately 2700 lbs. of clothing for a crew of six [4]. At an average cost of $18,000 per lb. of cargo during resupply missions, the estimated cost for not having an onboard laundry system is approximately $48.6 million [5]. Hauling 2700 lbs. of clothing to Mars—even if vacuum packed—has the added burden of occupying volume which could instead be utilized to store extra food, water, and spare parts.

NASA has already allocated funding to clothing studies to find fabrics that will provide astronauts with more comfortable, odor-resistant clothing [4]. NASA is currently planning on using merino wool, which is a soft, breathable, odor-resistant textile. Breathable fabrics are naturally odor-resistant since they provide skin bacteria less moisture from which to metabolize body odor molecules. While this solution may extend the wearability of clothing by a few days, it does not address the real need of having a laundry device onboard the ISS or the spacecraft that will ultimately carry humans to Mars.

The development or conceptualization of an onboard space laundering system is a surprisingly challenging project. In contrast, our current laundering system has become such a trivial part of life for so many us. It is common knowledge that laundry detergent, along with plenty of water, are needed to clean our soiled garments—and that having an electrically powered washer and dryer unit helps a great deal! But the chemistry behind our current laundering system is not only highly sophisticated, but has been improved by engineers and scientists over several decades. This means that an alternative laundering solution has a lot of “catching up” to do. To fully understand the complete set of requirements of an alternative laundering solution, it is helpful to review the function and requirements of our current laundry system, along with its advantages and areas of future improvement.

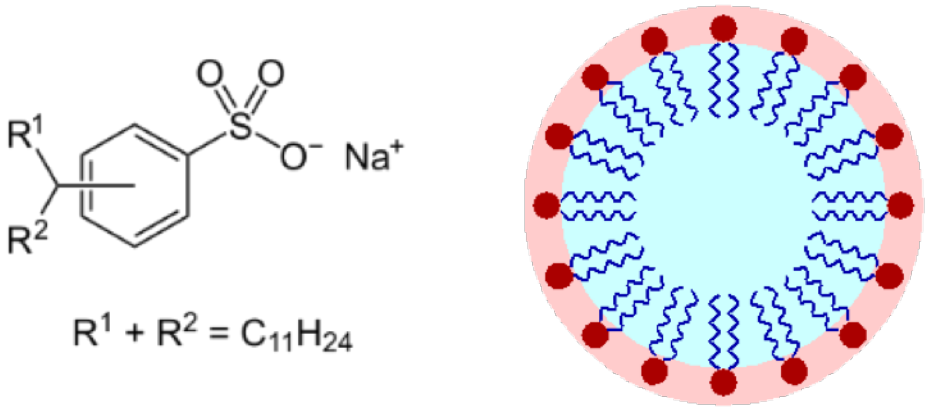

Figure 1: Chemical structure of typical laundry detergent surfactant (left) and corresponding micelle structure (right). Micelle structure by Stephen Gilbert. Reprinted from Wikimedia Commons.

Laundry detergents consist of a formulated mixture of surfactants known as alkyl-benzene-sulfonates [6], water softeners, bleaching agents, enzymes, optical brighteners, and fragrances. Surfactants help establish a chemical interaction between water and water-insoluble stains and debris. The end result is a micelle (Figure 1), which encapsulates the hydrophobic debris in an outward hydrophilic shell, which facilitates its extraction by water. The purpose of the water softeners is to capture calcium and magnesium ions to prevent the formation of soap scum, which drastically reduces the cleaning performance of any cleaning agent. Bleaching agents, which are not found in every detergent, are mainly composed of a sodium hypochlorite or hydrogen peroxide, and serve to disrupt the chemical bonds in dyes and stains that reflect light. Sodium hypochlorite and hydrogen peroxide also function as oxidizing agents that help with disinfection. Enzymes are utilized to remove biological stains (i.e. carbohydrates, lipids, proteins). Optical brighteners are fluorophores that re-emit incoming light at a higher wavelength, which causes a "whitening" effect. Finally, fragrances help mask any lingering odors that remain on the soiled fabric [7].

Clearly, laundry detergents need many components to function properly and to meet their extensive expectations. It is expected, for instance, that a good detergent will clean all kinds of fabrics, while preserving the clothing's color, mechanical behavior, and texture, and adding fragrance and softness. This is no easy feat, since the detergent solution needs to be chemically selective enough to extract and dissolve only dirt, greases, and biological fluids. The detergent also needs to find the perfect balance between being too chemically aggressive and too soft. If the detergent is too aggressive, wear, tear, and fading of the clothing will be immediately evident. On the contrary, if the detergent is too soft, then the laundering solution will be ruled ineffective.

The inherent advantage of our terrestrial laundry system is that the manufacturer can easily and precisely control the concentrations and types of chemicals and enzymes in laundry detergents to achieve high cleanliness with minimal clothing damage. These formulations have been optimized after years of testing across various textiles and stains. Another advantage is the plentiful use of water as a solvent, which not only facilitates the use and transport of enzymes and chemicals in and around multiple layers of clothing, but is also completely compatible with all garments. Moreover, after several agitating cycles, the water—containing encapsulated debris from the previously soiled garment—now serves its second purpose as an effective flushing agent.

However, even after years of research and progress in formulating more effective laundering detergents, it is still clear by any who wishes to renew their soiled clothing, that detergents are far from perfect—albeit the best solution available. On some

occasions, in order to effectively remove a stain, special spot treatments (often coming from anecdotal evidence) are required. Furthermore, rapid convective heat drying (an inseparable part of a modern, water-based laundry system) causes measurable, negative changes in the mechanical properties of textiles. These changes include shrinkage, pilling, loss of textile fibers, loss of ductility, and increase in fabric coarseness. Moreover, after approximately 20 wash cycles, materials can lose up to 50% of their tensile strength [8, 9]. These events are evidence that: (1) laundering remains an unsolved and unfinished problem, (2) that any realistic alternative to a water-based laundering system will face many immediate challenges—especially a non-liquid-based laundering solution, and, most important of all, (3) that terrestrial laundering has always imparted a degree of irreversible, mechanical damage to the fabrics being laundered.

The last three paragraphs have highlighted the rigorous requirements of our modern-day laundering solution, the inherent advantages of the cocktail-approach to detergent synthesis, and the inevitable damage to the fabric that is inseparable from the laundering process. This knowledge is both humbling, but also forgiving (since an alternative laundering solution need not be perfect since modern laundry technology is not). It is clear, though, that a space laundry system is faced with a very unique set of requirements. For example, the primary requirement of a space laundry system is the use of zero water—a requirement that greatly complicates the task. Furthermore, since our liquid and powdered detergents are completely ineffective without water, our actual laundering solution is left with no transferable value to our spacecrafts or the ISS. The second requirement is that the laundering solution occupy a minimum amount of space. This

requirement rules out other solid or liquid detergents, since they would also occupy valuable space onboard spacecrafts and the ISS. Logically, the minimization-of-space requirement preferentially selects gaseous-like states of matter as a necessary component in our space laundering solution. The third basic requirement of a space laundry system is that the laundering solution medium act like a detergent with bleach—meaning, it is able to 1) deodorize 2) disinfect and 3) serve its purpose without significantly or visibly damaging the fabric.

An agent capable of accomplishing these requirements is an electrically generated plasma (or ionized gas) under atmospheric pressure and temperature conditions. These kinds of plasmas are called non-equilibrium plasmas or “cold” plasmas. Research in the literature have shown that non-thermal plasmas, under the right conditions, are capable of disinfecting various microbes [10, 11], changing the chemistry of odorous molecules [12, 13], and being as compatible with various fabrics as standard processing and finishing treatments are [14, 15]. The best part is that this potential solution occupies very little space, and does not need any special equipment or resources, other than a high voltage AC power supply.

The research presented herein has proven low temperature plasma’s potential use as a space laundering medium through a series of tests and experiments. The first part of the project determined under what conditions plasma is, or is not, compatible with merino wool. The second part of the research focused on proving that plasma could disinfect

microbes at the same operational settings in which it remains compatible with merino wool. The last part of the research study focused exclusively on assessing plasma's deodorization capability of a specific body odor molecule.

Electron beams have also shown excellent disinfection properties. While the physical space requirements of an electron beam generator prohibit its implementation and use onboard spacecraft, electron beams can be used to pre-treat astronaut clothing. Scientific literature shows that an electron beam radiation dose of 10 kGy is sufficient to disinfect various microbes. Research within this report directly shows that a 10kGy dose of electron beam radiation does not impart any physical damage to either merino wool, cotton, or modacrylic. This statement is backed with tensile test data of 10 kGy treated fabrics, as well as SEM images, which show zero changes in surface morphology. Since electron beam treatment centers can quickly and efficiently treat pallets of various objects, this is already an underutilized tool with regards to extending the wearability of astronaut clothing.

The report is organized as follows: the section that follows provides the reader with the necessary background information to fully understand the entire contents of this report. The experimental method and procedures section contains all the necessary information on the "in-house" equipment used. These "in-house" equipment primarily consist of plasma-generating devices that were designed and manufactured at Texas A&M University. This is followed by the results section, where the results of various experiments are discussed independently of each other. The results section also contains

brief, but specific experimental procedures on how minor, but important, tasks were performed. The discussion section contains the storyline of the research project, and more importantly, serves to provide the connection between all experiments. The report ends with a conclusion section, followed by references and an appendix.

2. BACKGROUND

2.1 Body Odor Generation And Its Transfer To Textiles

It is worthwhile to have a brief discussion on the mechanism behind body odor production. First, it is important to understand that our skin contains three major kinds of sweat glands—eccrine, apocrine, and sebaceous. Of these three sweat glands, the apocrine gland, which is mainly located in the armpit and groin, is linked with the typical odor that many describe as body odor [16]. The eccrine and sebaceous glands, which are both present throughout our entire skin surface with some exceptions, are also linked to body odor production, but to a lesser degree.

Sweating is a normal bodily function that helps regulate an organism's body temperature by evaporative cooling. It is also a mechanism by which the body secretes metabolic waste products. The type of waste products is specific to the type of sweat gland. For example, eccrine sweat—which is secreted from the eccrine glands—is approximately 98% water and contains small amounts of sodium chloride, fatty acids, lactic acid, citric acid, ascorbic acid, urea, and urea acid. In contrast, apocrine sweat—which is secreted only from apocrine glands—contains water, protein, carbohydrates, cellular waste, and lipids. Sebaceous glands secrete an oily substance called sebum, which is meant to lubricate and/or waterproof mammalian skin. Since both the apocrine and sebaceous glands secrete fluids unto the same hair follicle, apocrine sweat also has sebum. Due to the differences in the composition of eccrine and apocrine sweat, these fluids can be

distinguished. Eccrine sweat is colorless and fluid, whereas apocrine is cloudy and viscous [16].

Interestingly, all sweat is originally odorless. According to Shelley and Horvath (1951) and Labow (1979), body odor is specifically a by-product of bacterial metabolism occurring near our sweat glands [16]. Apocrine and eccrine sweat are odorless when first secreted by our glands, and only after a few hours in the presence of bacteria, does any detection of body odor arise. Moreover, apocrine and eccrine sweat will not produce any odor in the absence of bacteria. In the presence of bacteria, eccrine sweat will produce a mild odor, while apocrine sweat will produce a stronger, pungent body odor [16].

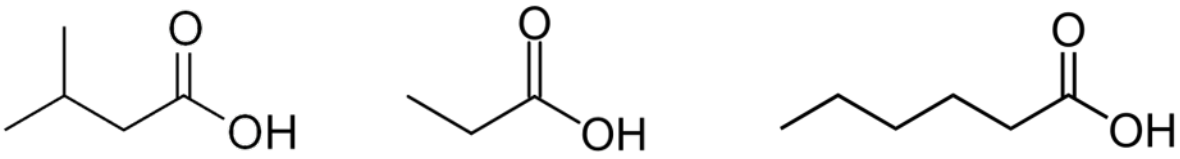

Figure 2: Carboxylic acids responsible for body odor (Left: Isovaleric Acid; Middle: Propionic Acid; Right: Hexenoic Acid)

One point of interest is that all of the major components of body odor have carboxylic functional groups. For instance, armpit bacteria produce isovaleric, propionic, and hexenoic acid (Figure 2). The importance of this is that carboxylic acids (electrophilic functional groups) are reactive, which suggest that interesting chemistry should occur under the presence of radicals and charged/energized species—which are precisely the kind of species that plasmas are composed of.

While we are dressed, our skin contacts our clothing. During these contacts, which vary in intensity and duration, there is a transfer of sweat, skin bacteria, and body odor molecules. After about 8-12 hours, the contacted clothing will have a noticeable body odor smell, at which point, the clothing is normally dispensed in a laundry hamper. Unfortunately, the transfer of bacteria from skin to clothing means that the bacteria will continue to metabolize the sweat on the fabric into odorous molecules long after its been stored in the laundry hamper. The transfer rate of sweat to the fabric is also problematic because higher volumes of sweat on the fabric lead to greater bacterial metabolic activity on the fabric.

To reduce body odor generation, and its transfer to worn textiles, a textile needs to transport sweat from human skin to the surroundings at a rate higher than the rate of bacterial metabolic activity. This chokes the resources that bacteria need to produce body odor molecules. The ability of textiles to transport moisture from the skin to the environment is known as breathability, and in general, a fabric's breathability is correlated with its odor-resistance.

For more information on body odor, please refer to "Human Body Odor—Etiology, Treatment and Related Factors" by Masumi Inaba and Yoshikata Inaba.

2.2 Common Textiles

2.2.1 Merino Wool

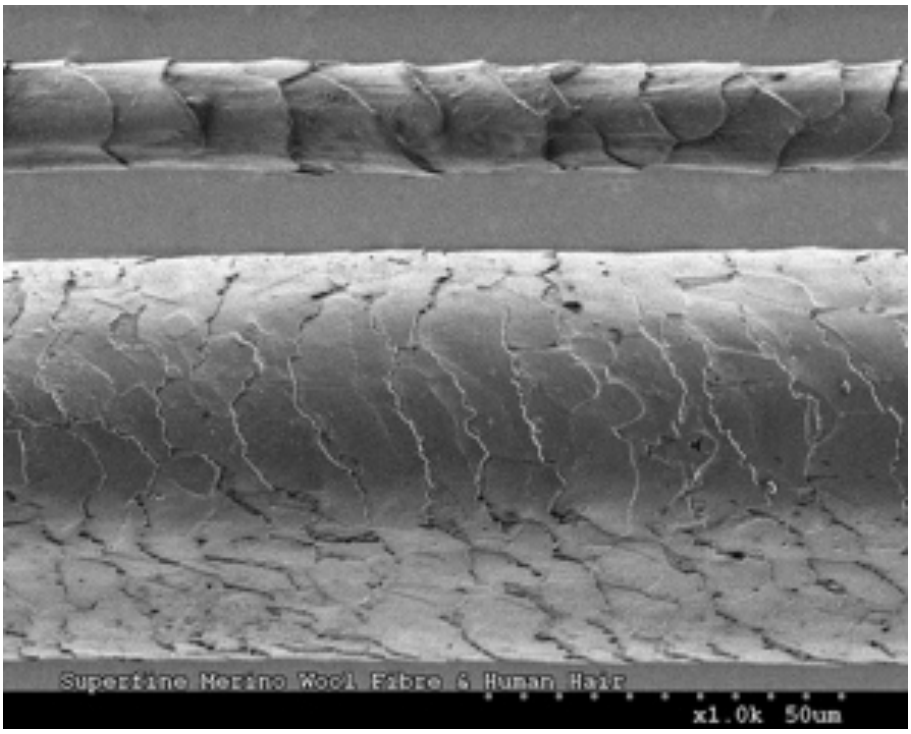

Figure 3: SEM image of a human hair (above) and a merino wool hair (below); Photo Credit: CSIRO, Reprinted from www.scienceimage.csiro.au/image/8115

Wool has been used extensively throughout history. There is even archaeological evidence pointing to its use as early as 6000 BC. Even today, wool continues to be a dominant fabric in the global textile industry. Wool's desirability has even led to the artificial selection of sheep, to produce more and softer wool. The breed of sheep renowned for its high-quality wool is the Merino. Though the breed originated in Spain (and was fiercely protected by Spain to continue dominating the wool trade), it eventually made its way to Australia. Today, Australian Merinos, which can produce up to 8 lbs. of

wool annually [17], are globally recognized as producing the highest quality of wool, and this recognition has helped make Australia the number 2 global exporter of wool.

Figure 4: Versions of merino wool fibers [A: Merino wool fiber displaying a faint scaly epidermis after certain finishing processes B: Example of a finer quality merino wool fiber C: Example of a body hair fiber of the merino sheep; Reprinted from page 38 of "The Chemical Technology of Textile Fibres: Their Origin, Structure, Preparation, Washing, Bleaching, Dyeing, Printing, and Dressing" by Georg Von Georgievics, published by London, Scott, Greenwood in 1902.

Wool is an animal fiber, and under the microscope, has a similar morphology to human hair (Figure 3). Typical merino wool fibers have a diameter range of 14um to 45um, and have a crimped configuration, with as many as 10 crimps per centimeter [18]. The overall structure of a merino wool fiber consists of three major components. The outermost layer of the merino wool fiber is known as the epidermis or cuticle. This layer is very scaly, and

has been likened to roof tiles for the manner in which each scale lies above the next scale. In fact, the ability of wool to felt, is directly related to the density of their scales [21]. The best wools have scales that singly wrap around the entire fiber, whereas, wools of lesser quality have multiple scales around the circumference of the wool fiber. See Figure 4 for examples.

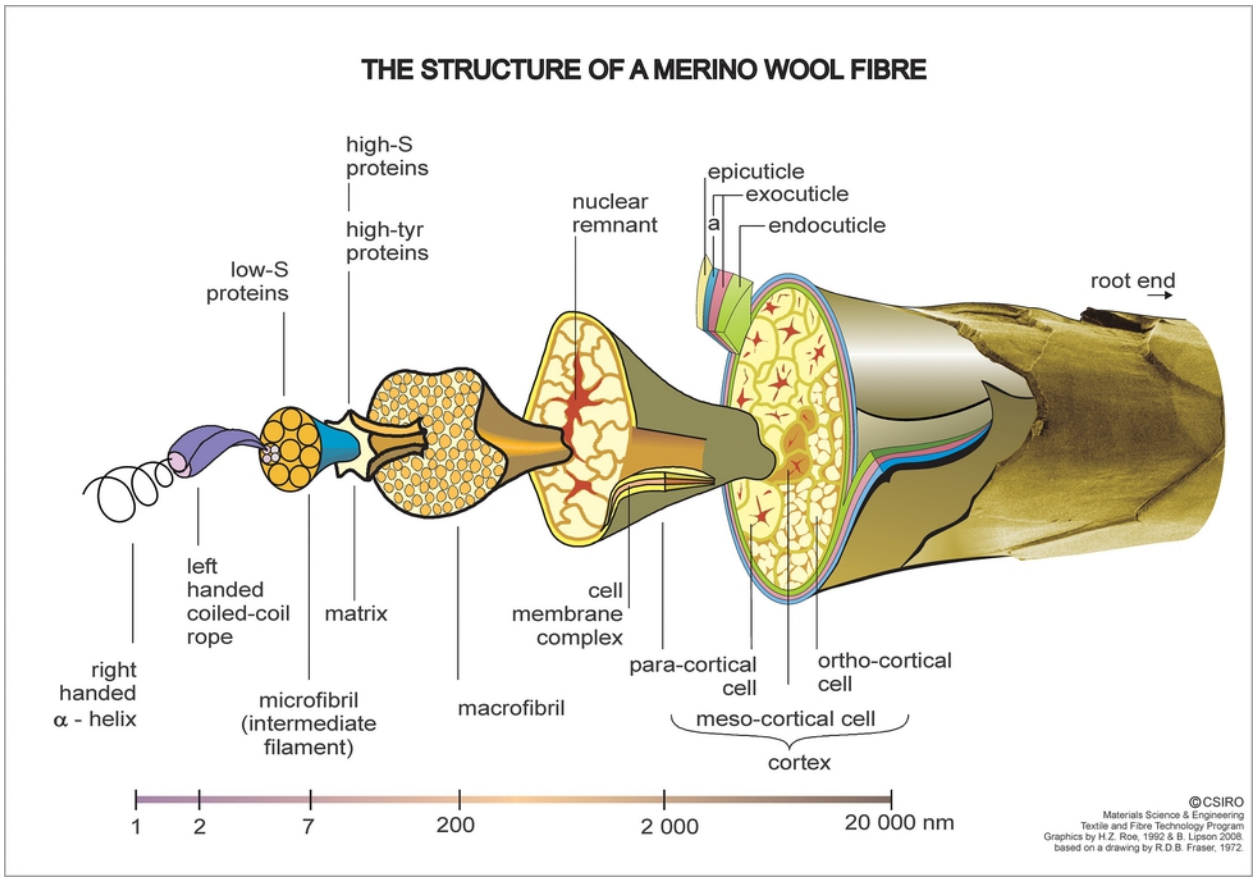

Figure 5: The structure of a merino wool fiber; Photo Credit: CSIRO, Materials Science and Engineering , Textile and Fibre Technology Program, Graphics by H.Z. Roe, 1992 & B. Lipson 2008. Based on a drawing by R.D.B. Fraser, 1972

Deeper into the center of the wool fiber, is the second layer, which is called the cortex. The cortex consists of a bundle of longitudinal cells (Figure 5). The innermost component is the medulla, which for the finest merino wool, consists of an empty space [20].

The macromolecular composition of merino wool consists of various proteins. It has been estimated that as many as 170 different proteins have been found across all wool types [18]. This variation helps explain the distinctive characteristics of wool across different breeds or regions. The chemical composition of merino wool is C, H, O, N, and S. Interestingly, wool is the only animal fiber to contain sulfur, and comprises about .8% to 3.8% of the total fiber weight [19].

Wool has very interesting properties. Its ability to keep us warm during chilly days is attributed to the air spaces between the fibers, which occur naturally thanks to the crimped configuration of wool fibers. Wool also has an interesting dynamic with water, since it is simultaneously anti-wetting and hygroscopic [19]. The scaly epidermis of the wool fiber, for instance, helps keep the wool anti-wetting [20]. This is important because as we sweat, merino wool is able to transport the moisture away from our bodies, and into the environment. This allows our sweating's natural evaporative cooling effect to be more efficient. Furthermore, the trapped moisture within the medulla of the merino wool also begins to evaporate, causing an additional evaporative cooling effect [21]. If, however, we begin to sweat faster than the merino wool can wick away moisture, the scaly epidermis opens, and the merino wool fiber begins storing the moisture in its medulla. Unlike other textiles, which can only absorb water at 8.5% of their dry weight, merino wool

can absorb as much as 30% of their dry weight, without becoming visibly wet [21]. This allows our sweat's evaporating cooling effect (facilitated by a dryer environment) to continue taking place. Similarly, during damp, cold days, the wool fiber can store water vapor from the air within the medulla, instead of allowing the water vapor to steal heat from direct skin contact. These combined properties make merino wool an excellent fabric for both warm and cold conditions.

Merino wool has additional properties that make it a fabric of choice. For example, the ability of merino wool to wick away moisture comes with a bonus: merino wool's odor-resistant property. Without our sweat, odor-causing bacteria have less of the perspiration they need to metabolize body odor molecules. Merino wool's moisture retaining ability also helps keep merino wool naturally static resistant—which is important for those working around electrically sensitive equipment.

Being mostly protein, however, wool is susceptible to acidity, basicity, and extreme heat. Under acidic conditions, the wool fiber's scaly epidermis is compromised, and begins to illustrate many striations along its length, while the ends of the fiber appear extensively shredded or split [19, 22]. This can be seen in Figure 6. On the other end of the pH scale, wool fibers begin to curl and exhibit random cracks throughout the epidermis (Figure 6). Upon being heated to 120 degrees Celsius, wool undergoes a slight decomposition, and at 200 degrees Celsius, the wool decomposes entirely [19]. For these reasons, neutral pH detergents, with a low heat drying cycle, are recommended for the washing of wool

fabrics. Alternative washing technologies should also aim to follow these recommendations.

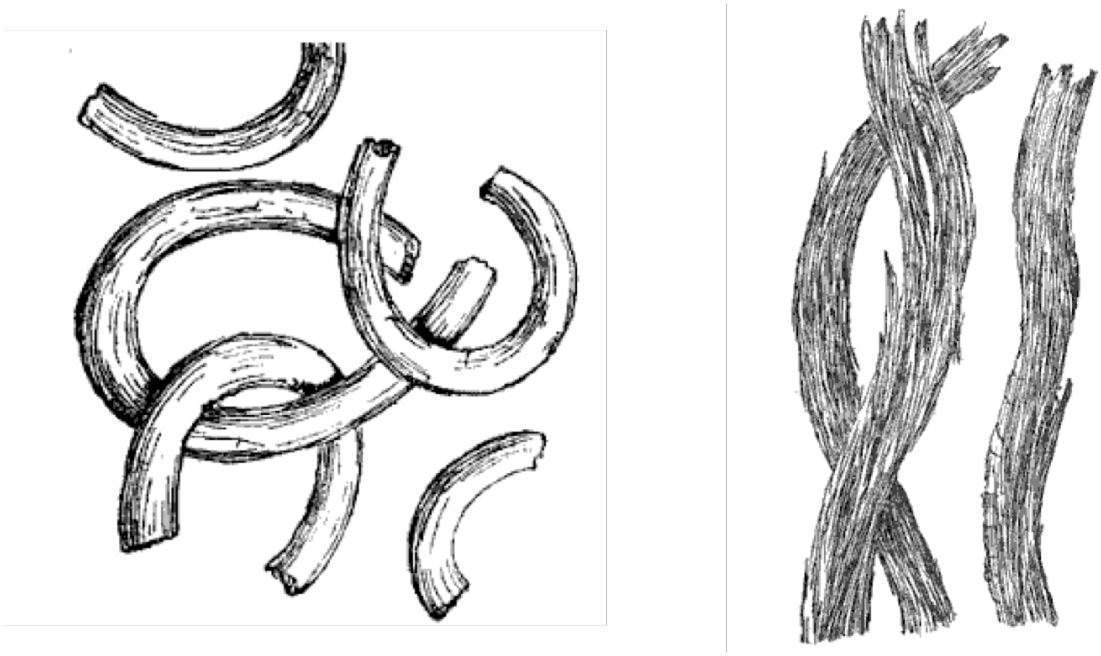

Figure 6: Example of merino wool fibers after alkali or acidic attack (Left: Example of Merino Wool after Alkali Attack; Right: Example of Merino Wool after Acidic Attack). Reprinted from page 41 of "The Chemical Technology of Textile Fibres: Their Origin, Structure, Preparation, Washing, Bleaching, Dyeing, Printing, and Dressing" by Georg Von Georgievics, published by London, Scott, Greenwood in 1902.

2.2.2 Cotton

Cotton is a natural, creamy-white fibrous compound that is sourced from cotton plants of the genus *Gossypium*. Upon fully sprouting from the cottonseeds, the raw cotton looks very similar to large cotton balls (Figure 7). A complex set of manufacturing and treatment processes ultimately change raw cotton into textile-grade cotton. However, the structure of cotton fiber remains the same, with very few exceptions.

Figure 7: The blooming process of cotton; Images taken from www.swicofil.com/products/001cotton.html

A cotton fiber can consist of three layers. The outer layer is a smooth, waxy layer known as the cuticle, which is comprised of pectin and protein. However, not all cotton have the cuticle, since it is removed after strong bleaching [19]. Directly underneath the cuticle is the primary wall, followed by the “secondary walls”. All walls are made almost entirely of cellulose, while the “secondary walls” tend to have a network of small strands of cellulose called fibrils.

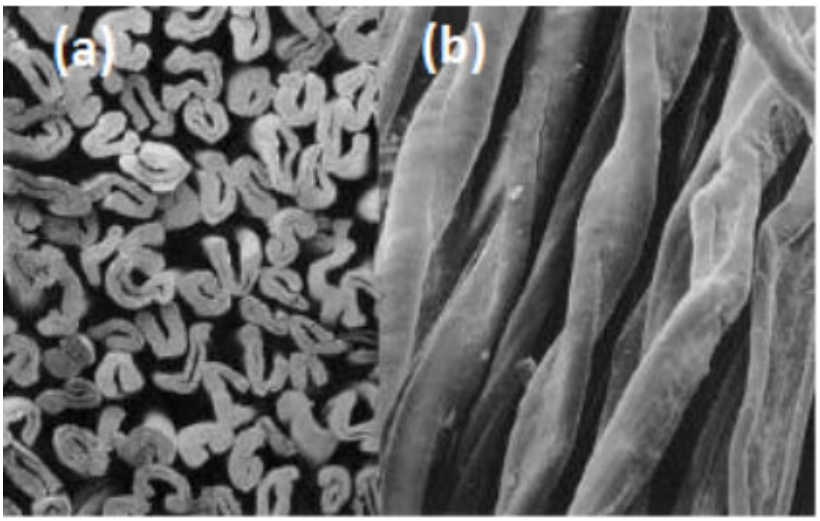

Figure 8: SEM Images of cotton fibers; (A) SEM cross-section view of cotton fibers demonstrating their kidney-like shape; (B) Longitudinal view of cotton fibers showing their ribbon-like structure with corkscrew convolutions; This image was taken from from www.swicofil.com/products/001cotton.html

The microscopic structure of a cotton fiber is that of a single, ribbon-like, elongated cell, that has certain corkscrew-like convolutions at random points along its length (Figure 8). Cotton fibers are typically 10-65 mm in length, have a diameter of 11-22 um, and can swell as it absorbs moisture [23]. Additionally, on one side of the flat cotton fiber is the lumen—a central, channel-like cavity where the vacuole of the cell once stayed. The lumen is very small compared to the cell wall of the cotton fiber, which gives the cross-section of cotton fibers a kidney-shaped appearance. These properties are responsible for cotton's comfortability.

The chemical composition of raw cotton is 87-91% cellulose, 7-8% water, .4-.5% wax, .5-.7% protoplasmic residue, and .12% ash [19]. Under extreme acidic or basic conditions, cotton fiber turns gummy, swells up, and bursts segments of the cuticle in various directions. Under controlled alkali conditions, the lumen contracts and the fiber becomes both shorter and thicker. Interestingly, these effects lead to a 15-20% increase in tensile strength, as well as noticeable increases in elasticity [19]. Cotton decomposes after prolonged exposure to temperatures of 300 degrees F and higher. Cotton is also susceptible to sunlight, is readily flammable, and can be affected by mold, mildew, and silverfish [19].

2.2.3 Modacrylic

Modacrylic is a synthetic copolymer, that by Federal Trade Commission guidelines, must contain no more than 85% of acrylonitrile, with the remainder consisting of several polymers such as vinyl chloride and/or vinylidene chloride [24]. Modacrylic exhibits excellent flame-retardant properties and can self-extinguish in the absence of an external flame [24, 25]. This property is attributed to the vinyl-chloride polymer of the modacrylic fiber. In addition, modacrylic is known to have excellent resistance to acids, weak bases, and organic solvents. However, modacrylic is sensitive to heat. At 250 degrees F, modacrylic will begin to shrink, and at 300 degrees F will lose its elasticity [26].

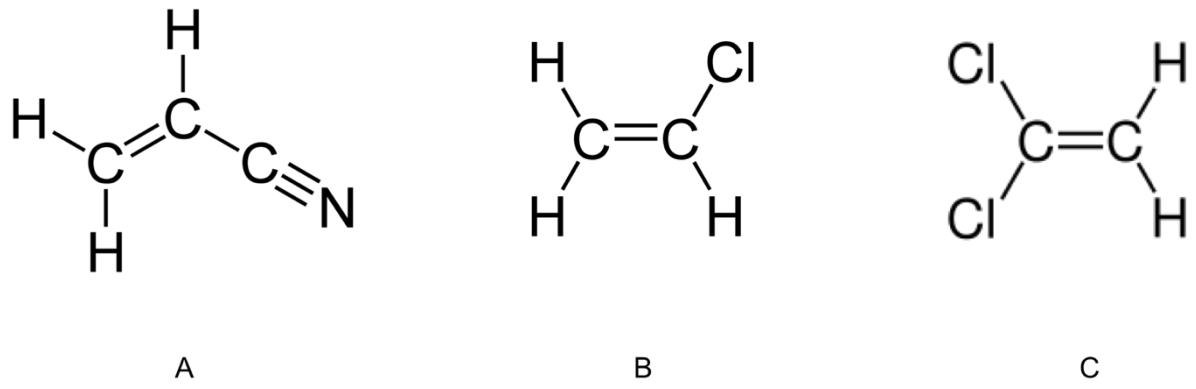

Figure 9: Monomers of modacrylic fibers: (A) Acrylonitrile (B) Vinyl Chloride (C) Vinylidene Chloride

2.3 Plasma Science

Plasma is a quasi-neutral gaseous mixture of neutral, radical, and charged species. Since plasmas have properties unlike those of solid, liquid, and gas phases, plasmas have been defined as the fourth state of matter. Plasmas have very interesting electromagnetic properties and can exist under various temperature and pressure conditions. On the astronomical scale, our Sun is essentially a ball of plasma. On a smaller scale, plasmas are found in fluorescent and neon lights, as well as lightening, the Aurora Borealis, and the sparks in our car's spark plugs. In fact, 99% of our observable universe is in the plasma state.

Plasmas can be generated in the laboratory by electrically ionizing a gaseous medium. This is typically done by connecting a power supply between two electrodes separated by an arbitrary distance. Upon turning on the power supply, an electric field is generated between the two electrodes. Since charged particles are accelerated by electric fields, randomly present electrons from cosmic background radiation begin to gain kinetic energy within this electric field. At a certain electric field strength (3 kV/mm for air in ambient conditions), a random electron is able to gain enough kinetic energy from the electric field to initiate an ionization reaction.

$$A + e^- \rightarrow A^+ + 2e^-$$
$$2A + 2e^- \rightarrow 2A^+ + 4e^-$$
$$4A + 4e^- \rightarrow 4A^+ + 16e^-$$

Figure 10: Electron avalanche mechanism

The first ionization reaction involves a neutral gas molecule and a high energy electron. Upon "colliding" with the neutral gas molecule, an ion and a low energy electron are produced. At this moment, there are now 2 electrons (the first one that initiated the ionization reaction and the second one, which was produced after the first ionization reaction). The two electrons then gain the required kinetic energy from the electric field to initiate two separate ionizations reactions. The two ionization reactions produce 4 total electrons, which go on to ionize other neutral atoms or molecules, thereby producing even more electrons. This chain reaction is called an "electron avalanche" and helps to ionize the non-conductive gas, and sustain the generated plasma (Figure 10).

Once the non-conductive gas in between the electrodes is appreciably ionized, it becomes conductive—an important characteristic of a plasma—under an event called electrical breakdown. Additionally, as energized species recombine or return to their ground state, photons in the visible light and UV range are released. These events give plasmas their vibrant colors.

Different gases, pressures, electrode geometries, and the absence or presence of dielectric materials will produce different plasmas. At ambient conditions, without a dielectric material, a spark discharge is made between the electrodes (e.g. automobile's spark plugs). At low pressures (1 mTorr - 3 Torr), a glowing plasma discharge is produced. At atmospheric pressure, along with the presence of a dielectric material covering the electrode, a dielectric barrier discharge (DBD) plasma is produced. Instead of a glow discharge, as is the case for the low pressure plasma, the DBD plasma consists of multiple filaments. The visual differences between an atmospheric pressure DBD plasma and a low pressure plasma can be seen in Figure 11. The purple color observed in the Figure 11 is due to nitrogen molecules returning to their ground state.

Figure 11: Dielectric Barrier Discharge (Left) and a Low Pressure Plasma Reactor (Right)

The dielectric barrier discharge's filamentary nature is a product of the dielectric material. A dielectric material is made of non-polar or polar molecules with zero free electrons. Under an electric field, the electrons and nucleus of the molecules in the dielectric pull in different directions, creating induced dipoles. This generates an opposing, yet proportional, electric field to the electrode's electric field. The dielectric also serves to

spread the net charge across the entire electrode surface area. Combined, these two features limit the current flowing through each of the filaments, and reduce the heat exchange between the filaments and surroundings.

Low pressure plasmas are also generated through an electron avalanche, but require less voltage than atmospheric plasmas. The reason is that in a low pressure environment, the gas density is lower, which decreases the collision frequency and increases the mean-free path of electrons. This means that an electron can gain more kinetic energy before losing its energy in a random collision. Since the electrons can gain the energy required to initiate an ionization reaction more readily in a less collisional environment, an electron avalanche can be initiated with a weaker electric field. This relationship is known as Paschen's Law.

An important feature of DBD plasma discharges and low pressure plasmas is their non-thermal or non-equilibrium property. By non-thermal or non-equilibrium, the plasma science community means that the temperature of the ions (~300 K) is not equivalent or equilibrated to the temperature of the electrons (~1100 K). This may seem to defy the basic principles of heat transfer, but due to the few, but elastic collisions between electrons and ions, and the small, mobile electron mass relative to the larger, slower ion mass, there is poor heat transfer between the electrons and the ions/neutrals. The slow heat transfer rate is also a result of these plasmas being weakly ionized (10^{-8} to 10^{-6}) and the natural cooling of the ions [27].

In contrast, thermal plasmas (i.e. lightening and spark discharges) are more fully ionized (10^{-3} to 10^{-1}), and the electron temperature and ion temperature are equilibrated ($T_e = T_i$). These kinds of plasmas can release large amounts of current and heat to their immediate surroundings.

Non-thermal plasmas (also known as “cold” plasmas) are ideal candidates to disinfect and deodorize soiled fabric because their non-thermal property ($T_e \neq T_i$) will not thermally stress the material, while the charged atoms and molecules of the plasma will destroy bacteria and its secreted odorous compounds. Plasma has already been applied in the elimination and removal of methane, butane, acetaldehyde, H_2S, VOCs, HAPs, NH_3, and odor in animal/fish houses [13]. Furthermore, the power consumption to operate either a DBD plasma reactor or low pressure plasma reactor is significantly lower than the power consumption to operate a traditional laundry washer.

Plasmas are indeed versatile. They have been successfully applied in lighting, semiconductors, TVs, and ozone generation. Their use as sterilizing agents is also well documented. Research on the sterilization and disinfection properties of plasmas has been conducted since the early 1970s. The primary motivation behind this research was to quickly and efficiently sterilize medical equipment without damaging thermally sensitive devices. As a result, there exists much literature documenting the reduction of bacteria colony forming units (CFU) via non-thermal plasma exposure. Plasma’s antimicrobial

activity has been exhibited in both weaker bacteria (E. coli) and stronger bacteria (Bacillus Stratosphericus and Deinococcus Radiodurans) [10].

In general, bacteria are susceptible to heat, radiation, oxidation, radicals, and pH [13]. These factors either affect their cellular membrane structure and function and/or DNA structure—which eventually leads to altered cellular activities, a loss of reproductive capabilities, or cell death. Since air plasmas generate reactive oxygen species (ROS) and reactive nitrogen species (RNS), radicals, and UV radiation, bacteria are naturally outmatched. The ROS and RNS predominantly include atomic oxygen, O_2*, superoxide, ozone, hydroxyl radicals, nitric oxide, and nitrogen dioxide.

However, Laroussi (2005) has shown that the generated heat and UV radiation in low temperature plasmas are too low to significantly effect bacteria viability. Instead, his research indicates that ROS, RNS, radicals, and electrons are largely responsible for the log reductions in CFU count in bacteria cultures directly exposed to low-temperature, atmospheric pressure plasmas.

In particular, it is believed that hydroxyl radicals react with the fatty acid components of the phospholipid bilayer of cell membranes to cause membrane disintegration, while oxidative species and RNS attack the regulatory proteins imbedded in the cell membranes. These effects are more pronounced with higher plasma exposure times. Furthermore, Laroussi believes that plasma-induced cell membrane surface charge

accumulation generates a strong enough electrostatic repulsive force to pull the cell membrane apart.

In summary, low temperature plasmas can be electrically generated with an AC or DC power supply, can be configured by changing the gas type, electrode geometry, and pressure, and have shown wide-ranging use in fields such as surface treatments, sterilization, and odor control.

2.4 Electron Beam Science

Electron beam technology is the result of combining fundamental properties of electricity and magnetism, with the ability of metals to emit electrons at high temperatures (i.e. thermionic emission). The purpose of an electron beam is to produce a beam of high-energy electrons. In order to accomplish this task, several components are needed. These include an a) electron source b) vacuum c) electron lens, and d) magnetic lens.

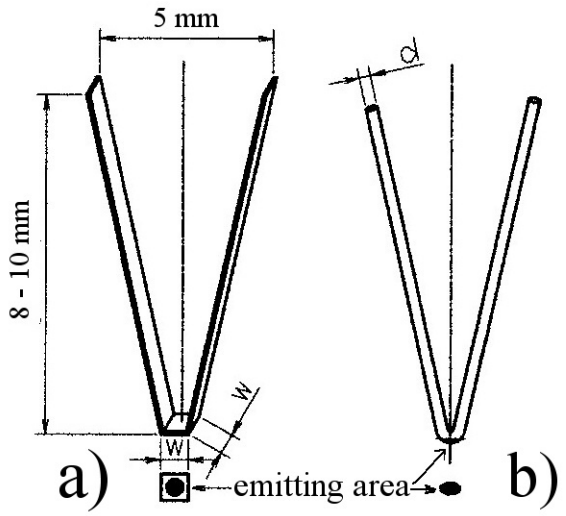

Figure 12: Tungsten Cathode Configurations (A) Strip configuration of the tungsten cathode (B) Wire configuration of the tungsten cathode. These electrodes serve as the electron source by the process of thermionic emission.

The electron source is typically a tungsten or LaB_6 (lanthanum hexaboride) hairpin-like filament (Figure 12). These compounds have high melting points, and can resist the high temperatures needed to literally "boil off" electrons from the metal. This process is called thermionic emission, and works by providing electrons with enough thermal energy to escape the electrostatic pull of the positive nuclei of the compound. As the electron escapes this potential energy barrier, it is important to keep that electron in a collision-free environment. Not doing so, results in unwanted outcomes such as the charge neutralization reaction that occurs if an electron collided against an ion. To avoid this, a vacuum (normally 10^{-3} to 10^{-10} Torr) is applied during electron beam processing.

Free electrons from thermionic emission typically only have energies of a few electron-volts (eV). To increase the energy of the electrons to their desired values, an electric field is used to accelerate the electrons. To prevent the electrons from diverging, an electrostatic lens, which is a cup-like cathode, is placed right after the electron emitter, but behind the anode. This produces a converging, radial field towards the hollow anode.

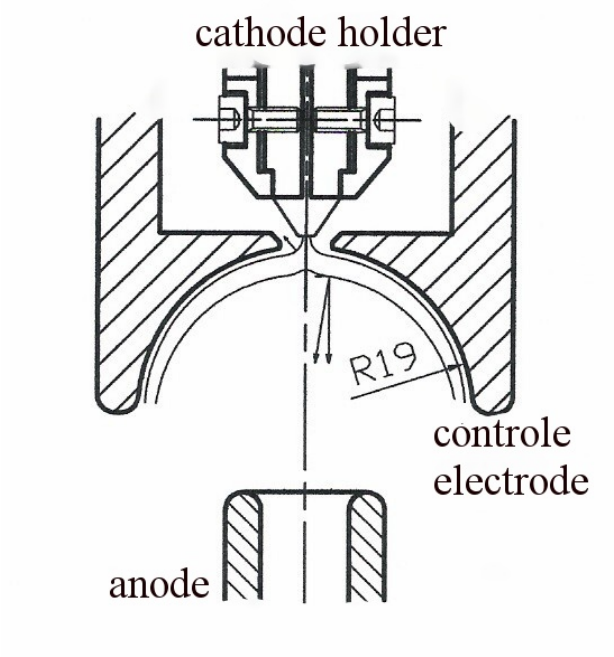

Figure 13: Electron Beam Electron Lens: Cup-like electrode functions as a secondary cathode by creating a converging electric field towards the anode. The radial components of the electric field help focus the electron beam, as the axial components accelerate the electrons to a higher kinetic energy. This electrode functions as the electrons lens.

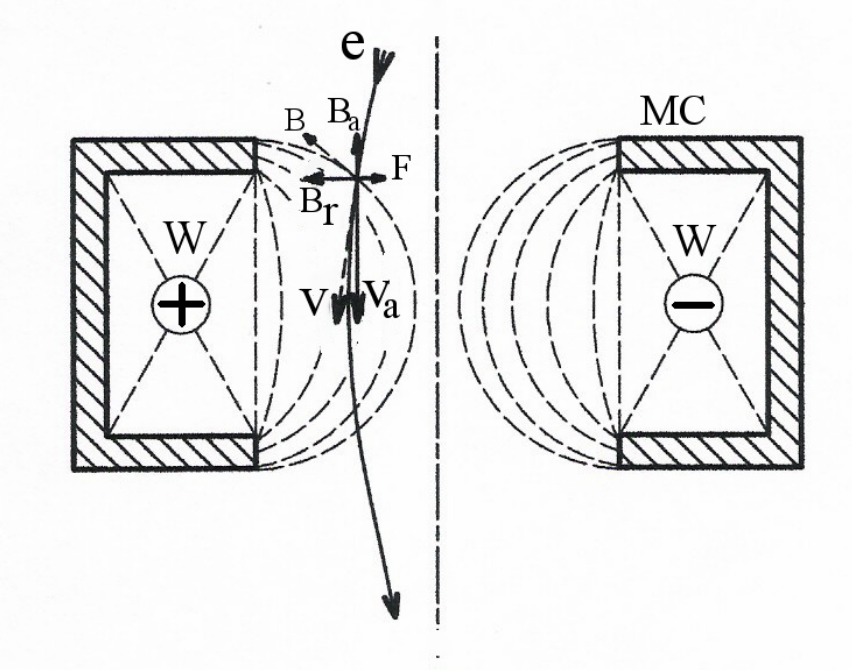

Figure 14: Electron Beam Magnetic Lens: magnetic coils producing a rotationally symmetric magnetic field. Note that the magnetic field has a radial component (B_R) and an axial component (B_A). The cross product between the axial velocity of the electron and the radial component produces a circumferential force. This force gives the electron a circumferential velocity. This circumferential velocity interacts with B_A and produces a radially inward force (shown as F). This is how a magnetic lens focuses an E-beam.

As the electrons converge into a beam, and ultimately begin to diverge again, a magnetic lens is employed to refocus the beam to a specific power density. Here, magnetism's property to affect the path of moving charged particles is applied. As the electron moves down with some unknown angle to the electron beam gun axis, it encounters a rotationally symmetric, yet curved, magnetic field (Figure 14). This magnetic field produces two forces, from the relation $F = q\ (v \times B)$. The magnitude of the first force is the product of the axial velocity of the electron with the radial component of the magnetic field and gives the electron a circumferential motion about the electron beam gun axis. This circumferential motion, in turn, produces the second force. The magnitude of the second

force is the product of the circumferential velocity of the electron with the axial component of the magnetic field. This produces an inward-facing force, which ultimately helps focus the electron beam.

The electron beam's power is calculated as the product of the accelerating voltage and beam current, and is easily controlled by either increasing the voltage between the cathode and anode and/or increasing the beam current by increasing the temperature of the tungsten or LaB_6 filament. The power density of the electron beam is controlled by changing the magnetic field strength of the magnetic lens.

3. EXPERIMENTAL METHODS AND PROCEDURES

3.1 Direct Dielectric Barrier Discharge Reactor Setup and Operation

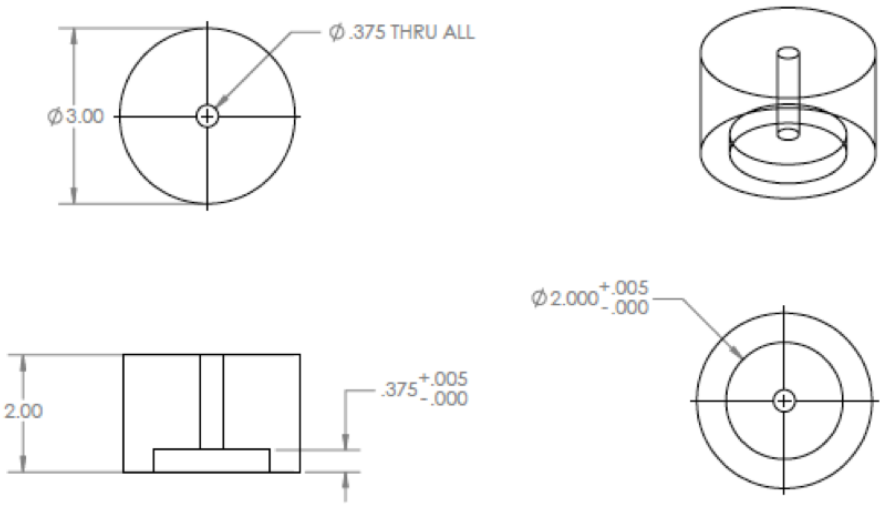

Figure 15: Drawing of DBD Reactor's Acrylic Housing

The dielectric barrier discharge reactor was manufactured at Texas A&M University (Figure 15). The housing was machined out of a 3.00” diameter acrylic cylinder. The center of the acrylic cylinder has a .40” bore to accept a conducting 3/8-16 all-thread. The bottom part of the acrylic cylinder was machined to have a height of .375 inches and an inner diameter of 2.00” to accept the copper electrode.

The copper electrode was CNC machined from a copper plate (Figure 16). The copper disc has a 2.00” outer diameter and is .375 inches thick. The center of the copper disc was bored and tapped to have a .25” long 3/8-16 thread.

The DBD reactor was assembled by passing the steel all-thread through the acrylic housing, and screwing it into the copper disc. The copper disc was kept flush with the bottom of the acrylic housing by tightening a 3/8-16 nut on the 3/8-16 all-thread against the top of the acrylic housing (Figure 17).

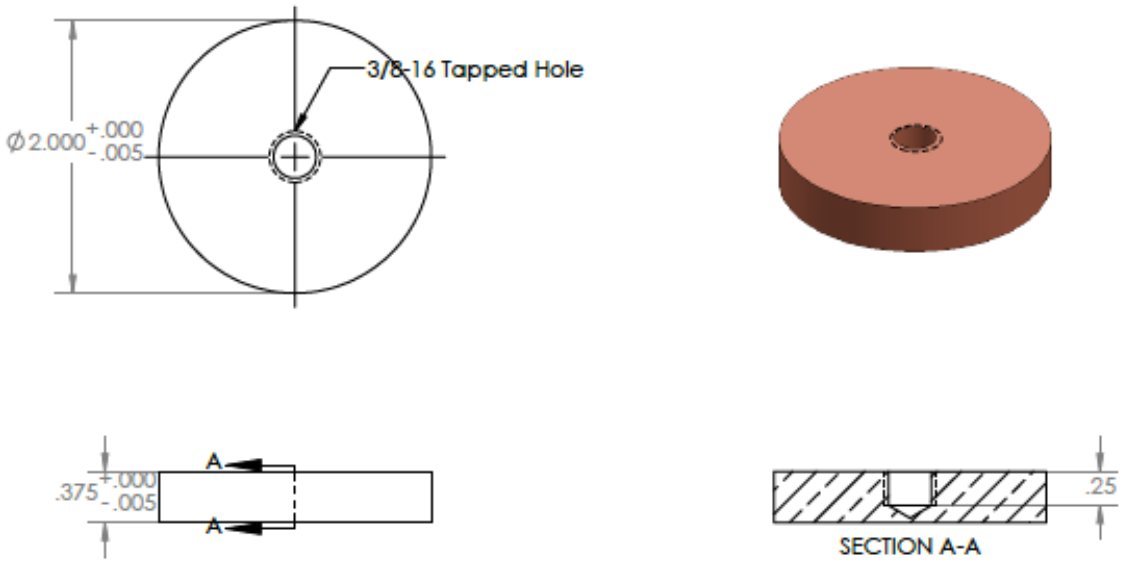

Figure 16: Drawing of Copper Electrode Disc for DBD Reactor

The dielectric barrier chosen for our experimental setup was a ¼” thick, 3.00” OD quartz plate. This dielectric barrier was secured to the copper electrode through a high temperature silicon glue. Special care and attention were taken to minimize air gaps in between the copper electrode and the quartz dielectric barrier. This was done by adding

excessive amounts of silicon glue between the copper and the quartz, and pressing down on the quartz plate with the rest of the assembly until the excess silicon glue squeezed out of the edges. The excess silicon glue was quickly wiped away from the edges to prevent the silicon glue from setting. After ensuring that there were no air gaps between the copper and the transparent quartz plate, the DBD reactor was set down (quartz plate down) and left to set overnight.

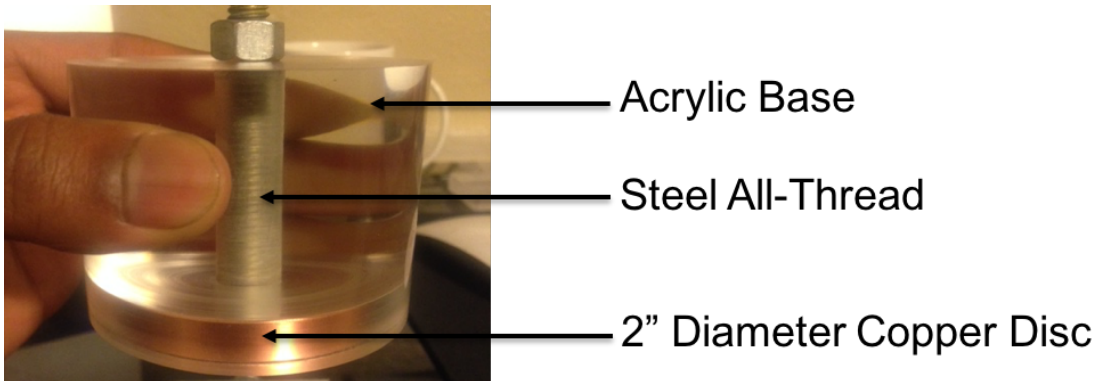

Figure 17: Assembly of Atmospheric Pressure DBD Reactor

The final DBD reactor assembly step was securing an insulated, conducting wire to the steel all-thread by using a combination of threaded nuts and washers to clamp down on the terminal pin connector of the conducting wire.

The DBD is operated by positioning the DBD reactor above a ground electrode. The vertical distance between the DBD reactor and the ground electrode is changed and measured via a micrometer. The DBD filaments are more uniform with a 1-2 mm gap

distance. Larger distances require more power for DBD discharges to become evident. At any given power density, larger distances reduce the DBD filament density, and increase the probability of etching holes into your fabric.

For these reasons, our DBD reactor was operated with at a power density of 1.27 W/cm^2, a gap distance of 1 mm, a power supply frequency of 22 kHz, and at ambient air conditions. DBD reactor operating times varied according to the specific experiment.

3.2 Indirect Dielectric Barrier Discharge Setup and Operation

The following experimental procedure is very similar to the direct DBD method of operation. The major difference is that in an indirect setup, the experimenter allows the plasma species to passively diffuse onto the substrate. This is achieved by placing the substrate (i.e. liquid) below the two electrodes, instead of in between the two electrodes—as is done in the direct DBD configuration. Furthermore, to allow the plasma species to diffuse through the bottommost electrode and onto the substrate, a stainless-steel mesh is used as the ground/bottommost electrode. To maintain a 1mm gap between the electrodes, a circular non-conductive spacer is placed in between the high voltage electrode (that already has a quartz plate) and stainless-steel mesh ground electrode. A cross-sectional view of this setup is shown below for further detail.

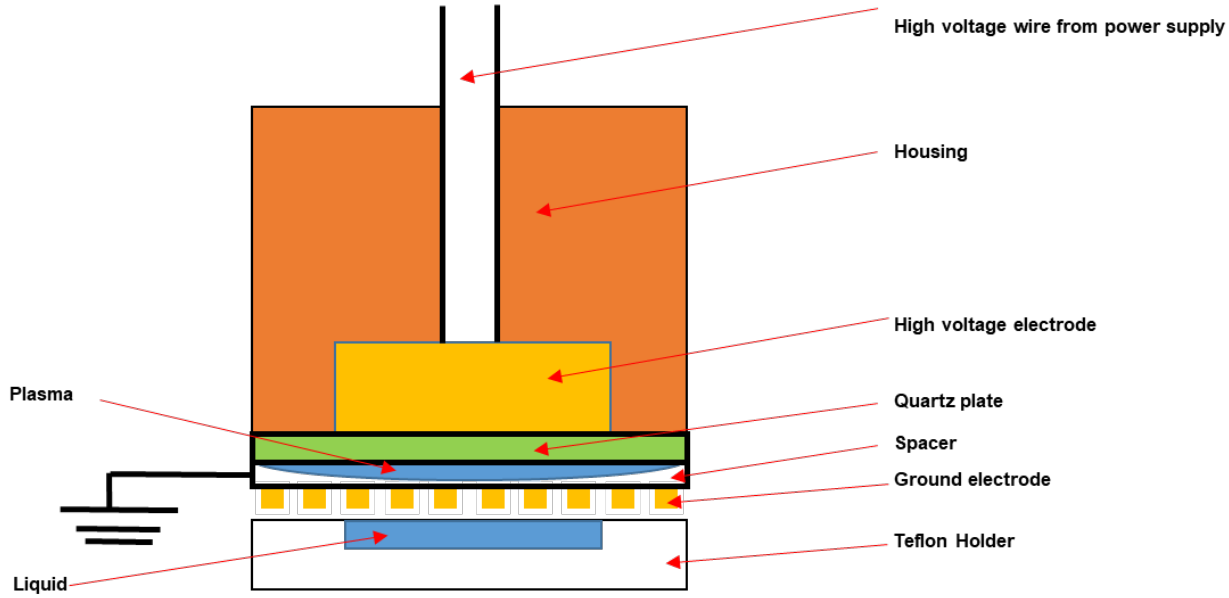

Figure 18: Cross-sectional View of an Indirect DBD Reactor. Note how in contrast to the DBD reactor in Figure 17, this indirect DBD has both electrodes (shown here in yellow) above the substrate. The substrate in this diagram is the liquid, which is poured into the teflon holder. Photo Credit: Josef Sebastiaan

Once the voltage across the two electrodes exceeds the electrical breakdown of air within the 1mm gap, a dielectric-barrier-discharge plasma is generated. This DBD plasma is visible only within the 1mm region between the electrodes (Figure 19). However, plasma species are now free to diffuse through the slots of the stainless-steel mesh ground electrode and interact with the substrate below.

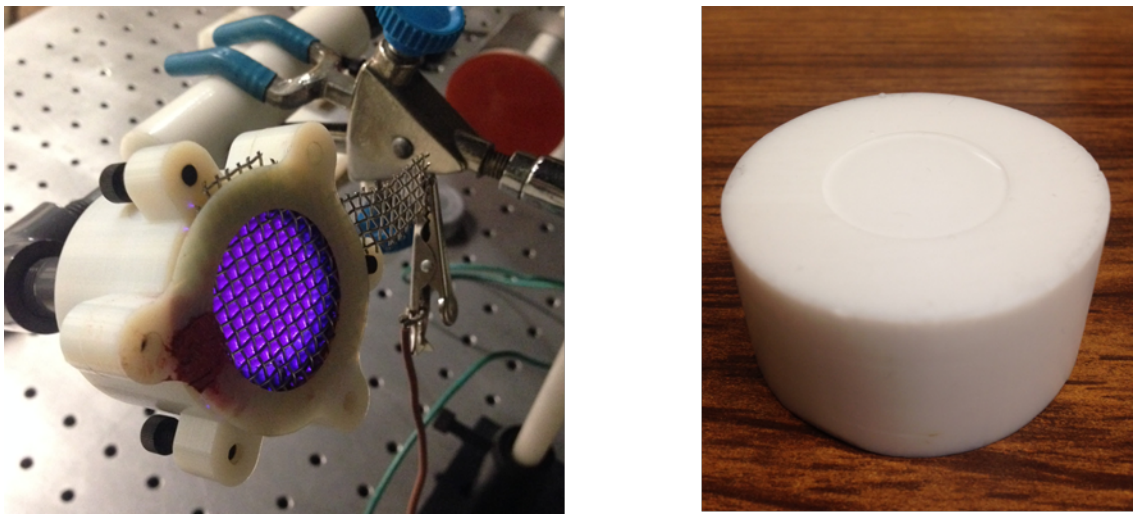

Figure 19: Indirect DBD Reactor Showing Plasma Filaments (left) and Teflon-made liquid sample holder (right)

If the chosen substrate is a liquid solution, the Teflon liquid-sample holder can be filled with up to .85 mL of the solution. The Teflon liquid sample holder is a cylindrical piece of Teflon with a recessed hole. An image of the Teflon sample holder is provided in Figure 19, and in the image of the complete setup (Figure 20).

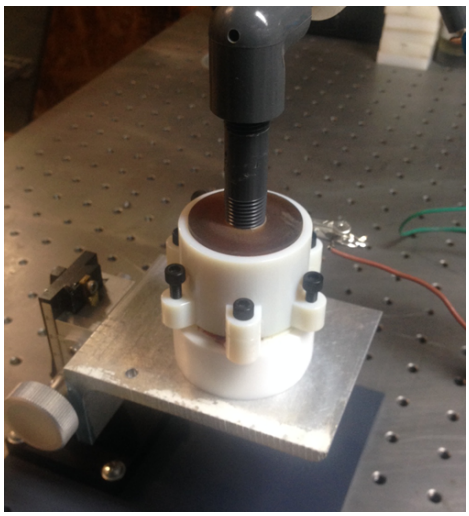

Figure 20: Experimental Setup of an Indirect DBD Reactor. Plasma species generated in between the electrodes are able to diffuse into the liquid sample below

3.3 Low Pressure Plasma Reactor Setup and Operation

The Low Pressure Plasma Reactor—or LPPR—was assembled at Texas A&M University. The LPPR consists of a 3.00” diameter x 36” long acrylic cylinder glued to stainless steel flanges on both ends. A Teflon gasket is inserted in between the stainless steel flanges and end caps, while a stainless steel clamp tightens this seal from the outside.

The flanges at both ends of the LPPR have 4 threaded holes that are equally spaced. Two sets of all-threads are passed through these holes. The first set of 4 all-threads are steel conducting all-threads measuring approximately 90% of the length of the LPPR. The second set of 4 all-threads are shorter non-conducting all-threads measuring approximately 20% of the length of the LPPR. Both sets of all-threads are mechanically joined via 4 female-female connectors. This configuration is needed in order to establish an electric potential between the two electrodes. Without the non-conducting all-thread, both ends of the LPPR would have the same electric potential. One of the end caps of the LPPR, there is a port that connects to a vacuum pump. Along this same mechanical line, a needle valve is added that allows the operator to regulate the vacuum pressure inside the LPPR. The AC power supply is connected to the LPPR by using a threaded nut to clamp down the terminal end of the wire to one of the steel-all thread rods. The other end of the LPPR has a grounding strap attached for electrical safety.

The LPPR is operated by closing the needle valve, tightening the seal clamps, turning on

the vacuum pump, and slowly increasing the voltage of the AC power supply. At a specific voltage, the user will begin to see the low pressure plasma.

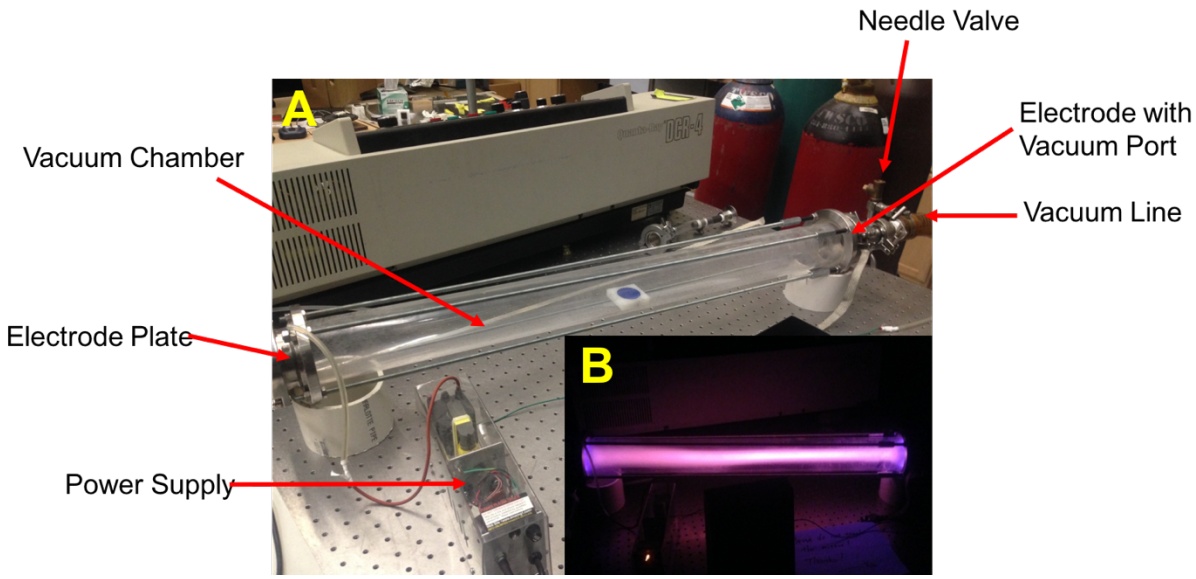

Figure 21: Low Pressure Plasma Reactor (LPPR) in off (A) and on (B) position

3.4. Electron Beam Setup and Operation

The electron beam generator is housed at Texas A&M University's Electron Beam Center for Food Science Research. Samples are placed inside a cardboard box and exposed to the electron beam through a conveyor belt system. The speed of the conveyor belt system determines the E-Beam dose (measured in kGy) of the samples.

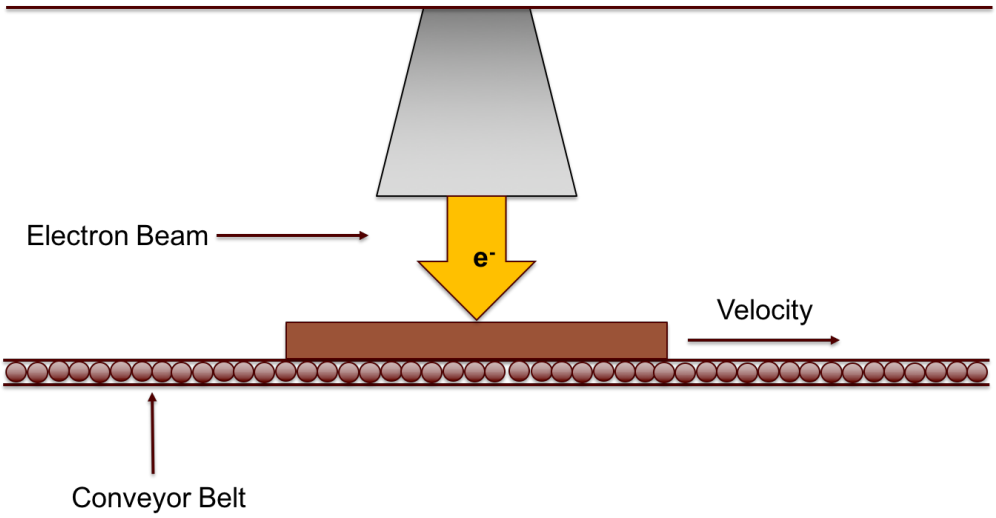

Figure 22: Electron Beam Treatment Setup Diagram

3.5 Fabric Sample Holder Setup and Operation

DBD treatment is dependent on the distance between the DBD reactor and the ground electrode. In order to obtain a uniform DBD treatment, fabric samples had to be held down evenly across the ground electrode.

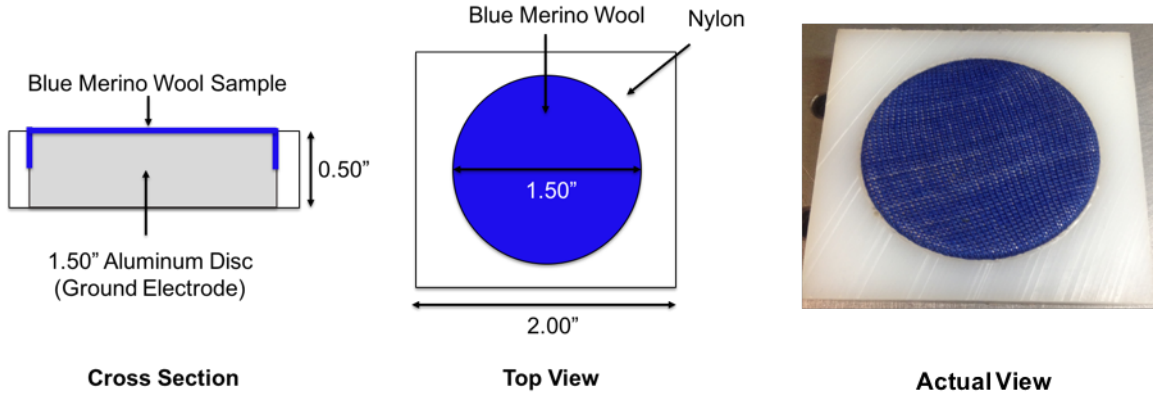

Figure 23: Fabric Holder Dimensions and Setup: This setup is used to straighten and secure fabric samples during DBD plasma exposure. The fabric shown is commercially available blue merino wool.

This was made possible by machining 1.50” OD ground electrodes, and cutting 1.50” circles into 2” x 2” x.50” nylon squares. A 2” diameter circle of fabric is then placed down onto the ground electrode, and the hollow nylon square is placed over it. The tight clearance between the ground electrode OD and the nylon fabric ID requires a degree of mechanical force to fully cover the ground electrode with the nylon fabric holder. The tight clearance also causes minor stretching of the fabric as the nylon fabric holder passes over the ground electrode (Figure 23).

4. RESULTS

4.1 Plasma-Induced Wettability Changes

Wettability was measured indirectly through the contact angle that a 10 uL droplet of distilled water made when placed at the center of untreated and/or treated fabric. After placing the 10 uL droplet of water, a photograph was taken and then loaded into a photoimaging software (Toup) that had an angle measuring tool. During all contact angle measurements, the treated or untreated fabric were held down over the aluminum electrode with the nylon fabric holder to facilitate the placement of the horizontal component of the contact angle. Fabric fibers in front of the 10 uL water droplet complicated the precise placement of the base of the contact angle measuring tool. Therefore, contact angle measurements presented here have an estimated degree of error of +/- 15 degrees. Water droplets were routinely placed at the center of the fabric because the center was most likely to have received the highest exposure to plasma reactive species.

4.1.1 DBD Plasma

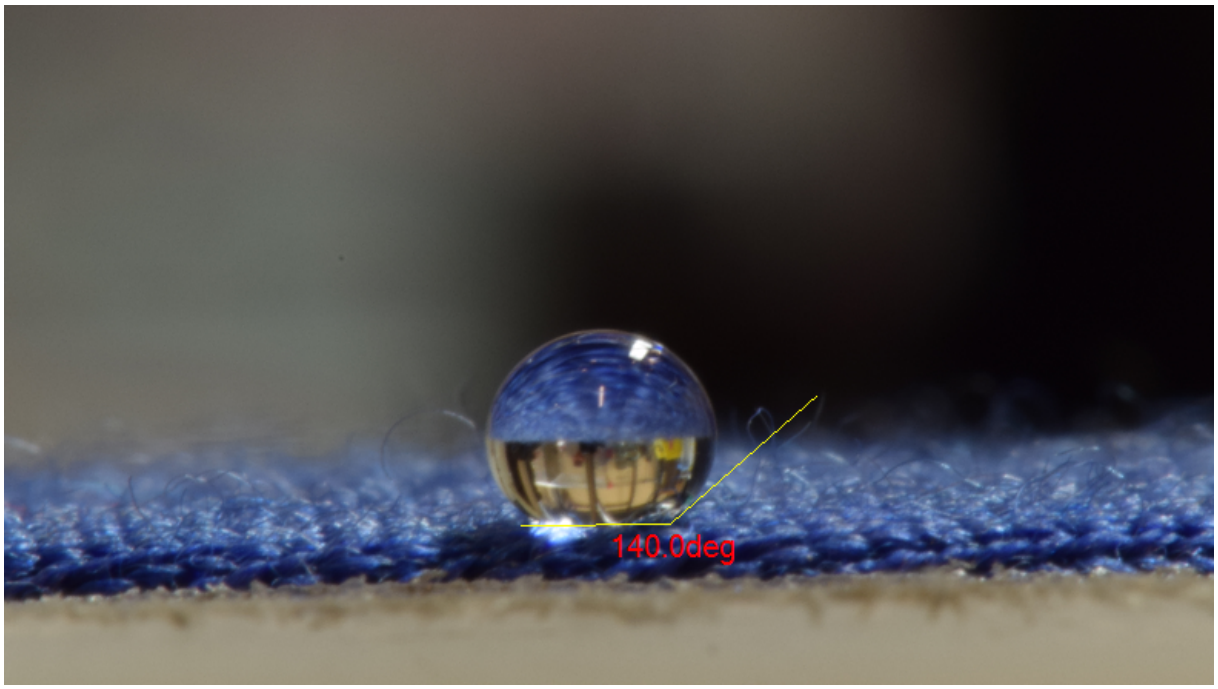

Figure 24: Initial Water Contact Angle on Untreated Merino Wool. A 10uL droplet of distilled water on untreated blue merino wool makes an approximate contact angle of 140 degrees. Note: The white surface near the bottom of the image is the nylon fabric holder.

Untreated merino wool has a water contact angle of approximately 140 degrees, which indicates very low wettability (Figure 24). Direct exposure to DBD generated plasmas changes merino wool's characteristic low wettability to high wettability. In other words, DBD plasmas make merino wool hydrophilic. Though the exact reaction mechanism behind the change in wettability is unknown, it is hypothesized that the charged oxygen and nitrogen species of the plasma temporarily bind to the merino wool fiber, thereby creating a thin hydrophilic layer which facilitates the transport and absorption of water through the merino wool fibers.

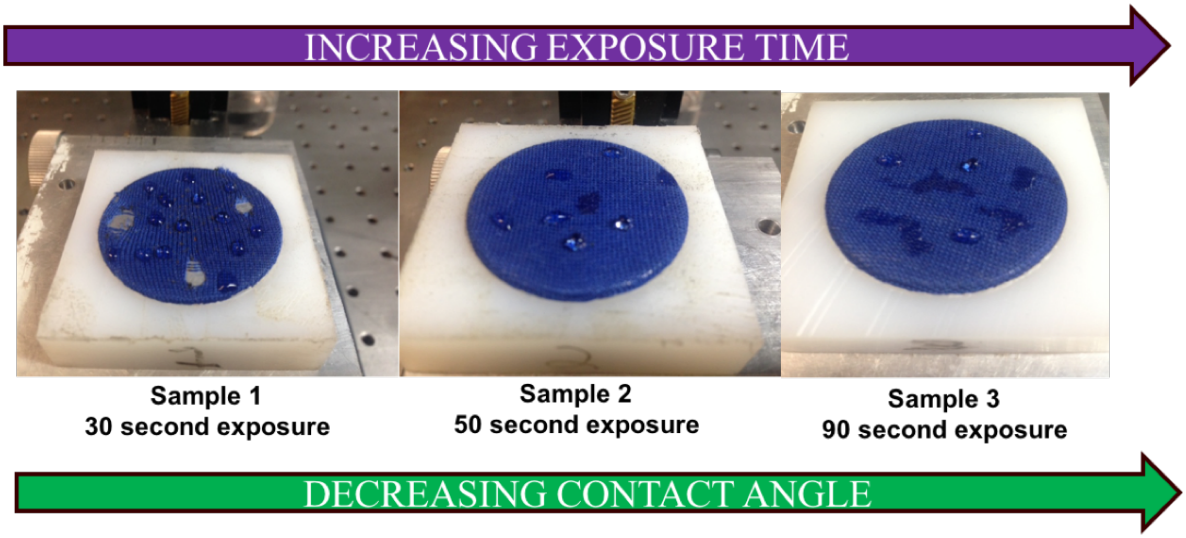

Figure 25: Wettability vs DBD Exposure Time Study. These results showed that increased plasma exposure time leads to higher degrees of water absorption.

A wettability vs plasma exposure time study (Figure 25) showed that at a power density of 1.27 W/cm^2 and a gap distance of 1 mm, a plasma exposure time of 120 seconds (2 mins) was needed to achieve a complete and uniform change in wettability. Interestingly, this is approximately the same amount of time needed to kill *B. Stratosphericus* and *D. radiodurans* under the same operating conditions.

4.1.2 Low Pressure Plasma

Merino wool experiences a wettability change after exposure to low pressure plasmas. Similar to merino wool's wettability change with DBD plasmas, the wettability of merino wool under low pressure plasmas is also a function of exposure time. During short plasma exposure times (0-10 seconds), surfaces of fabric farthest away from the axial center of

the cylinder will experience little to no wettability changes. This also means that folded areas of longer fabrics will not show any signs of wettability changes.

4.1.3 Electron Beam

A total of nine samples of blue merino wool were taken to the Electron Beam Center. Six samples were held down over aluminum electrodes, two samples were held down over acrylic electrodes, and the last sample was held down over an acrylic electrode and wrapped in heat-shrink plastic.

All blue merino wool samples were exposed to an E-Beam dose of 52.2 kGy. At approximately 10 minutes after E-Beam treatment, each of the samples were tested for wettability changes by using a 10 uL droplet of distilled water.

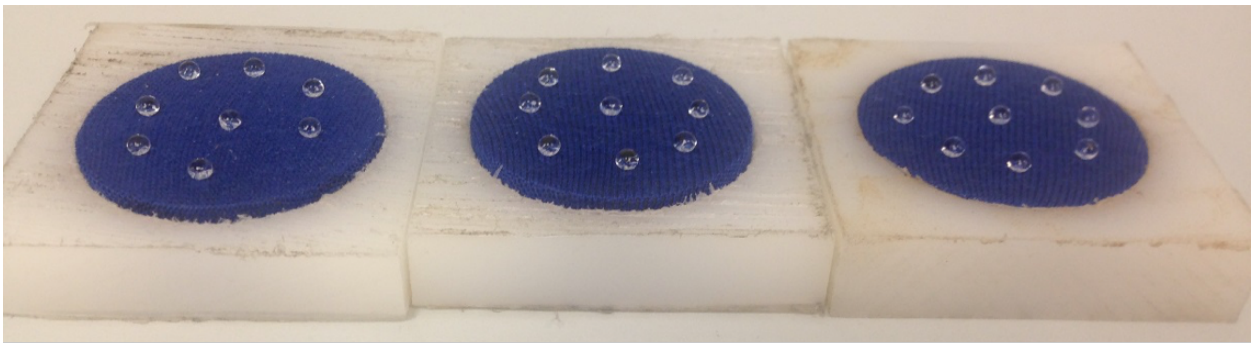

Figure 26: E-Beam Treatment of Blue Merino Wool at 52.2 kGy with Different Configurations (Listed)

As can be seen from Figure 26, none of the samples experienced any changes in

wettability, regardless of whether the sample was heat sealed, placed over an acrylic disc, or placed over an aluminum disc. In all of the images, the water droplets had contact angles higher than 90 degrees, which indicates low wettability.

These results are very important. First, it shows that electrons do not participate in the wettability change mechanism of blue merino wool. This means that the positively-charged species of the LPPR and DBD reactor are the likely participants in the wettability change of the merino wool. Second, an E-Beam dose of 52.2 kGy is known to kill an entire culture of bacteria. Visual inspection of the blue merino wool did not reveal any damage to the fabric. The significance of this is that E-Beam treatment of merino wool is a potential solution in extending the wearability of astronaut clothing by providing them “super clean” garments before launch time.

To summarize, an E-beam dose capable of killing a culture of bacteria did not cause any wettability changes or any visual changes in the mechanical properties of the blue merino wool. This suggests that electron-beam pre-treatment of fabric is a potential solution in extending the wearability of astronaut laundry. In fact, as discussed later, tensile testing revealed negligible changes between the mechanical properties of E-beam treated merino wool and untreated merino wool. This experimental result provides additional support for pre-cleaning astronaut clothing before long-duration space missions.

4.1.4 Wettability Lifetime

After repeatedly verifying that DBD and LPPR treatment affect the wettability of merino wool, a question arose as to whether the wettability change was permanent or temporary. This was the motivation behind the wettability lifetime studies for DBD treated blue merino wool samples.

Each blue merino wool sample was exposed to DBD plasma treatment at a distance of 1mm, a power density of 1.27 W/cm^2, and an exposure time of 2 minutes. A single water contact angle test was performed on each fabric after a multiple of 10 minutes after the DBD treatment. The results of the wettability lifetime study are shown in Table 1 below.

The blue merino wool's hydrophobicity began to return post-treatment. At 50 minutes post-DBD treatment, a contact angle of 66° was measured. At 60 minutes post DBD treatment, a higher contact angle of 75° was measured. After 3 days, a water contact angle test was performed on the same samples. Each of the samples had an average contact angle of 127°. Clearly, these results show that the return of the initial wettability state is a function of time after plasma treatment.

Table 1: Wettability Lifetime Study (three different days labeled on left vertical axis) NOTE: [1-1 means Day 1, Sample 1, 2-3 means Day 2, Sample 3.

	Test Sample	Δt	ΔT	Contact Angle
	Control	N/A	N/A	140°
12/02/16	1-1	0 min	24 °F	0°
	1-2	10 min	19 °F	0°
	1-3	20 min	25 °F	0°
	1-4	30 min	26 °F	0°
	1-5	40 min	19 °F	0°
	1-6	50 min	25 °F	66°
	1-7	60 min	21 °F	75°
02/10/17	2-1	70 min	19 °F	0°
	2-2	80 min	23 °F	0°
	2-3	90 min	24 °F	0°
02/14/17	3-1	100 min	28 °F	82°
	3-2	110 min	22 °F	52°
	3-3	120 min	25 °F	54°
	3-4	130 min	20 °F	38°

However, the return of the initial wettability state is not only a function of time after plasma treatment. While attempting to add additional data to the first data set in Table 1 above, it was found that blue merino wool samples treated on 2/17/2017 retained high wettability characteristics at 70, 80, and 90 minutes post DBD treatment, even though the DBD treatment of the fabric was the same as the DBD treatment on 12/6/2016 (1mm gap distance, 1.27 W/cm^2 power density, 20-22 kHz power supply frequency, 2 minute treatment time).

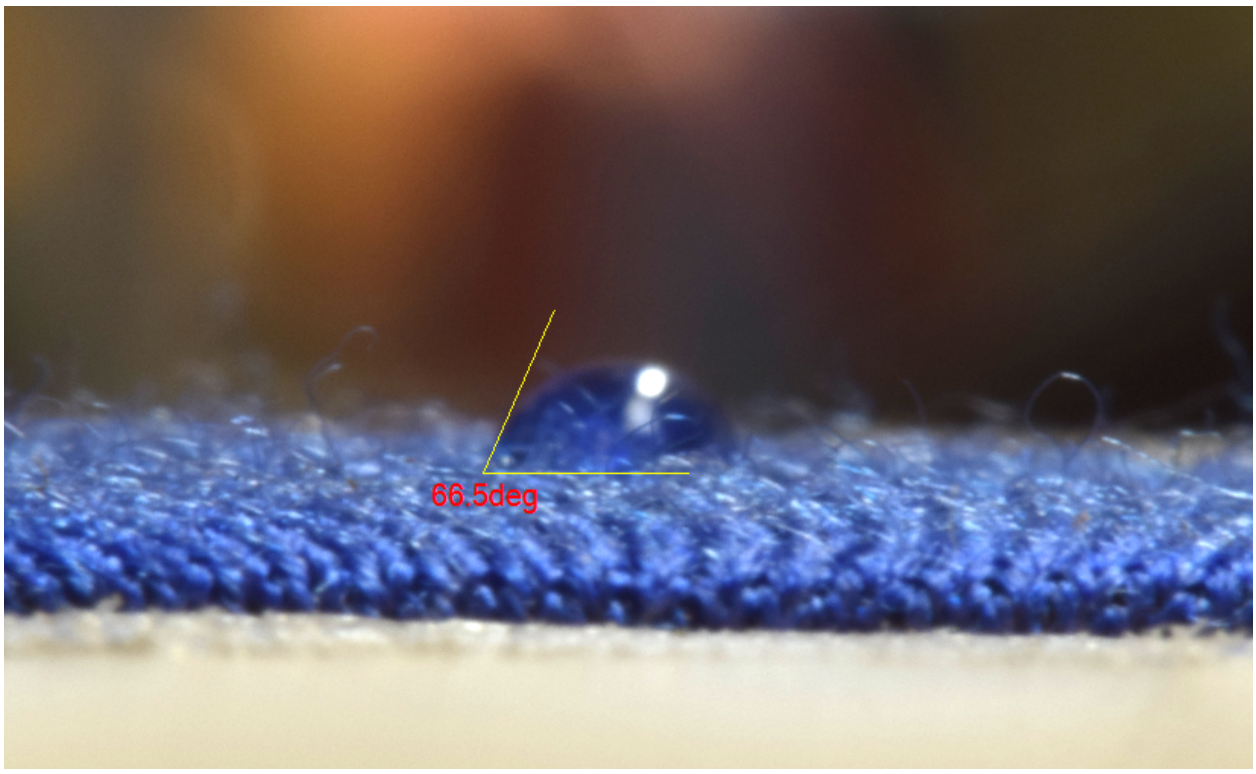

Figure 27: Return of Low Wettability Contact Angle. Sample 1-6 (Day 1, Sample #6) with a contact angle of 66 degrees 50 mins after a 2 min DBD plasma treatment. The image is blurry because the water droplet is being slowly absorbed into the DBD treated merino wool

This experiment was carried out again a few days later, and there was a partial decrease in the wettability of the blue merino wool samples at 100, 110, and 120 minutes post DBD treatment as shown by the increasing contact angle of 10 uL of distilled water droplets.

Fitting this data set into an inverse exponential decay function, a time of 4 days is found to be the amount of time necessary post plasma treatment for the fabric to regain 90% of the initial wettability state.

While only a minor attempt was made to determine the time required for the fabric to regain its initial wettability properties, the real purpose of this study was to answer whether the wettability change was permanent or temporary, and if temporary, after what unit of time, a return to the initial wettability state could be seen. The answers to these questions is that the wettability change of blue merino wool after a 2 min DBD treatment is temporary and begins to return to its initial wettability state after a 3-4 days.

4.1.5. Effect of Contaminants (Dirt and Oil)

The presence of contaminants on the merino wool affect the wettability lifetime of the plasma-induced wettability change. This was clearly seen after rubbing dirt or oil on the blue merino wool fabric. Interestingly, the contact angle of the untreated dirt-laden or oil-laden merino wool was still greater than 90 degrees (thereby showing low wettability). However, the wettability lifetime post DBD treatment at 2 min, 1mm gap distance, and 1.27 W/cm^2 power density was greatly increased with the presence of contaminants.

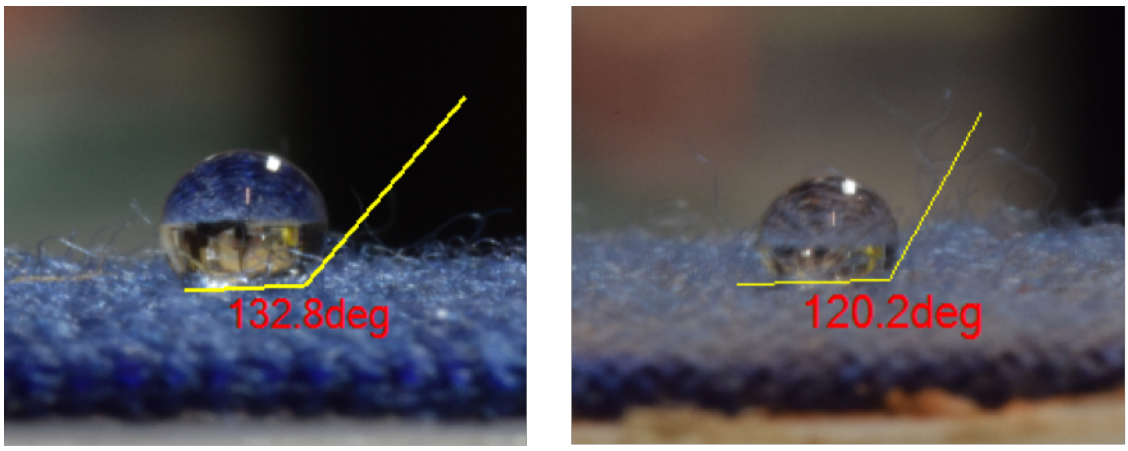

Figure 28: Water contact angles on untreated oil stained (left) and dirt stained (right) blue merino wool samples. Both showed low wettability.

Though the DBD treated, dirt contaminated samples of merino wool remained wettable for the same amount of time as the DBD treated, vegetable oil contaminated fabrics, there was a difference in the absorption rate of the 10 uL water droplet. The DBD treated vegetable oil stained fabric had a smaller spread, yet faster absorption rate. The DBD treated dirt stained fabric had a slower absorption rate, but the water droplet spread out a lot farther throughout the fabric.

Please note that a contact angle of zero degrees was recorded in DBD treated fabrics during the wettability lifetime studies—even though there was an initial contact angle directly after placing the 10 uL water droplet—because by the time the camera took a photo, the water droplet had been absorbed by the DBD treated blue merino wool, and a contact angle could not be measured.

Table 2: Wettability Lifetime Study for Stained Merino Wool

Vegetable Oil Stained Merino Wool

Sample	Contact Angle Test After	Contact Angle
Control	N/A	120°
1	15 min	0°
2	30 min	0°
3	45 min	0°
4	60 min	0°
5	75 min	0°
6	90 min	0°
7	105 min	0°

Dirt Stained Merino Wool

Sample	Contact Angle Test After	Contact Angle
Control	N/A	133°
1	15 min	0°
2	30 min	0°
3	45 min	0°
4	60 min	0°
5	75 min	0°
6	90 min	0°
7	105 min	0°

Table 2 shows that contaminants such as dirt and vegetable oil greatly extend the wettability lifetime of plasma-induced wettability changes on blue merino wool. Coincidentally, during this study, it was found that DBD treatment of vegetable oil-stained blue merino wool produced a very strong and foul odor. The purpose of this project is to deodorize fabric with atmospheric DBD plasmas or low pressure plasmas. This result was slightly discouraging because it is possible that human skin oils will be transferred onto merino wool shirts, and after DBD or low pressure plasma treatment, a pungent smell—instead of a neutral or pleasant one—will be made.

4.2. Plasma Penetration of Fabric

4.2.1 DBD Plasma Penetration of Fabric

The question of whether the DBD plasma affected the opposite side of a single layer of fabric led us to carry out another study—the backside contact angle test. This consisted of DBD plasma treating the merino wool for 2 minutes, at a gap of 1 mm, and at a power density of 1.27 W/cm^2. After the DBD treatment, a 10 uL distilled water droplet was placed approximately 1 cm to the left of the center. After measuring the contact angle on the top surface, the fabric was flipped upside down, and a 10 uL distilled water droplet was placed approximately 1 cm to the right of the center. After measuring the contact angle on the bottom surface, the two contact angles were compared across different post-treatment times.

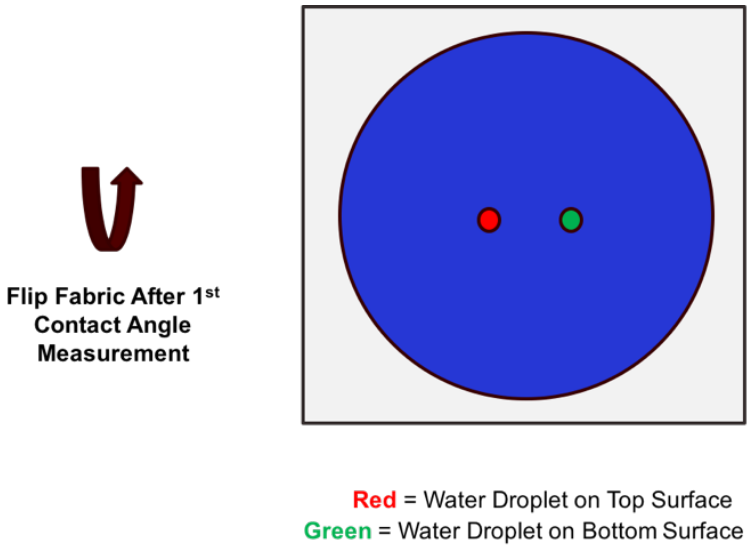

Figure 29: Backside Contact Angle Test Procedure

This test revealed that both sides of the fabric surface were affected by the plasma. Figure 30 shows that both sides of the fabric had 0° contact angles, which means both sides of the fabric became completely wettable after directly treating only one side of the fabric. This result agrees with similar findings in the scientific literature [28, 29].

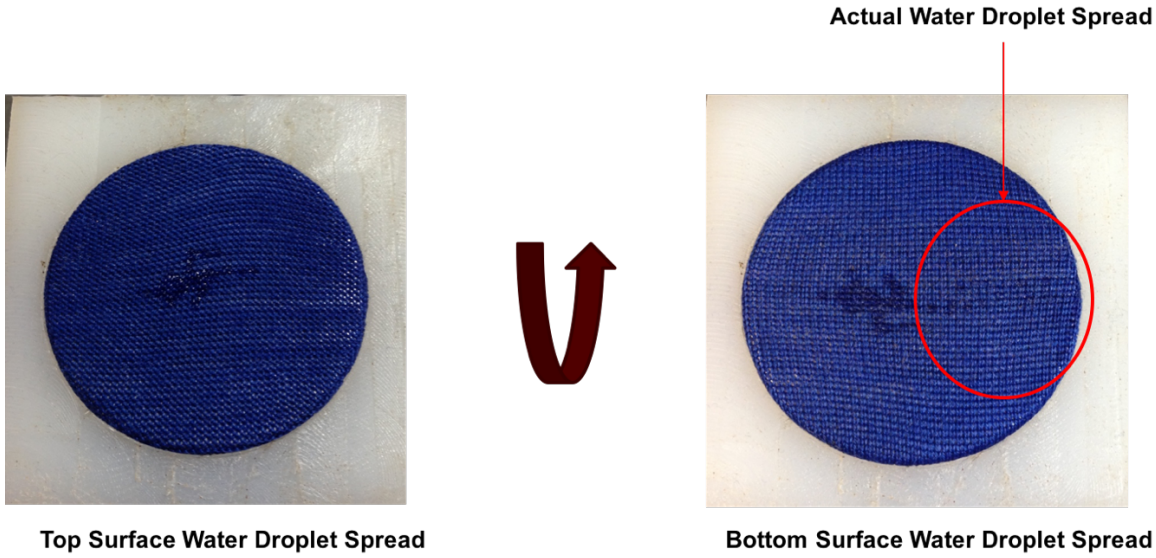

Figure 30: Backside Contact Angle Test Results: (Left shows 1st water droplet on closest surface to DBD reactor, while right shows different water absorption pattern after 2nd water droplet dropped on fabric surface furthest way from DBD reactor.)

Penetration analysis with multiple layers of fabric could not be conducted. The reason is that additional layers of fabric completely shielded the ground electrode, which prevented DBD plasma generation. DBD plasma generation was still possible with two layers of fabric. However, with two layers of fabric on top of the ground electrode, only a few filaments form, and the fabric undergoes strong, random hole formation. This is clearly seen in the Figure 33.

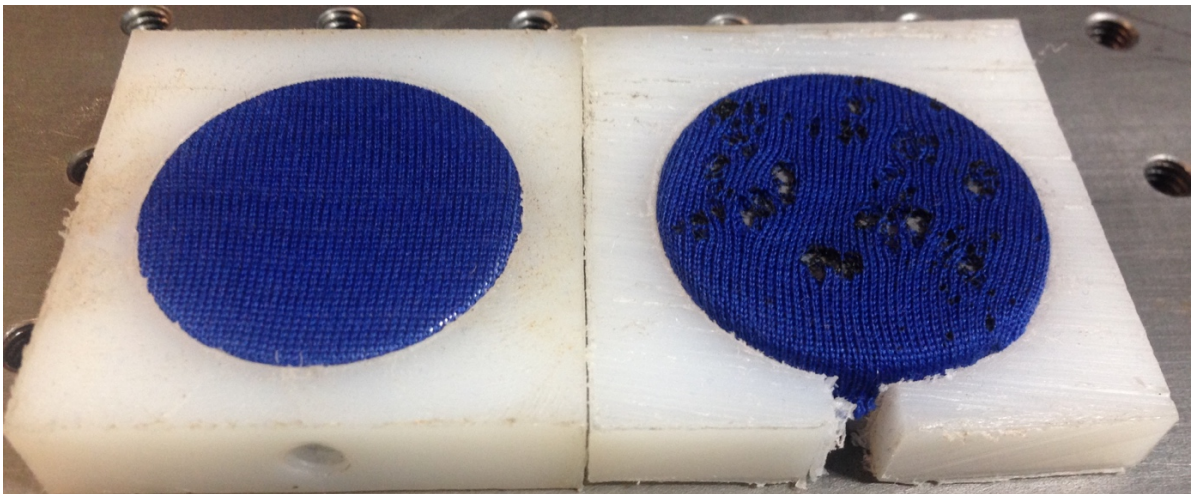

Figure 31: DBD treatment of multi-layered fabric (Left setup has only a single layer of blue merino wool. The right setup has two layers of merino wool. After treatment, the multi-layered sample underwent significant hole formation.)

Furthermore, it was found that if the fabric is not significantly stretched across the ground electrode, there is a smaller effective electrode surface area, which decreases the DBD filament density, which increases each DBD filament intensity, which leads to random, hole formation.

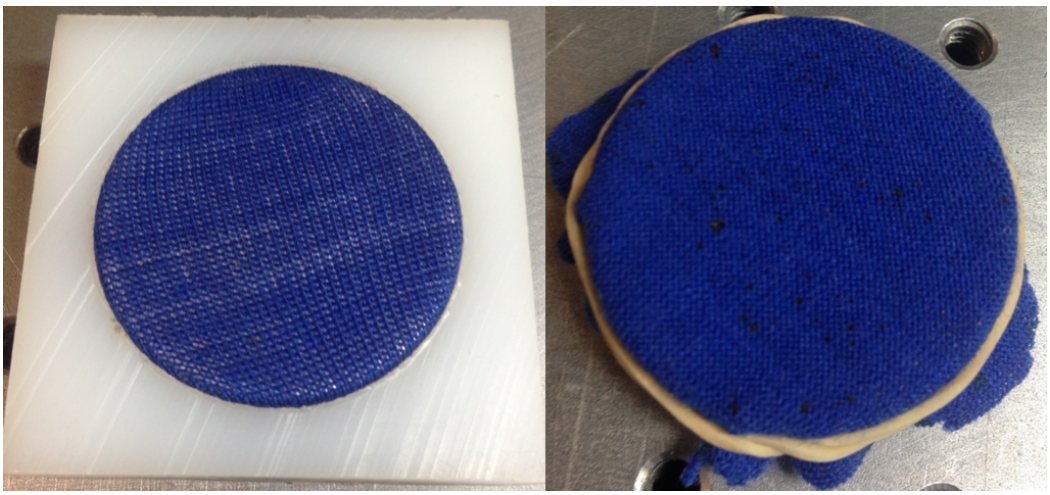

Figure 32: DBD treatment of stretched and unstretched fabrics (Left setup has a single layer of merino wool secured by a tight fitting nylon fabric holder. Due to the tight fit, the fabric is stretched. The right setup has a single layer of merino wool and is not stretched as it is only held down by a rubber band)

Lastly, it was found that at a power density of 1.27 W/cm^2, and a distance of 7mm above the fabric sample, the DBD reactor made holes in the blue merino wool in only 5 seconds. Figure 33 shows hole formation in three different samples.

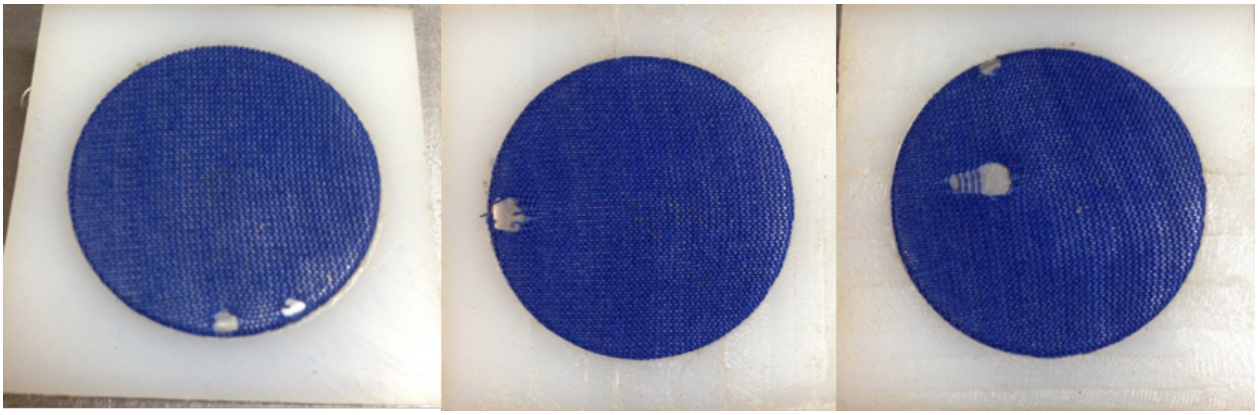

Figure 33: DBD treatment of fabrics at various gap distances (three separate samples of single-layered blue merino wool showing hole formation after 5 second exposure to a DBD reactor at 1.27 W/cm^2 and a gap distance of 7mm. Though not shown here, holes were also formed at gap distances of 5mm and 6mm.)

Cumulatively, these results suggest that atmospheric DBD treatment of fabric would have to occur with a gap distance of 1mm-2mm, one layer at a time, over sufficiently porous or stretched fabric, and for a duration of 2 minutes to achieve both uniform plasma penetration/treatment of the fabric and the prevention of random hole formation.

4.2.2 LPPR Plasma Penetration of Fabric

To measure the penetrative capability of low pressure plasmas, six 1” x 1” merino wool fabric samples were stacked and stapled together (Figure 34). This collection of fabric samples was then placed in the middle of the LPPR for 15 minutes at a power density of .016 W/cm^2. After the 15 minutes of low pressure plasma treatment, the collection of samples was removed from the LPPR, unstapled, and spread across a flat plate according to each fabric sample’s stacking order. As soon as this was completed, a 10 uL droplet of distilled water was then placed on each of the six fabric samples. Photographs were taken in order to measure the contact angle afterwards.

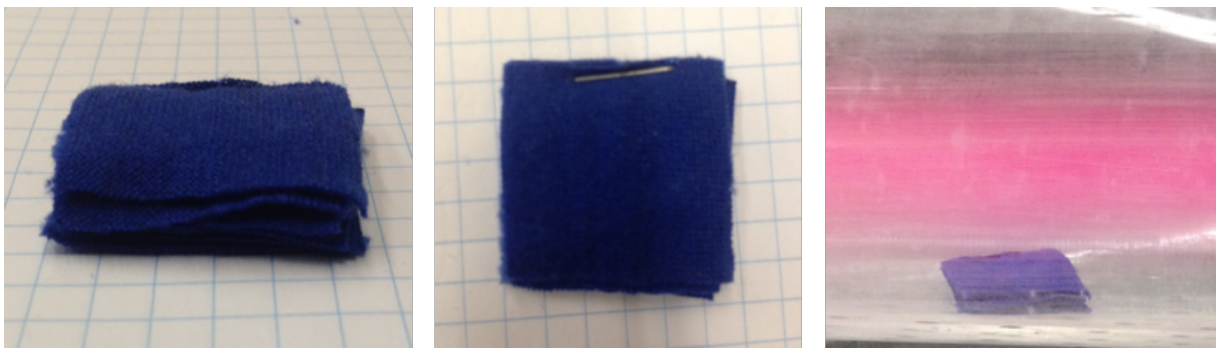

Figure 34: Stapled stack of 1" x 1" blue merino wool samples in LPPR

At sufficiently long plasma exposure times, the charged species of the low pressure plasma can penetrate multiple layers of fabric. In our LPPR multi-layer penetration study, the charged species of the LPPR penetrated up to six layers of merino wool fabric (approximately 6 mm of total thickness) in 15 minutes at a power density of .016 W/cm^2.

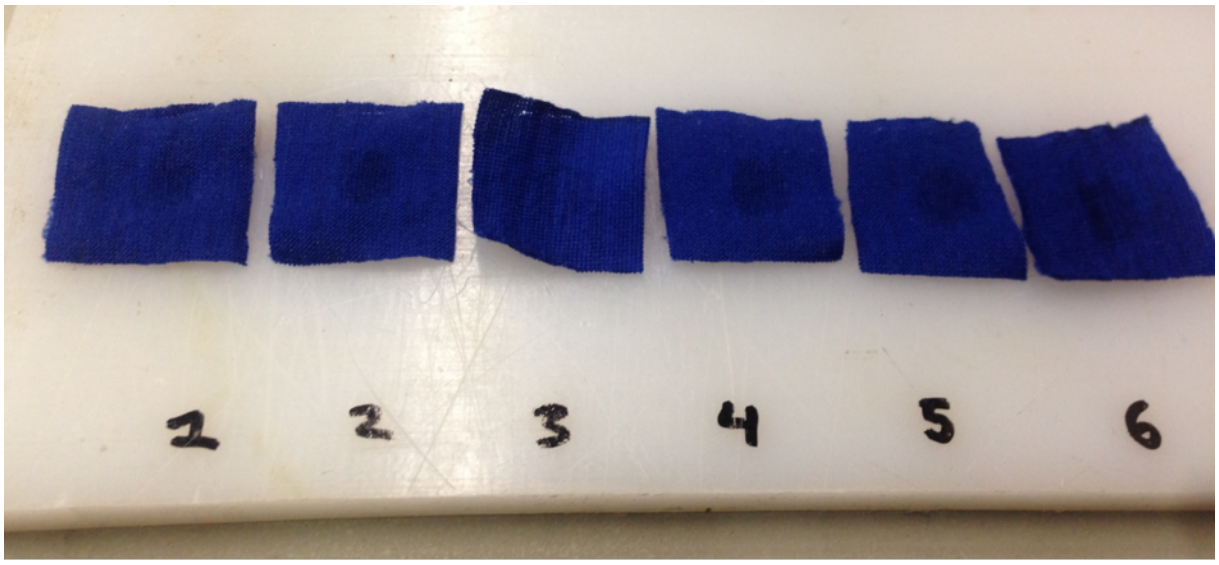

All six samples showed complete wettability
(1 = topmost layer; 6 = bottommost layer)

Figure 35: Results of LPPR penetration test. Note the water droplet absorption in each of the square tiles of blue merino wool.

Figure 35 shows the results of this multi-layer penetration study. As can be seen from the six 1" x 1" fabric samples of merino wool, each sample had a contact angle of 0 degrees, indicating a complete wettability change.

The fact that each merino wool layer was completely wettable after 15 minutes of LPPR treatment indicates that 1) additional layers would have seen at least partial wettability changes and/or 2) shorter times (i.e. 8-10 minutes) may have yielded complete changes in wettability. This agrees with scientific literature on plasma penetration [30, 31].

The goal of this study was not to determine the exact plasma exposure time required to effect complete wettability in all layers. The purpose of this study was to prove that with adequate exposure time in the LPPR, the low pressure plasma species can penetrate any depth in porous material such as merino wool. The importance of this result is that mechanical agitation of soiled clothing is not a strict requirement in the design of a LPPR-based laundry device. Lastly, it is worth pointing out at this stage that the LPPR is capable of plasma treating a multi-layered component (i.e. a shirt that is folded upon itself several times), while DBD reactors do not have this capability.

4.3. Plasma-Assisted Disinfection of Bacteria Inoculated Fabric

4.3.1 DBD Treatment without Fabric

A 100 uL of a 1.46 x 10^9 CFU/mL *E. coli* solution was prepared in TBS Broth, and added directly on top of the aluminum electrode. The gap between the DBD reactor and the aluminum electrode had to be increased to 3 mm in order to account for the contact angle of the *E. coli* broth droplets. After centering the aluminum electrode with the *E. coli* broth

droplets underneath the DBD reactor, the DBD reactor was operated at 1.27 W/cm^2 for a duration of 2 minutes.

After the DBD treatment, part of the solution appeared to have evaporated, while the contact angle of the remaining E. coli broth droplets had decreased and spread out over a large area of the aluminum electrode. This solution was pipetted into a micro-cuvette. The rest of the electrode was washed twice with a total volume of 200 uL of TBS. This volume was then added to the same micro-cuvette. In the end, the experimental sample consisted of a micro-cuvette of 300 uL of DBD treated or untreated E. coli culture.

For the control, a second 100 uL of E. coli broth solution was added to a different aluminum electrode. However, this culture of E. coli was not exposed to the DBD plasma. Instead, it was promptly pipetted into a second micro-cuvette, and washed twice with a total volume of 200 uL of TBS and added to the same control sample micro-cuvette.

A baclight study was performed on the the treated and control E.coli solutions in the micro-cuvettes. The baclight study—via red fluorescence—showed that the DBD treated E. coli solution had experienced extensive membrane damage during the DBD plasma treatment, while the control *E. coli* solution—via green fluorescence—showed intact membranes (Figure 25). These results show, as much of the scientific literature already has, that DBD treatment will kill an E. coli population through cell membrane damage.

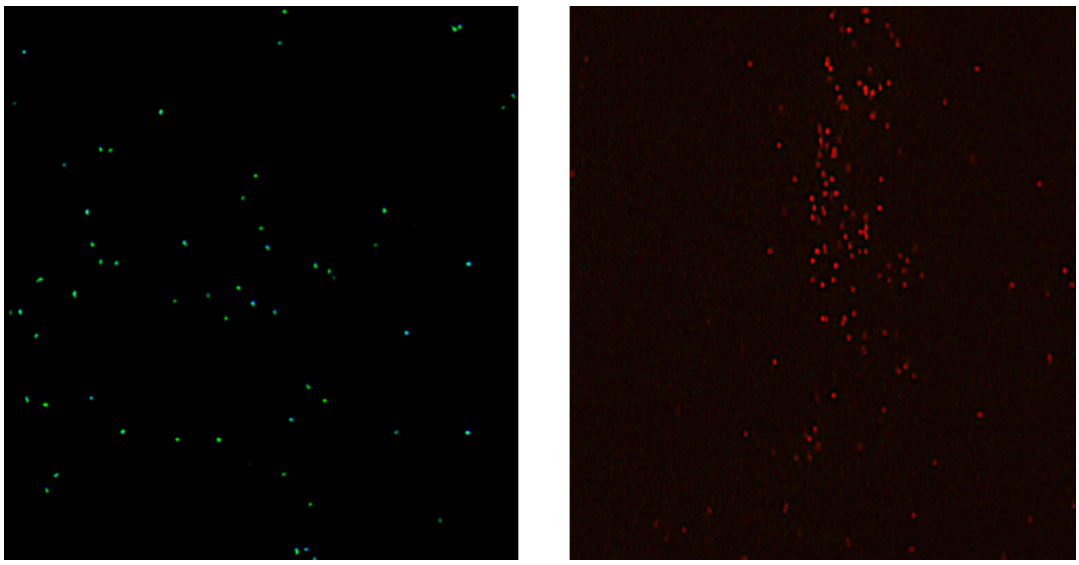

Figure 36: Baclight analysis of DBD treated and untreated E.coli samples (Left: Control E.coli culture (No DBD plasma treatment); Right: DBD treated E.coli culture at 1.27 W/cm2 with a gap distance of 3mm for 2 minutes)

4.3.2 DBD Treatment with Blue Merino Wool

An *E. coli*-inoculated merino wool sample was prepared by placing 100 uL of 1.46 x 10^9 CFU/mL *E. coli* broth solution at the center of a merino wool fabric circle and inserting it into a sterilized plastic bag. The naturally low wettability of the merino wool did not allow the E. coli solution to seep into the fabric. Therefore, absorption was forced by pressing the E. coli solution into the fabric. After 30-60 seconds, the E. coli solution was preferentially absorbed by the merino wool since the sterilized plastic bag was less wettable than the merino wool. Using the same procedure just mentioned, a second *E. coli* inoculated merino wool sample was prepared for the control.

Both inoculated merino wool samples were placed over aluminum electrodes and secured

in place with the nylon fabric holders. Only one of these samples was placed under the DBD reactor at a gap distance of 1mm, a power density of 1.27 W/cm^2, and a treatment time of 2 minutes. The other sample was held as the experimental control. The reason that the gap distance was returned to 1mm, is that there were no droplets to consider, and to remain consistent with the rest of DBD treatments that occurred at a gap distance of 1mm.

After DBD treatment, the inoculated merino wool samples were inserted into separate test tubes of 100 mL of TBS. The control and treated test tubes were vortexed for 1 minute. Next, 10 uL of each test tube were plated from each test tube into separate petri dishes. The plates were then incubated for 3 days and counted.

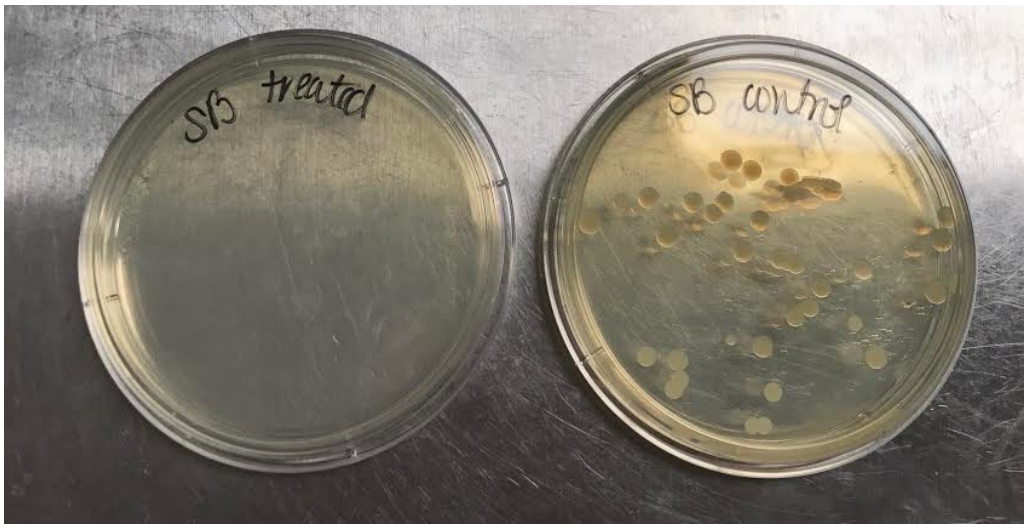

Figure 37: CFU count differences between plasma treated and untreated E.coli samples. After 3 days of incubation, there were strong differences in the CFU count across treated and untreated bacterial solutions (Left): DBD Plasma Treated E.coli Culture with zero CFU count, (Right): Control sample of E.coli Culture

As can be seen from Figure 37 the DBD treated inoculated merino wool did not show any growth after 3 days. The control clearly had growth and had a total CFU count of 73.

While the recoverability (5×10^{-5}) of the E. coli from the merino wool is abysmal, it was consistent with all trials. Furthermore, the test tube containing the treated E. coli-inoculated merino wool fabric was left in a warm water bath for further evidence: after 3 days, this test tube had visible bacterial growth, albeit less than the growth seen in the control test tube left in the same water bath for the same amount of days.

The DBD treatment of E. coli-inoculated fabric proves a few things. First, DBD treatment is also effective at treating inoculated textiles. However, it appears that DBD treatment is most effective at treating uniform media, and slightly less effective at treating non-uniform media like fibrous textiles. Second, the fibers of the fabric may be providing a certain degree of protection for the bacteria against the reactive oxygen and reactive nitrogen species of the DBD plasma treatment. This may partly explain the bacterial growth in the test tube containing the E. coli-inoculated merino wool. Another reason for this growth is that some of the E. coli-wetted merino wool was safeguarded by the nylon fabric holder during plasma treatment. Third, plasma treatment alone is not capable of physically removing bacteria from the fabric. This was proven by the poor recovery fraction (5×10^{-5}) after 1 minute of vortexing the test tube.

A few months later, a second study of the disinfection potential of DBD treatments with blue merino wool was performed. This time, instead of a power density of 1.27 W/cm^2, a

DBD power density of 0.85 W/cm^2 was chosen. All other parameters and experimental procedures were kept the same as the first DBD disinfection study. The DBD disinfection studies with blue merino wool were repeated to ensure that a softer plasma treatment (i.e. one that would impart less damage to the merino wool fibers) would still provide some degree of disinfection. The results of this study were exciting and can be found in the Table 3 below. It was found that a 10-min 0.85 W/cm^2 DBD treatment provided a net 2.7 CFU log reduction. This means that excluding the loss of bacteria that occurs during the vortex-aided extraction process, the 10-min 0.85 W/cm^2 DBD treatment destroyed 99.8% of the *E. coli* bacteria.

4.3.3 LPPR Treatment with Blue Merino Wool

To assess the relative disinfection capabilities of different plasma treatments, a disinfection test with the LPPR was administered using the same starting E. coli concentration (1.46 x 10^9 CFU/mL) as the previous DBD disinfection studies mentioned earlier in this report.

After having prepared a new E. coli batch with a concentration of 1.46 x 10^9 CFU/mL, the blue merino wool was inoculated following the same procedures used to prepare E. coli inoculated blue merino wool samples for the DBD disinfection studies. Once the blue merino wool absorbed the 100 uL droplet of E. coli stock solution, the blue merino wool sample was placed over aluminum electrodes, and held down with the nylon fabric

holders. This last step was performed solely to better compare the disinfection results from the DBD and LPPR plasma treatments.

Using forceps to grab the corner of the nylon fabric holder, the sample was carefully inserted into the center of the LPPR. The center of the LPPR was chosen due to plasma symmetry about the center. The plasma is symmetric about the center of the LPPR because the power supply continually alternates the direction of the electric field, making both sides of the LPPR approximately equal in terms of plasma species concentrations.

Once the sample was properly positioned at the center of the LPPR, the LPPR was sealed shut, and the vacuum pump was turned on until the chamber pressure reached -96 kPa (40 Torr). This is the maximum vacuum that the vacuum pump could achieve. After seeing a steady -96 kPa readout from the analog pressure gauge, the power supply was turned on to generate the low pressure plasma at a power density of 0.016 W/cm^2. This power density is calculated by dividing total power (measured by an oscilloscope) by total surface area of the inside of the LPPR.

Each sample was left inside the LPPR for a specific amount of time at constant power density. After the treatment was done, the power supply was turned off, then the vacuum pump, and finally, the pressure relief valve was opened to increase the LPPR chamber pressure to ambient conditions. After following these steps in sequence, the cover of the LPPR is carefully removed, and a pair of forceps used to carefully retrieve the sample.

The LPPR treated, inoculated blue merino wool is then placed in 10 mL of TBS and vortexed for 1 min. Afterwards, 10 uL of the vortexed solution is serial plated and serial diluted across 5 petri dishes and incubated for a CFU count the next day. The results are shown in Table 3.

As Table 3 shows, all LPPR treatments of *E. coli*-inoculated merino wool showed a reduction of CFU. However, unlike the linear trend that was observed between increased DBD exposure time and increased CFU reduction, the LPPR treatments showed no clear trend between plasma exposure time and CFU reduction. Furthermore, the longest LPPR treatment of inoculated merino wool had one of the lowest CFU reductions of all the LPPR treatments.

The vacuum only control was calculated to have an effective .80 CFU log reduction. If it is assumed that the CFU reduction due to vacuum was fairly constant across all treatments, then by subtracting .80 from the rest of the values in the “Treatment Log Reduction” column, it is readily seen that the low pressure plasma was moderately effective on the 1 min and 4 min LPPR treatments. The moderate effectiveness of the plasma in the 1 min and 4 min samples, as well as the absence of a positive trend between treatment time and CFU reduction hints at the possibility that experiment’s treatment times were too low. Nevertheless, the range of CFU log reduction after the LPPR treatment was 0.06 to 1.03.

Table 3: CFU Log Reduction of E. Coli
(Note: Infinite means too many CFUs to count; Treatment Log Reduction = Total Log Reduction – 1.51 (Log Reduction due to Extraction))

			Plate Counts						
	Sample	Parameters	1E-03	1E-04	1E-05	1E-06	Log (CFU/mL)	Total Log Reduction	Treatment Log Reduction
DBD Reactor	A	30 sec @ 0.85 W/cm2	Infinite	91	5	0	6.83	1.39	-0.12
	B	45 sec @ 0.85 W/cm2	Infinite	136	2	1	6.81	1.41	-0.10
	C	10 min @ 0.85 W/cm2	1	0	0	0	4.00	4.22	2.71
	D	30 sec @ 0.43 W/cm2	-	85	11	1	6.99	1.23	-0.28
	E	45 sec @ 0.43 W/cm2	-	180	2	0	6.78	1.44	-0.06
	F	10 min @ 0.43 W/cm2	-	14	1	0	6.07	2.15	0.64
Mini-LPPR	G	10 min @ 0.04 W/cm2	210	16	0	1	6.51	1.71	0.20
	H	1 min @ 0.04 W/cm2	Infinite	8	0	0	5.90	2.32	0.81
	I	2 min @ 0.04 W/cm2	391	35	3	1	6.65	1.57	0.06
	J	3 min @ 0.04 W/cm2	336	23	1	0	6.30	1.93	0.42
	K	4 min @ 0.04 W/cm2	48	0	0	-	5.68	2.54	1.03
	L	5 min @ 0.04 W/cm2	377	8	1	0	6.16	2.06	0.55
Control	No. E. coli	No Bacteria Added	0	0	-	-	0.00	-	-
	Vacuum Only	E. coli exposed to 5 min vacuum only	110	5	1	0	5.91	2.31	0.80
	Extract Only	E. Coli added (no plasma or vacuum) and extracted	Infinite	23	6	1	6.71	1.51	0.00
Initial E. Coli Concentration			-	-	Infinite	254	8.22		

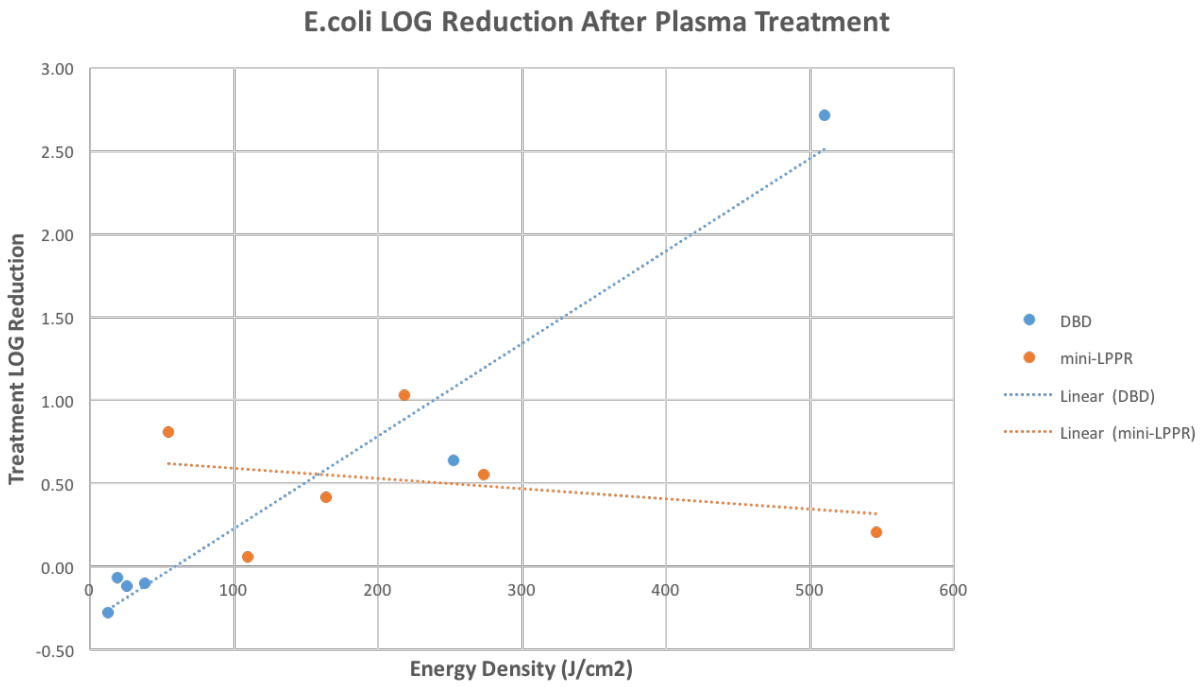

Figure 38: Comparison of the disinfection capabilities of the DBD reactor vs LPPR reactor. The DBD reactor displays a linear trend between exposure time and CFU log reduction. LPPR reactor does not show a linear trend. This is perhaps because the LPPR treatment times were on the low side.

A comparison of the disinfection potentials of both the DBD and LPPR are shown in Figure 38 below. Future work in the disinfection potential of low pressure plasmas should aim to have a 10-60 min LPPR treatment time range. It is likely that the CFU log reduction would begin to display proportionality with treatment time.

4.4. Plasma's Effect on Fabric's Tensile Strength

The mechanical properties of fabrics can be tested through several methods. The chosen and preferred method for this project was the ASTM D5035 Tensile Cut Strip method.

Other testing methods require either larger sample sizes, more complex geometric modifications to the fabric samples, or more sophisticated testing equipment. The cut strip method (ASTM D5035) requires only a 1” x 6” strip of the fabric and a standard tensile testing machine. Convenience aside, this method was also chosen because the 1” x 6” strip of fabric could easily be treated with the DBD reactor.

It was observed that cutting the fabric strip with scissors mechanically stressed the fabric along the edges, which caused a curling effect of the strip of fabric. Concerned that these stresses would affect the quality of our data, an alternative cutting method was desired. The use of a rotary cutter was found to significantly reduce or eliminate the amount of curling observed after cutting the 1” x 6” fabric strip (Figure 39).

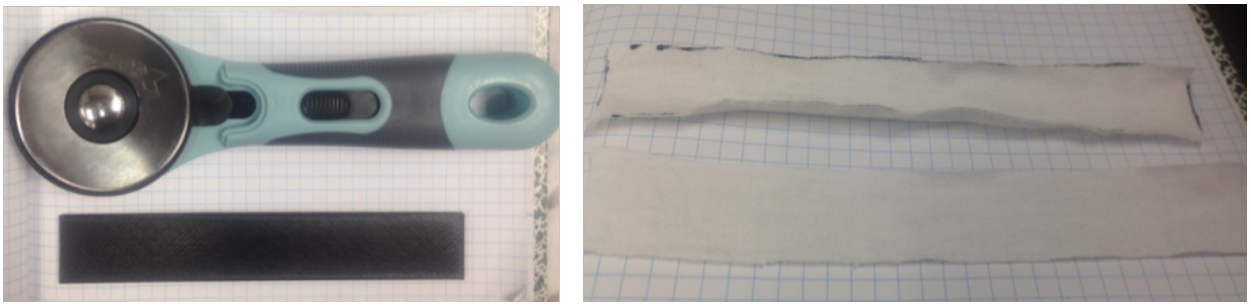

Figure 39: Effect of cutting mechanism on fabric sample quality. (Left) Rotary Cutter and 1" x 6' ABS Template used to make cut strips; (Right) Difference in curling by using either scissors (top) or a rotary cutter (bottom)

The ASTM D5035 method requires that the jaws be 1.00” high and at least .50” wider than the fabric sample. In order to adhere to the specifications of the ASTM D5035 method, 1.50” wide x 1.00” high ABS jaws were 3D printed (see Figure 40). However, the clamping surface of the jaws was intentionally kept completely flat. This was done to

reduce localized stresses in the fabric along the jaw edge, thereby reducing the likelihood of the fabric breaking at the jaw (aka jaw break).

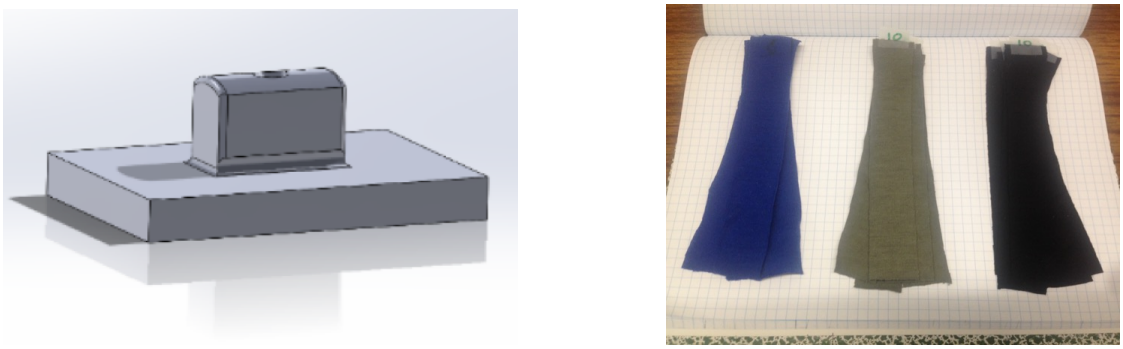

Figure 40: Materials and samples for tensile test (Left: 3D printed ABS jaw with flat contacting surface; Right: Example of 1" x 6" fabric strips that were used for treatment and tensile testing.)

For the tensile test study of this project, fabrics were treated with DBD plasmas, low pressure plasmas, and E-beam. The DBD plasma treatment was administered at a power density of 1.27 W/cm^2 for 2 minutes at a gap distance of 1mm. The LPPR was operated at power density of 0.91 W/cm^2 for 5 minutes. Only one fabric sample was loaded inside the LPPR at a time. Prior to generating the plasma inside the LPPR, the vacuum was turned on for a duration of 30 seconds. This was done for consistency and to check the vacuum pressure before initiating the experiment. The E-beam treatment was carried out at a dose of 10 kGy via the conveyor belt system outlined in experimental procedures. For elastic modulus vs treatment type box plots for all treated fabrics, please refer to the appendix. Elongation vs treatment type box plots that are not provided in the results section can also be found in the appendix.

4.4.1 Blue Merino Wool

DBD treatment of the 1” x 6” strip of blue merino wool produced too many holes for valuable tensile test results due to the fabric strips not being porous or stretched enough. However, low pressure plasma treatment of blue merino wool seems to have strengthened the blue merino wool (Figure 41). The average maximum load of blue merino increased by approximately 20% after the LPPR treatment. This is more clearly seen in the box plot shown below (Figure 42). E-beam treatment of blue merino wool had negligible effects on the max load rating of the blue merino wool. The LPPR and E-beam treatments had a minimum effect on the ductility of blue merino wool. For blue merino wool, the severity of the treatment is electron beam, LPPR, and DBD (in increasing order).

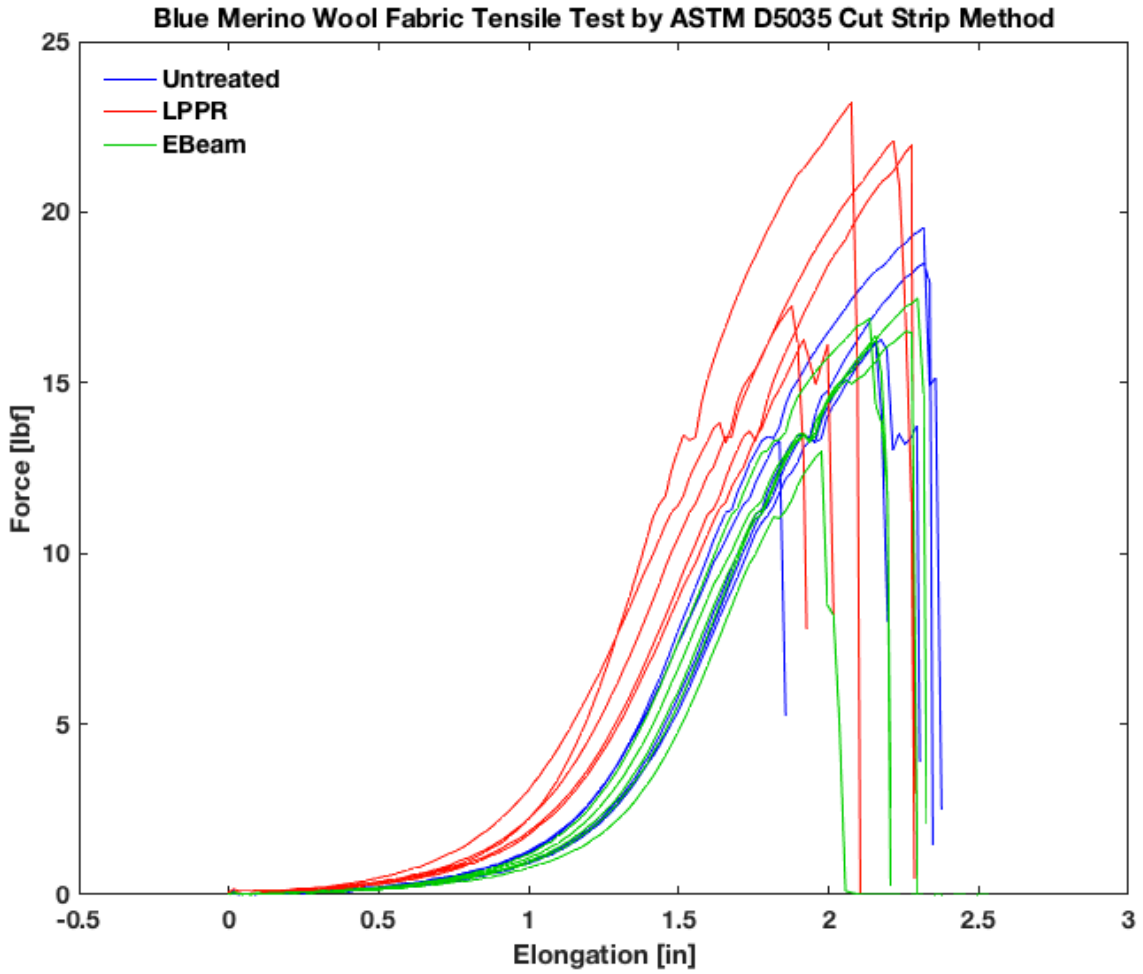

Figure 41: Force vs Elongation plot of LPPR and E-Beam Treated Blue Merino Wool. More than 50% of the LPPR treated blue merino wool had maximum loads greater than the maximum load seen in untreated blue merino wool. E-beam treated blue merino wool had negligible changes.

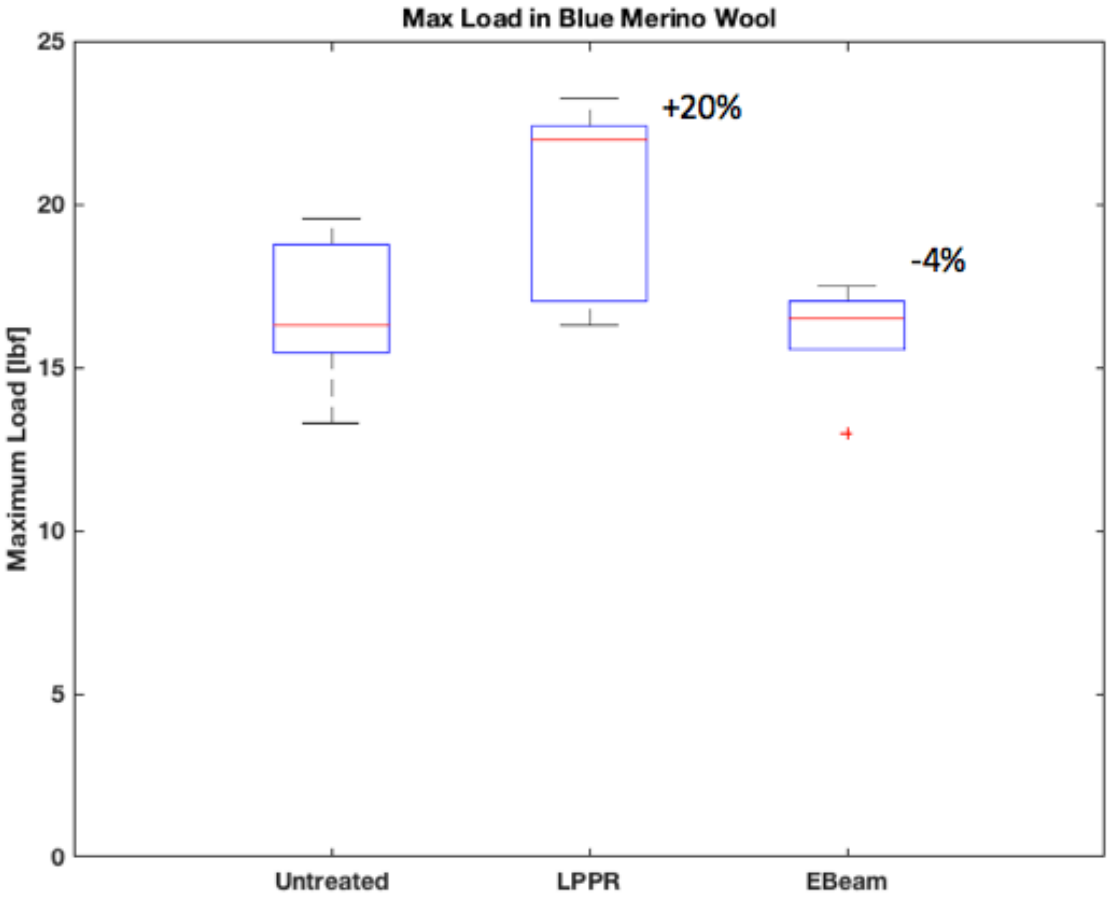

Figure 42: Box plot of maximum observed loads during each tensile test of treated blue merino wool. LPPR treatment increased the average maximum load of blue merino wool by 20%. E-beam had negligible changes in the strength of the blue merino wool.

4.4.2 Black Merino Wool

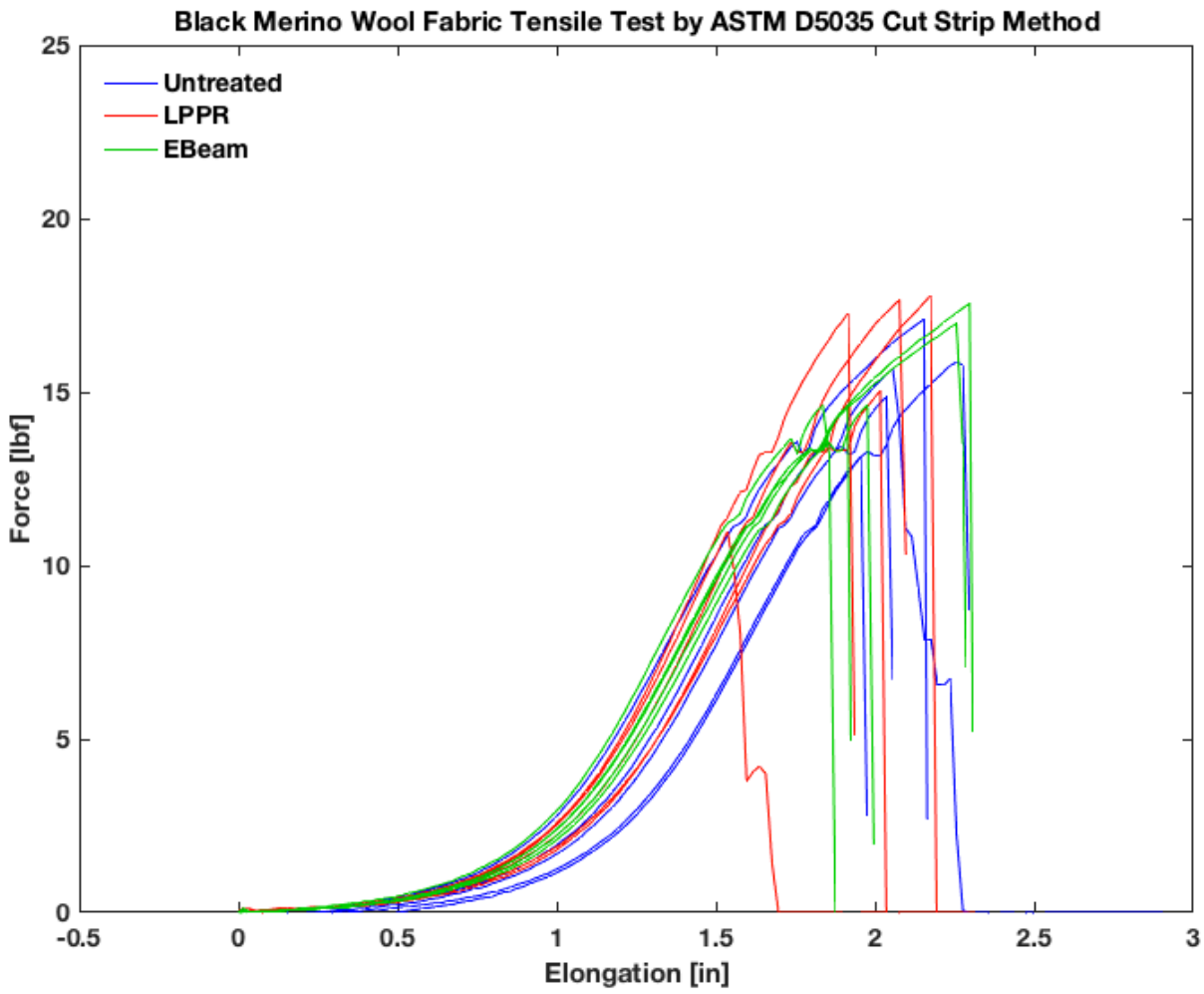

Figure 43: Tensile Test of Treated Black Merino Wool (Note: Red trace that significantly deviates from the rest of the Force vs Elongation traces was due to a textile fabrication/processing error). LPPR and E-Beam treatments caused negligible changes in the strength and ductility of black merino wool.

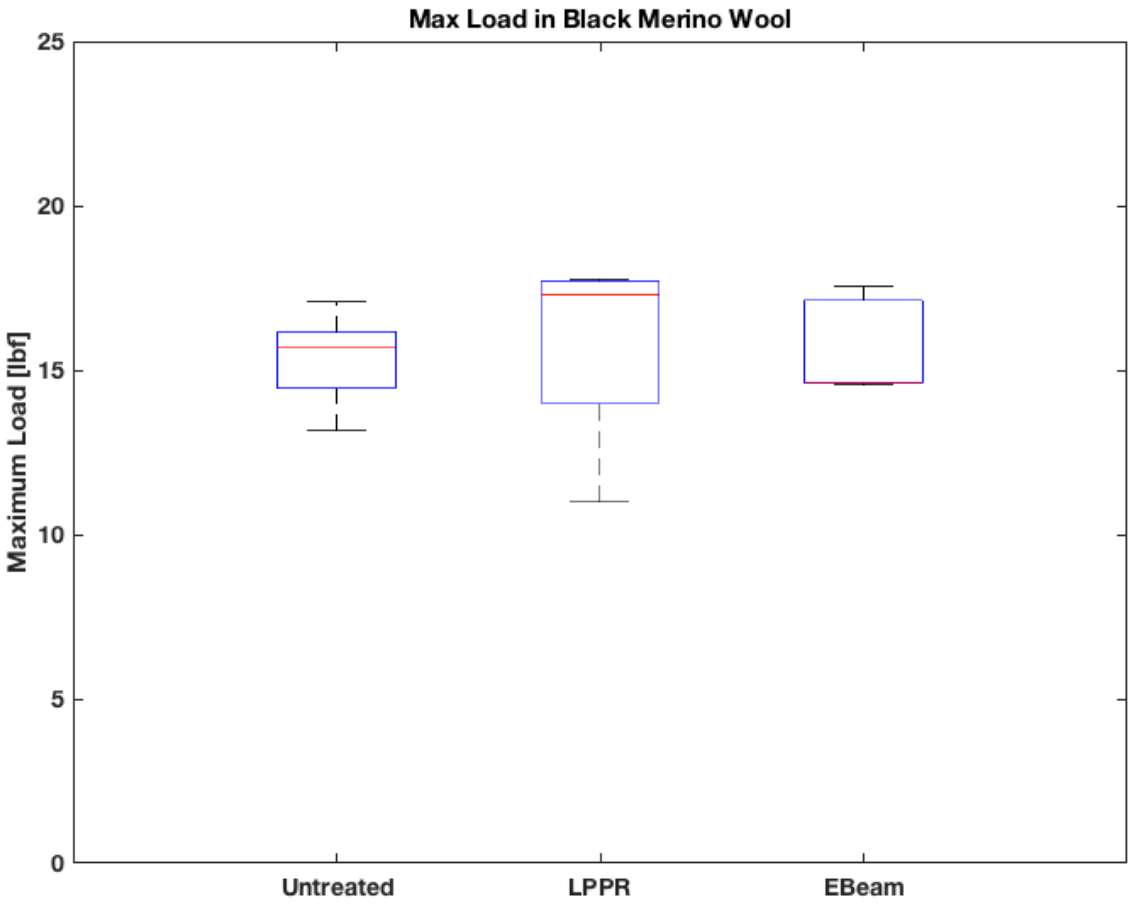

Figure 44: Boxplot for maximum load observed during each tensile test of treated black merino wool. Overall range of values across all categories are very similar, indicating that 0.016 W/cm^2 LPPR and 10 kGy E-Beam treatments had negligible effects on the mechanical properties of black merino wool.

DBD treatment of 1” x 6” black merino wool fabric strips also produced too many holes for significant tensile testing to take place. Low pressure plasma treatment of black merino wool did not have as strong of an effect than it did with blue merino wool. In general, LPPR and electron beam treatment had a negligible effect on the mechanical properties of black merino wool. This is clearly seen in Figure 43 and Figure 44. LPPR and E-beam treatment are both recommended for black merino wool treatment.

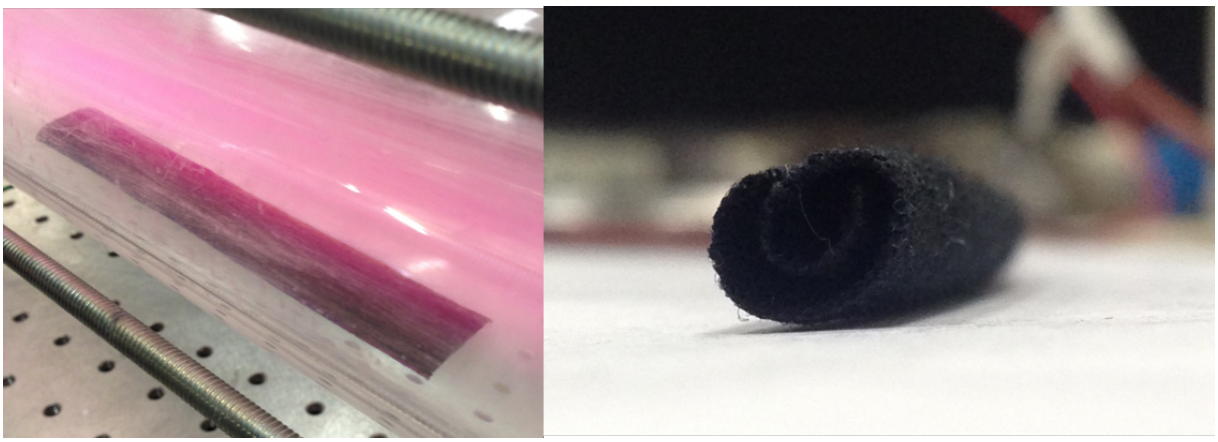

Figure 45: Curling behavior of black merino wool during LPPR treatment. The left image shows the initial state of the black merino. After 5 minutes of a 0.016 W/cm2 LPPR treatment, the 1" x 6" fabric strip curled into a cinnamon stick form.

An interesting phenomenon occurred while the black merino wool underwent LPPR treatment. After 5 minutes of LPPR treatment at 0.016 W/cm^2 power density, the black merino wool strip rolled up into a cinnamon-stick-like configuration (Figure 45). Black merino wool was the only fabric that displayed this behavior. To be clear, blue merino wool did *not* show this curling behavior either. It is possible that this curling was due to a combination of chemical interactions between the black dye and the low pressure plasma species and the differential surface exposure to plasma species.

4.4.3 Green Modacrylic

DBD treatment of 1” x 6” modacrylic fabric strips also produced too many holes in the fabric for a tensile test to be performed. Interestingly, LPPR treatment significantly decreased the strength of the modacrylic cut strip. The average maximum load of the modacrylic dropped approximately 23% after a 5 min 0.016 W/cm^2 LPPR treatment. This

can be seen in Figure 46 and Figure 47 below. Once again, electron beam treatment produced the least amount of change in the mechanical properties of the fabric. It is interesting to observe that of all fabric samples, modacrylic had the least amount of variability. In the force vs. elongation chart, this is seen by the tight grouping within different treatments. In the box plot, this is seen by the small IQRs and overall ranges.

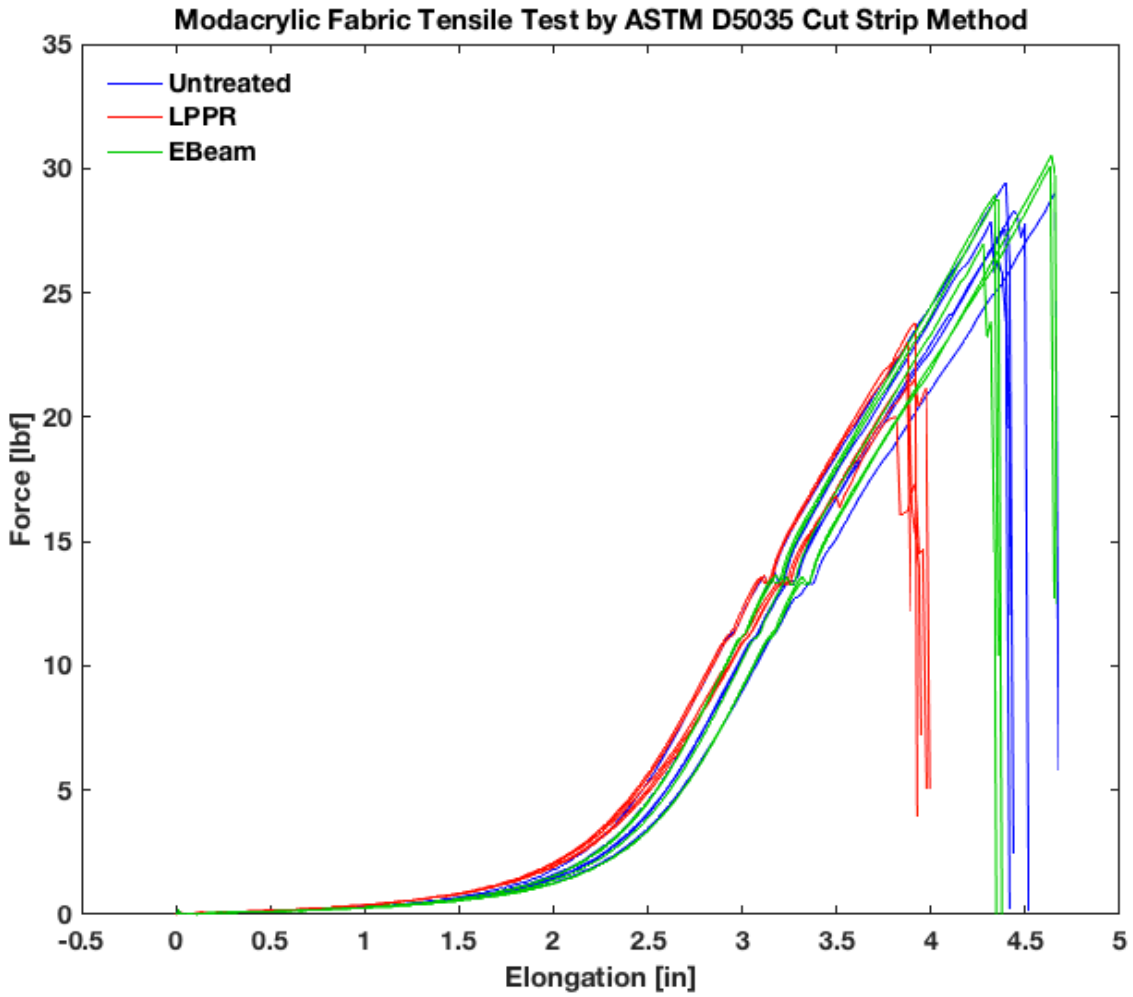

Figure 46: Tensile test of treated green modacrylic. A 0.016 W/cm2 LPPR treatment significantly reduced the tensile strength of the fabric. While this plot shows E-Beam treated modacrylic as slightly stronger, there are many other E-beam treated samples behind the graphs of the untreated green modacrylic, which ultimately averages out the maximum load of the E-beam treated samples.

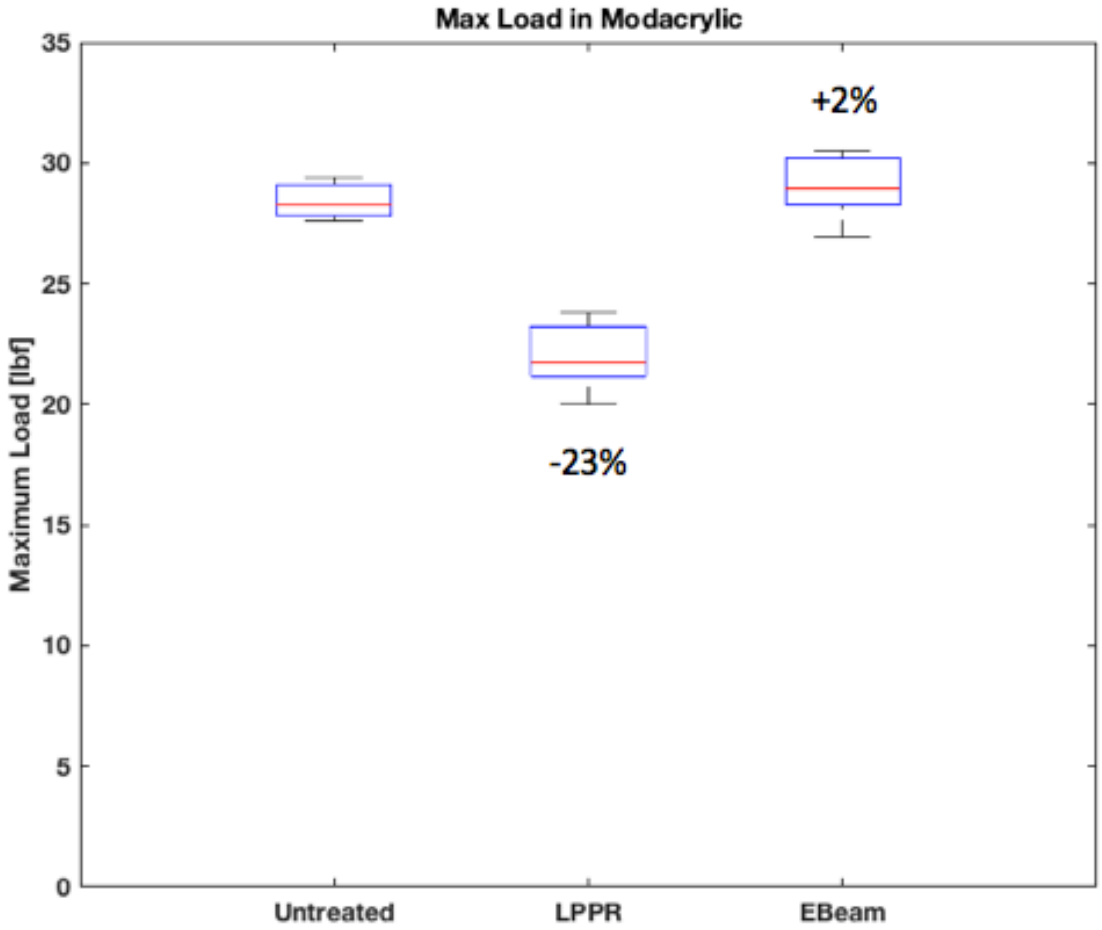

Figure 47: Boxplot for maximum load observed during each tensile test of treated green modacrylic. The 0.016 W/cm2 LPPR treatment reduced the average strength of green modacrylic by 23%. None of the maximum loads of the tested LPPR-treated samples overlapped with the untreated modacrylic maximum loads. E-beam treatment had negligible effects on the strength of the green modacrylic.

4.4.4 White Cotton

DBD treatment of 1” x 6” cotton strips did not produce as many holes in the fabric, as was the case for blue merino wool, black merino wool, and modacrylic. This allowed us to tensile test the cotton strips. Interestingly, the fabric strip breaks did not coincide with the location of the visible holes (Figure 48).

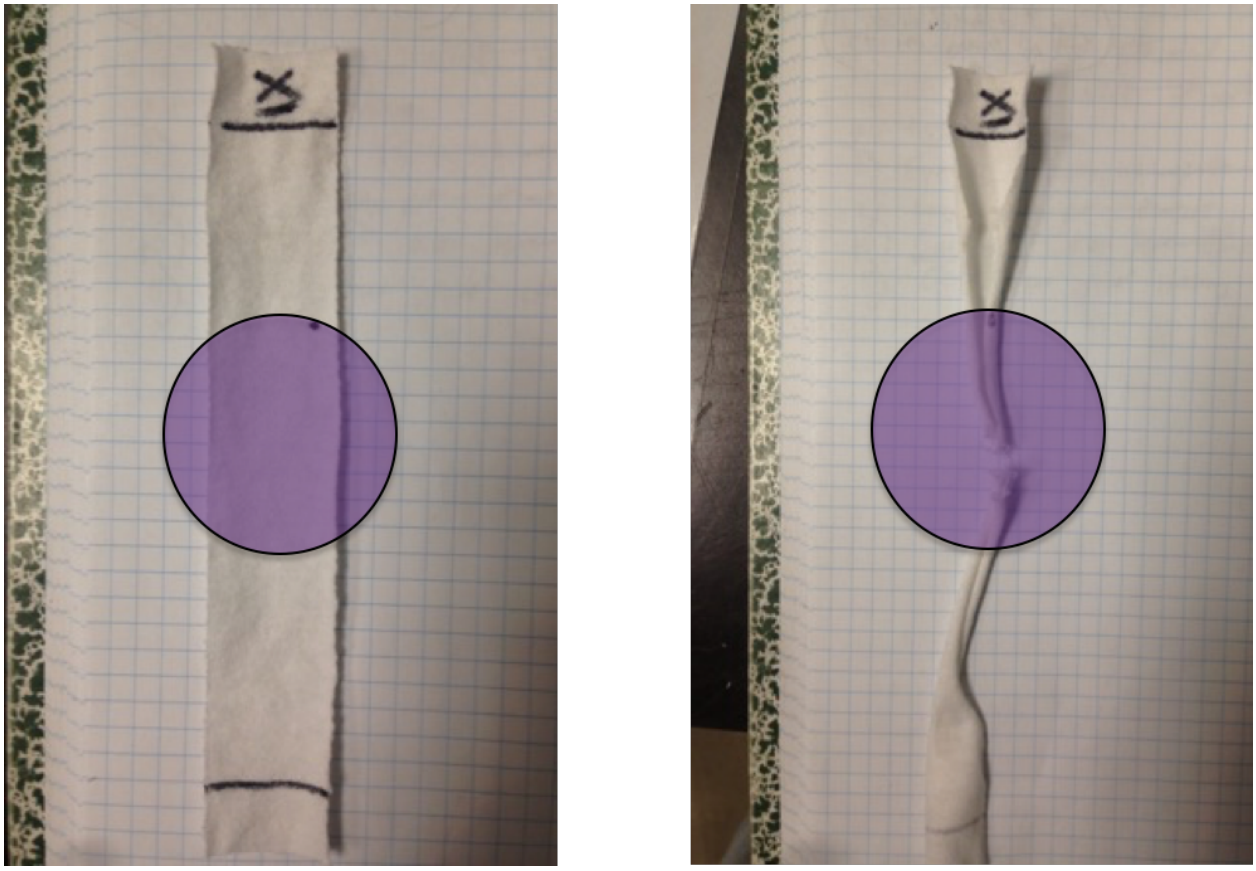

Figure 48: Example of DBD treated cotton strip before and after tensile test. Black dot in the left image represents the only hole formed after a 2-min, 1.27 W/cm2 DBD treatment at a distance of 1mm from the fabric. Purple circle represents DBD filament coverage during treatment. The right image shows that the hole occurred at the edge of the DBD coverage. The right image also shows that the cotton strip failed near the center of the DBD treatment, and not the hole.

This suggests that even though the hole reduced the cross-sectional area of the fabric, there are locations above or below the hole that were weakened much more significantly because of the DBD generated plasma species than a simple area reduction. This conclusion is further supported by a side experiment which showed that with untreated cotton, the fabric breaks at the location of the pre-made 0.080" diameter holes (Figure 49).

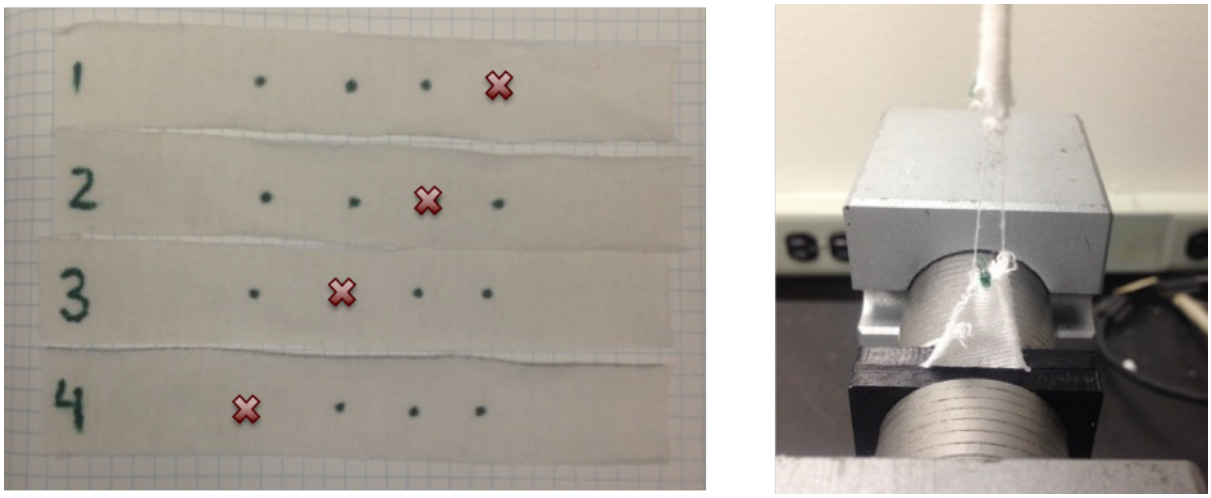

Figure 49: Side experiment to examine the correlation between hole placement (marked by the maroon x) and fabric failure point. With the exception of one jaw break (sample 4), all samples broke where the holes were located (right). Since sample 4 and sample 1 are symmetric, one can safely assume that without a jaw break, sample 4 would have failed at the hole location.

DBD treatment caused an average 40% drop in the max load at break (Figure 51), and a significant reduction in the elongation at break of the cotton strips (see box plot in Figure 52). LPPR and E-beam treatment of 1" x 6" cotton strips did not affect the mechanical properties of the fabric as much as the DBD treatment did. However, both LPPR and E-

beam treatments did cause a loss in the ductility of the of the cotton fabric, while not discernibly changing the max load rating of the cotton fabric.

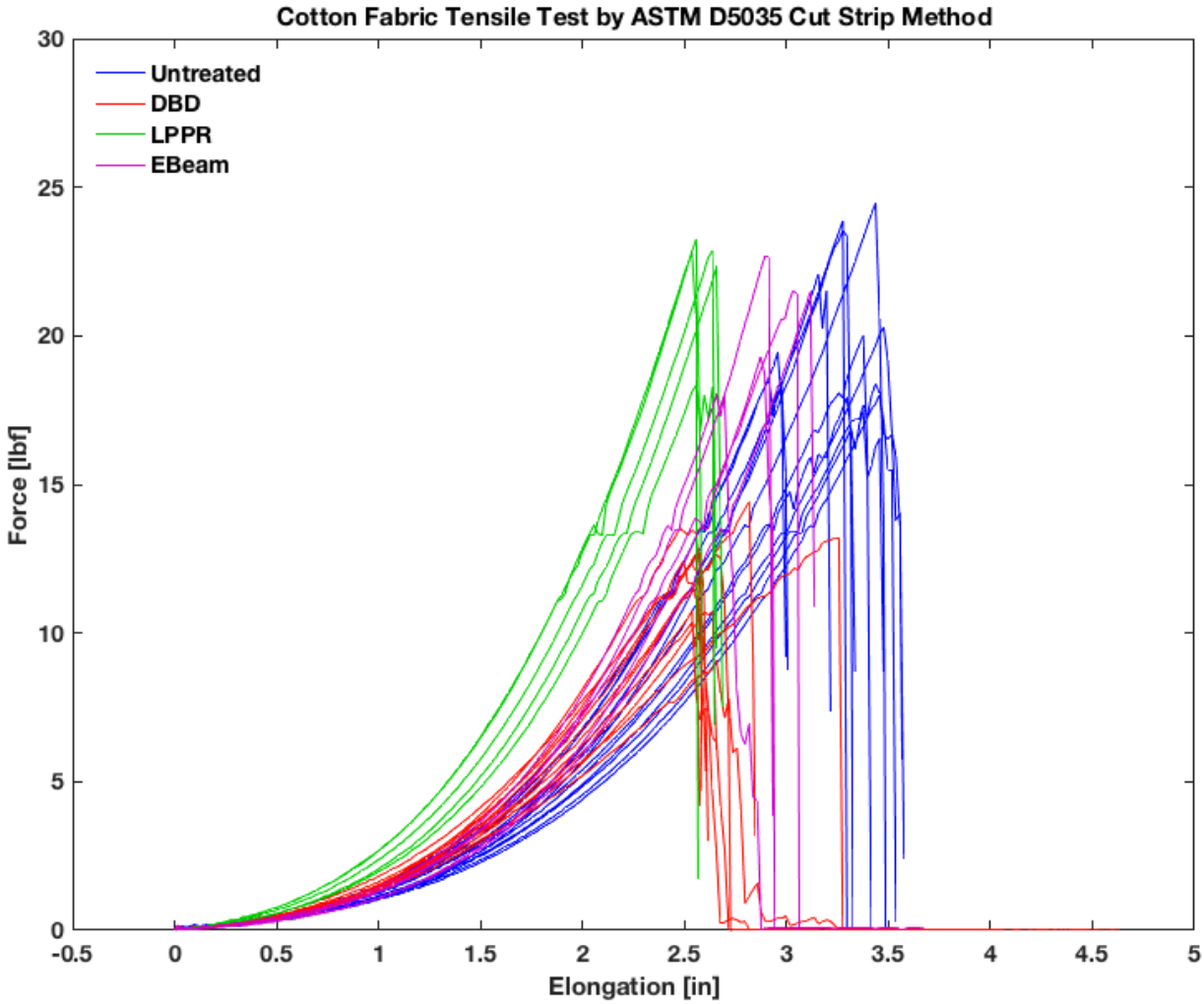

Figure 50: Force (lbf.) vs elongation (in.) plot for tension tested cotton samples after separate DBD, LPPR, and E-Beam treatments. With the exception of the DBD treatment (red), all remaining treatments did not significantly alter the maximum tensile loads seen. However, all treated samples (shown in green, red, and magenta) are to the left of the control (shown in blue). This indicates a loss in ductility.

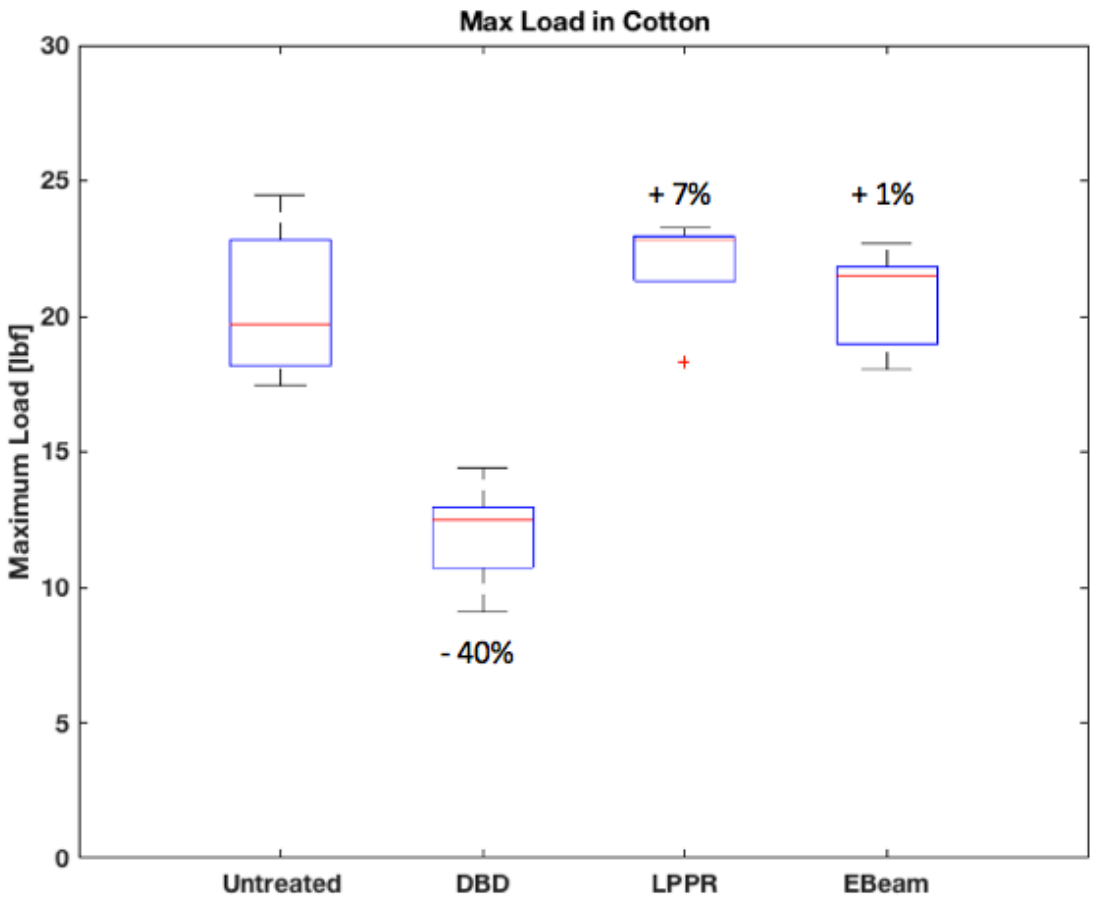

Figure 51: Box plot for maximum load observed during each tensile test of treated white cotton fabric strips. A 2-min 1.27 W/cm^2 DBD treatment caused an average 40% decline in the tensile strength of the white cotton. 5-min 0.016 W/cm^2 LPPR treatment and a 10 kGy E-beam treatment did not significantly affect the tensile strength of white cotton.

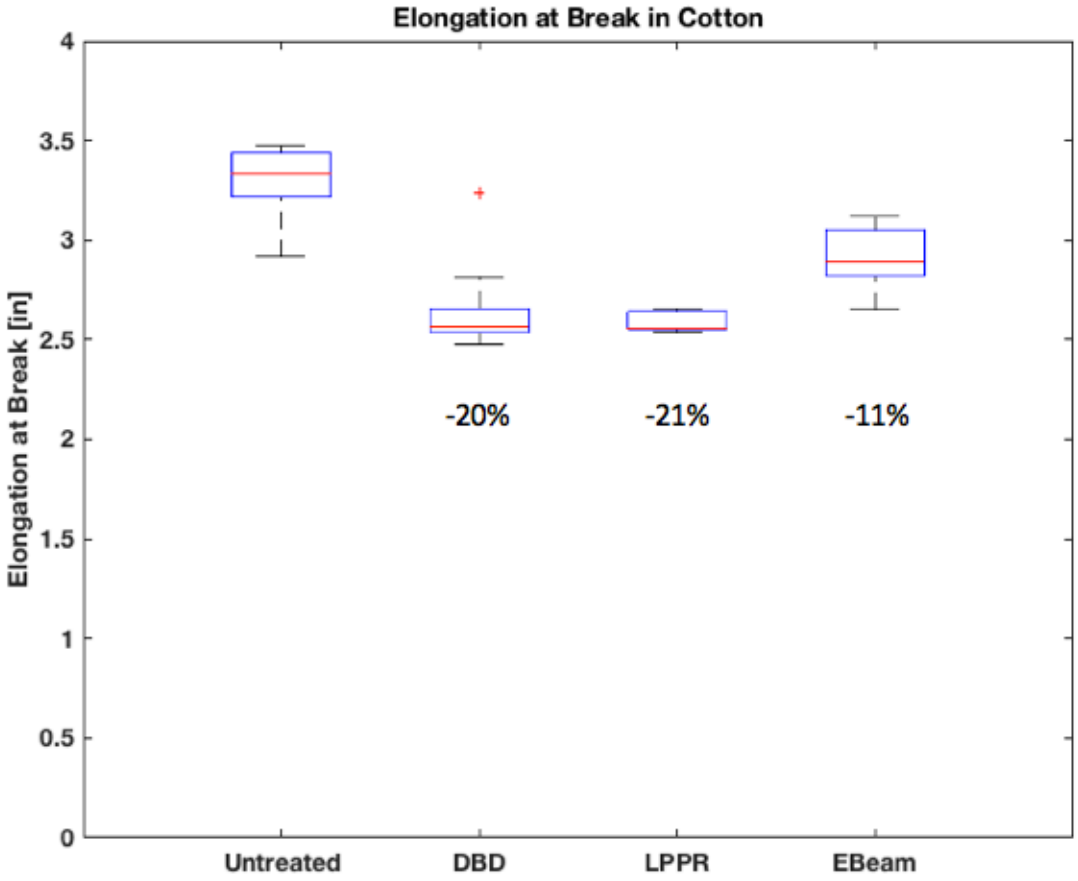

Figure 52: Box plot for maximum elongation in treated cotton fabric strips. All treatments significantly reduced the ductility of white cotton. This was interesting given that the LPPR and E-beam treatments did not significantly affect the elongation of

4.5 Plasma-Induced Morphological Changes in Various Fabrics

4.5.1 Two Minute DBD Treatment at 1.27 W/cm^2

DBD treatment of blue merino wool at 1.27 W/cm^2 at a gap distance of 1 mm for 2 minutes will produce minor changes in the visual appearance of the blue merino wool fabric (Figure 53). These changes can hardly be seen without the aid of an optical microscope.

The visual changes consist of discoloration (blue to orange), minor fading (bright blue to dark blue), and the formation of a viscous, glue-like substance. This effect seems to be specific to the blue dye of the blue merino wool. Black merino wool that is treated under similar conditions does not undergo any visual changes.

It is important to stress that while the worst-case images are shown here, a 2-min DBD treatment at a power density of 1.27 W/cm^2 causes minimal changes to the fabric as a whole. The majority of the surface area of the 2-min treated blue merino wool sample looks indistinguishable from the untreated version. This is a common theme throughout all the DBD treatments.

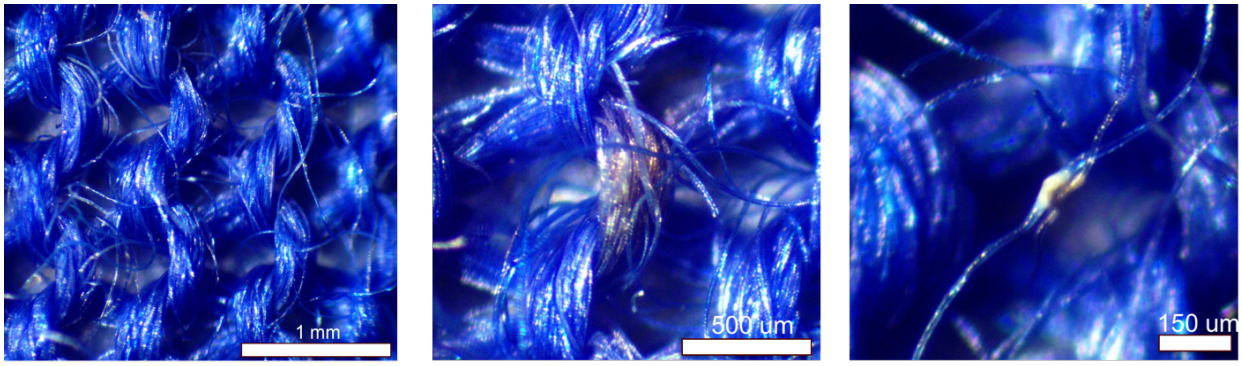

Figure 53: Optical micrographs of DBD treated blue merino wool. (Left: Untreated blue merino wool fabric; Center: 2-min 1.27 W/cm^2 DBD Treatment; Right: Same fabric sample as [center], but different location. These were the worst-case images. The rest of the merino wool sample looked identical as the untreated blue merino wool. This is confirmed by the condition of the merino wool fibers seen in the background.))

In Figure 54, you can see the untreated structure of a blue merino wool fiber sample used extensively throughout this research report. It shows the characteristic scaly nature of a

merino wool fiber. It is interesting that the SEM images prove that the merino wool fibers selected for the merino wool shirt are of fine quality.

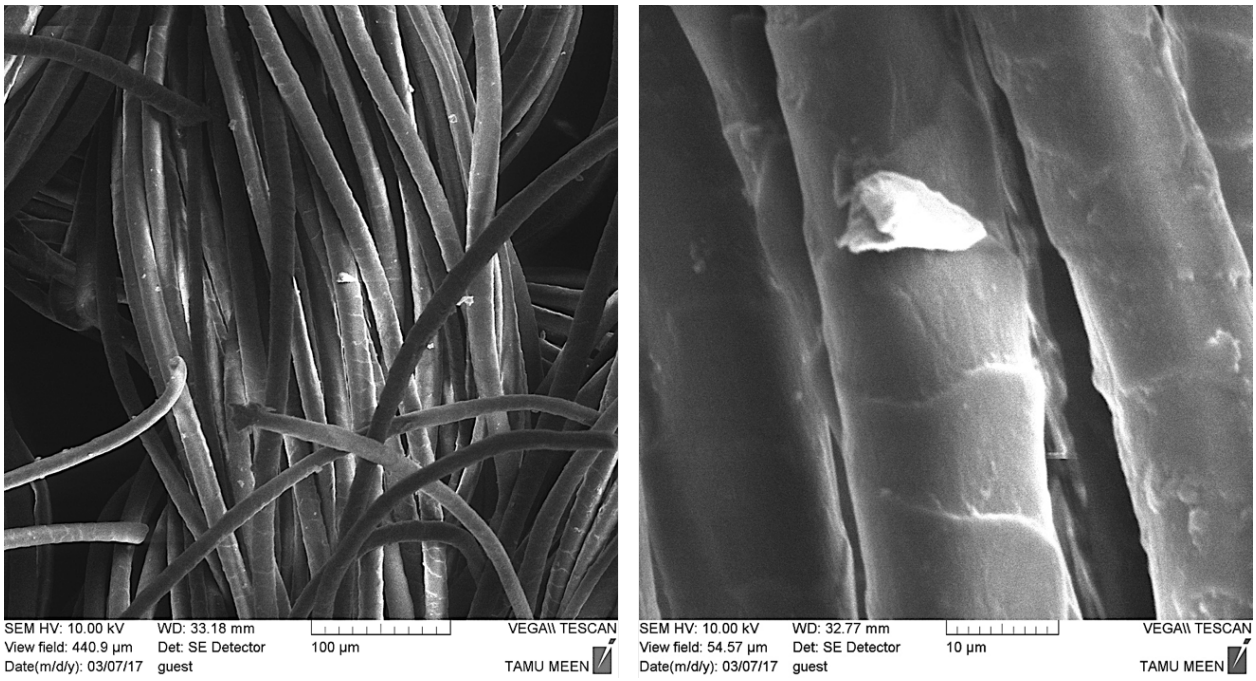

Figure 54: SEM images of untreated blue merino wool sample. All blue merino wool samples were sourced from the same shirt. Left: Fiber bundle shows the cuticle across several fibers. Right: An image of higher magnification displaying the scaly epidermis of the merino wool fiber. According to the literature and information provided in the background of this report, these merino wool fibers are of fine quality since only 1-2 scales are needed to cover the circumference of the fiber.

In Figure 55, the SEM images blue merino wool after a 2-min DBD treatment at a power density of 1.27 W/cm^2 are shown. These images provide evidence that DBD exposure time has a surface-level effect on the fibers. The worst-case fiber of a 2-min treated sample shows the disappearance of the cuticle and the appearance of a wax-spotted fiber. However, much of the 2-min treated blue merino wool sample was unaffected. This

is broadly seen by the presence of the cuticle in the background of the SEM image of Figure 55.

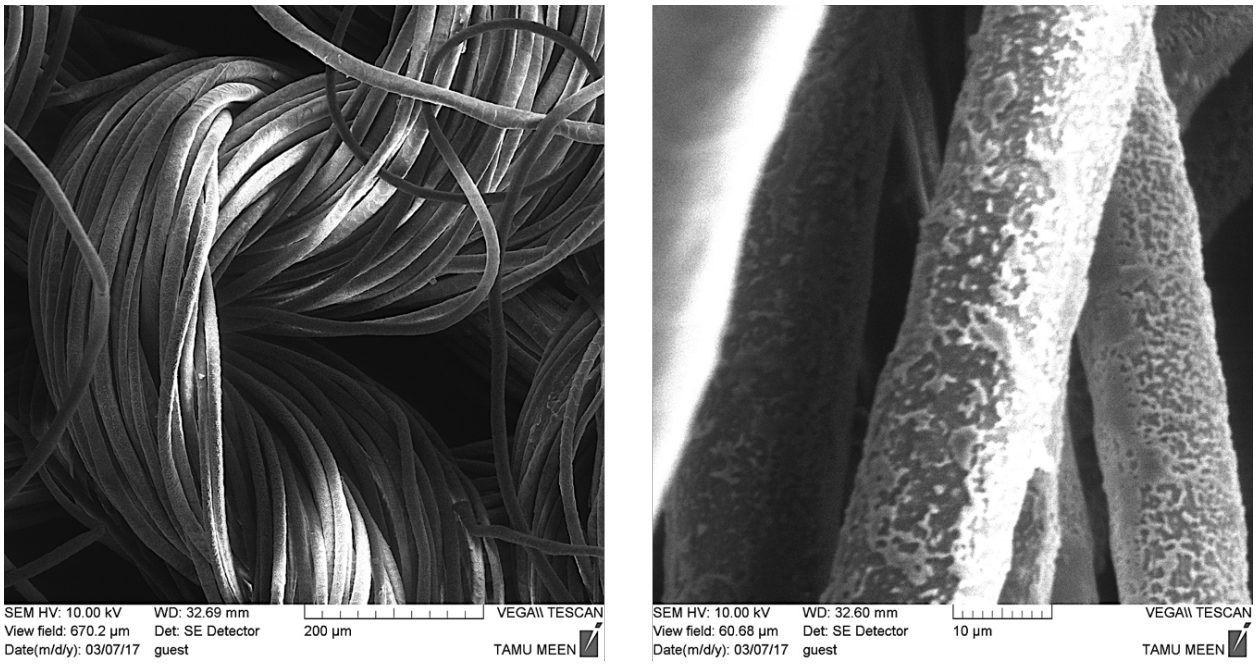

Figure 55: SEM images of blue merino wool after 2-min 1.27 W/cm^2 DBD treatments. Left: Blue merino wool fiber bundle displaying an unaffected epidermis across multiple fibers. Right: Strongest response seen in 2-min 1.27 W/cm^2 DBD treated blue merino wool sample. The cuticle is gone on these fibers, and in its place, is a waxy residue that seems to have been overlaid around the fibers.

4.5.2 Fifteen Minute DBD Treatment at 1.27 W/cm^2

DBD treatment of blue merino wool at 1.27 W/cm^2 at a gap distance of 1 mm for 15 minutes will produce significant changes in the visual appearance of the blue merino wool. These changes can be seen without the aid of a microscope. These changes consist of a strong discoloration (blue to orange), strong fading (bright blue to dark blue and/or purple), and localized formation of wax-like substances. The formation of the wax

substance is often, but not always, a precursor to a fiber break point. These changes can be seen in Figure 56 below. Macroscopically, a 15-min DBD plasma treatment will also cause blue and black merino wool to “pill”. This pilling effect can be seen in the right image of Figure 57. For the images of the pilling effect on black merino wool and green modacrylic, please refer to the appendix. Cotton did not display any pilling.

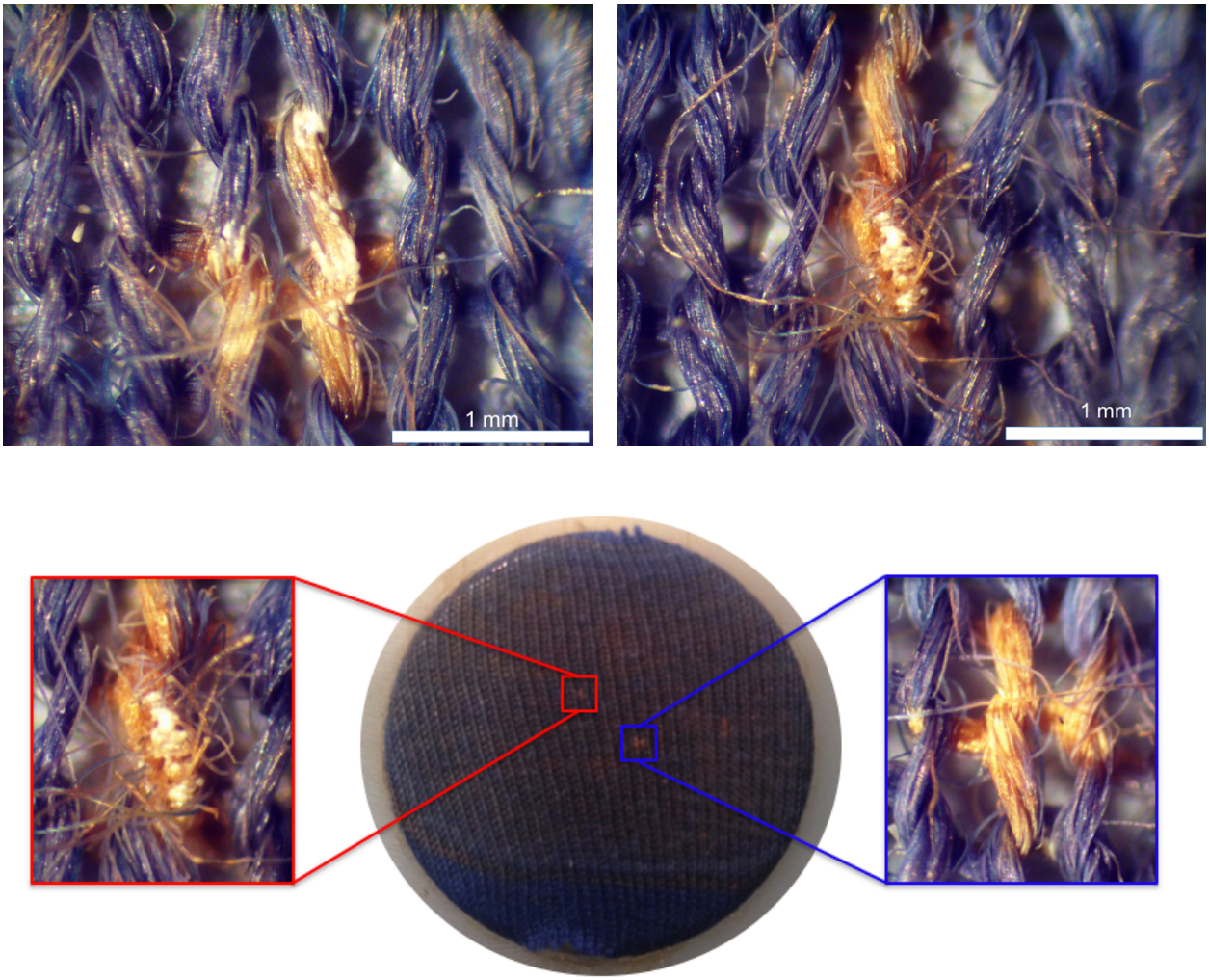

Figure 56: Blue merino wool after a 15 min exposure to the DBD Reactor at 1.27 W/cm^2 at 1 mm gap distance. The top optical micrographs show two locations that were severely affected by the DBD plasma. The bottom images show that these drastic effects only covered a small fraction of the entire treated surface. While the rest of the merino wool has an orange appearance, the fibers did not display the wax-like formation seen in the top row. Please note that these images were the worst-case found.

Figure 57: Photographs of untreated and DBD treated blue merino wool. (Left: Untreated Blue Merino Wool; Right: 15 min, 1.27 W/cm^2 DBD treated blue merino wool.) This image shows the change in macroscopic appearance between the new blue merino wool and the recently DBD treated merino wool. Some of these changes are pilling and small, brown burn spots. Please note that this sample does not have an overall change of color from blue to orange, as did the sample in Figure 56.

Curiously, these effects were entirely absent in black merino wool, green modacrylic, and white cotton when exposed to the same exact DBD treatment (15-min, 1.27 W/cm^2 at 1mm gap distance). Figure 58 shows the before and after optical micrographs of each fabric. With the exception of the pilling—which is only appreciable with the naked eye—there is no difference between the micrographs of the untreated and treated fabrics (Figure 58).

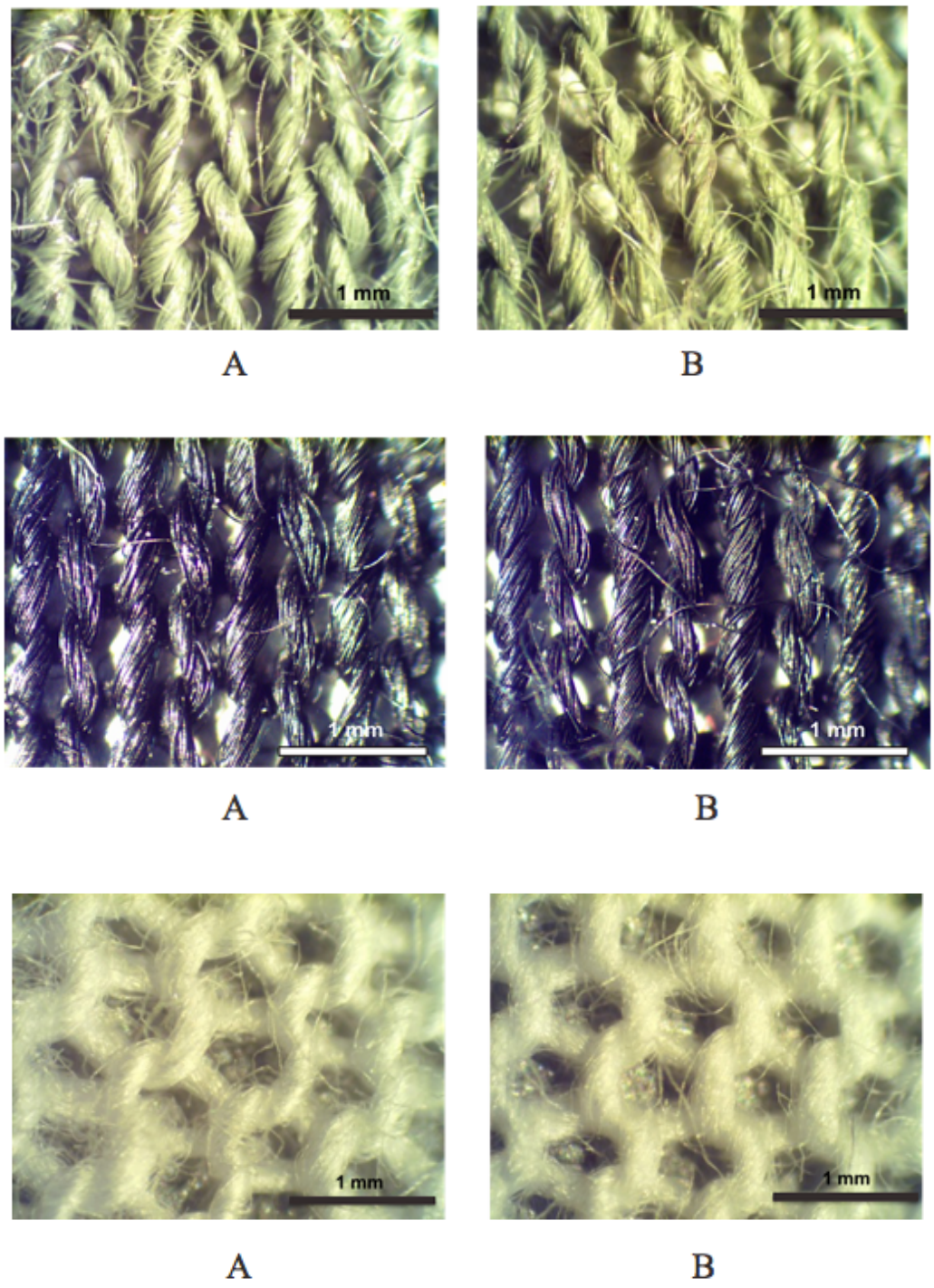

Figure 58: DBD treatment visual effect on other fabrics (A: Untreated Fabrics; B: Fabrics after a 15-min 1.27 W/cm2 DBD Treatment; Top Row: Green modacrylic; Middle Row: Black Merino Wool; Bottom Row: White Cotton)

Please note that all SEM images of 15-min 1.27 W/cm^2 DBD treated fabrics are of blue merino wool only. In Figure 59, the SEM images of the 15-min 1.27 W/cm^2 DBD treated blue merino wool show considerable degradation of the cuticle structure of the blue merino wool fiber. This left image of Figure 59 captures two different fibers, each with a different amount of damage. The fiber to the right edge of the view field appears to be at the stage of losing its cuticle: the smoothness and rough shape of the cuticle are still seen, but instead of overlapping another scale, its edges have been by etched away. In the left image of Figure 59, there appears to be a high density of thin scales falling off of the fiber. Also, at the lower right corner of the same image, a thin, twisted, scale-like structure seems to be the discontinuity between an etched fiber (above the scale-like structure) and a smooth one (below the scale-like structure). This seems to suggest that the DBD plasma may be unwrapping the fiber's cuticle. However, since this unwrapping is not seen in less plasma-exposed blue merino wool, it seems the plasma simply etches away at the surface of the merino wool fiber, while occasionally incising certain segments of the fibers.

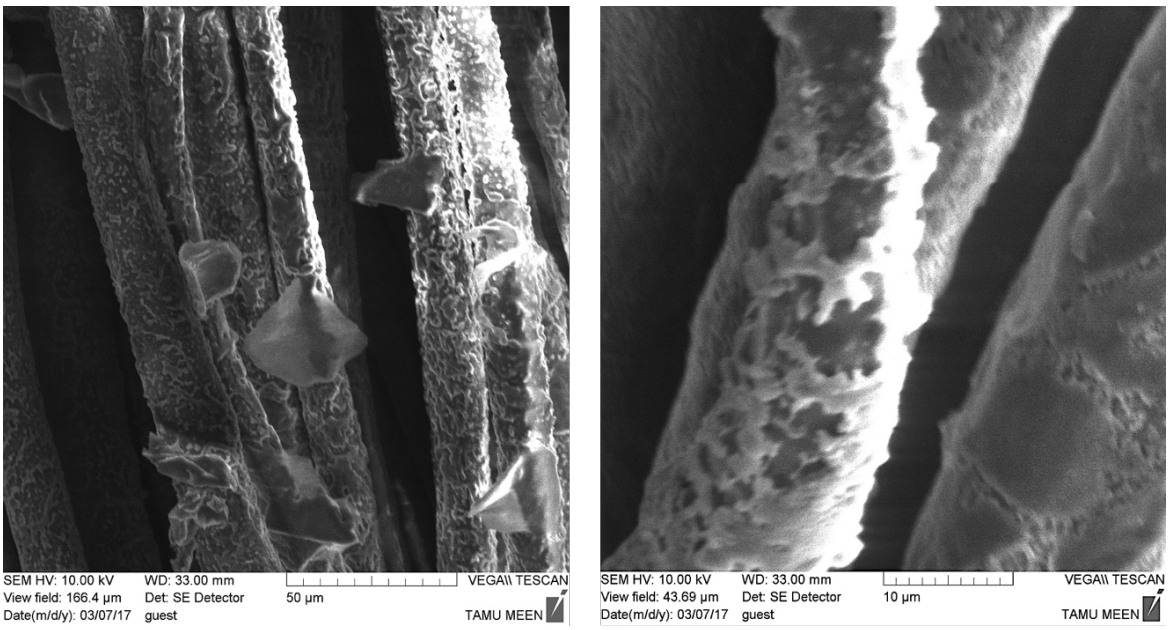

Figure 59: SEM images of blue merino wool after a 15-min 1.27 W/cm2 DBD treatment. Left: Merino wool fiber bundle showing the disintegration of the cuticle. Right: Worst-case example of plasma-induced damage to the blue merino wool fiber. To the right, it appears that part of the cuticle is still present as the rest has been slowly etched away.

The fiber to the left edge of the left image in Figure 59 shows the most damage of any merino wool fiber seen while scanning the fabric via the SEM. This image shares similar characteristics to the waxy-deposit observed in the color micrographs of Figure 56. With increased DBD plasma exposure, the affected fibers seem to be covered in this wax-like substance. It is unclear if this interaction is exclusively between the DBD plasmas and the merino wool, or if batch merino wool processing chemicals also play a role. Lastly, it is interesting that the damage seen in Figure 56 and 59 differ from the damage seen in merino wool fibers after alkali or acidic attack (Figure 6).

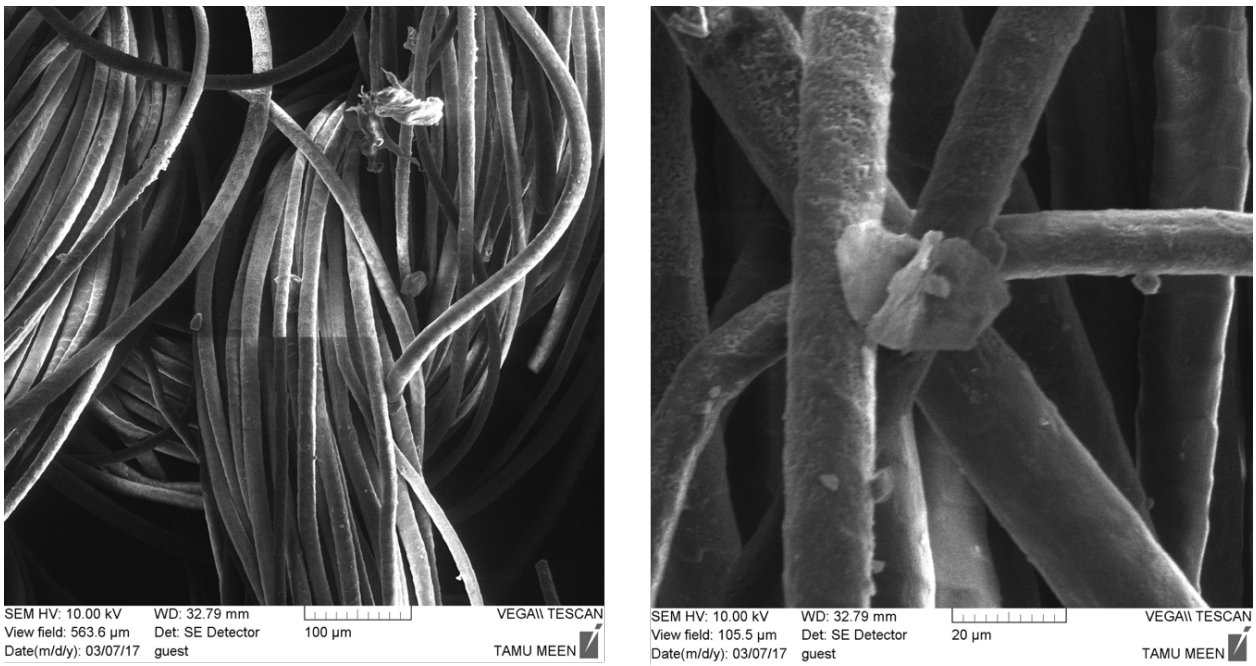

Figure 60: SEM images of another location of the blue merino wool sample that was also exposed to 15 min of a 1.27 W/cm2 DBD plasma. In the left image, you can see a perfectly unharmed merino wool cuticle. Note that in the fiber bundle (left), there are many fibers that retain their cuticle. This shows that many fibers are not as severely affected as the fiber close-up in Figure 59.

Once again, it is important to stress that although a 15-min DBD treatment at a power density of 1.27 W/cm^2 is too harsh for the blue merino wool, there are still many fibers in the background of the SEM images (Figure 60) that appear completely unaffected. This is even more true for merino wool fibers after DBD treatments of lower intensity.

4.5.3 Ten Minute DBD Treatment at 0.85 W/cm^2

All fabrics were exposed to a 10-min DBD treatment at 0.85 W/cm^2. Under this treatment, all fabric types began to display minor signs of plasma-related damage. For blue merino wool, this manifested itself as an increase in porosity (or poke-a-dots) across the scaly

cuticle of the merino wool fiber. As can be seen from the SEM image in Figure 61, only a small fraction of the blue merino wool fibers within the captured image seemed to be affected. The rest of the fibers look indistinguishable from the untreated blue merino wool.

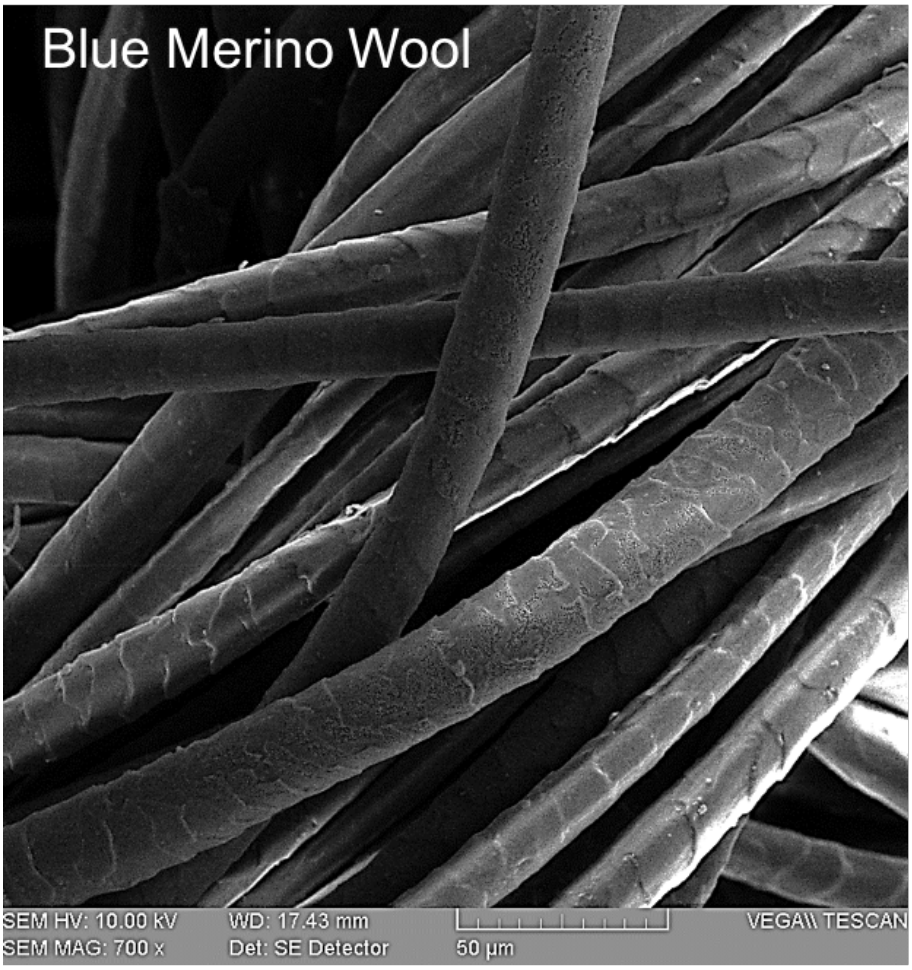

Figure 61: SEM image of blue merino wool fibers after a 10-min 0.85 W/cm2 DBD treatment. Plasma does not cause widespread damage to the fibers. Instead, only some of the fibers appear to be affected. The fibers in the background look the same as untreated merino wool fibers. Please note the vertical merino wool fiber: the cuticle is present near the bottom, but seems to be slowly etched away further up the fiber.

For black merino wool, a 10-min DBD treatment at 0.85 W/cm^2 seemed to have a slightly smaller effect on the surface morphology of the merino wool fibers. An overview SEM image of a merino wool fiber bundle shows that many of the black merino wool fibers continue to display their scaly cuticle (Figure 62). Images of higher magnification were hampered by apparent issues of the platinum-palladium coating for this specific sample set.

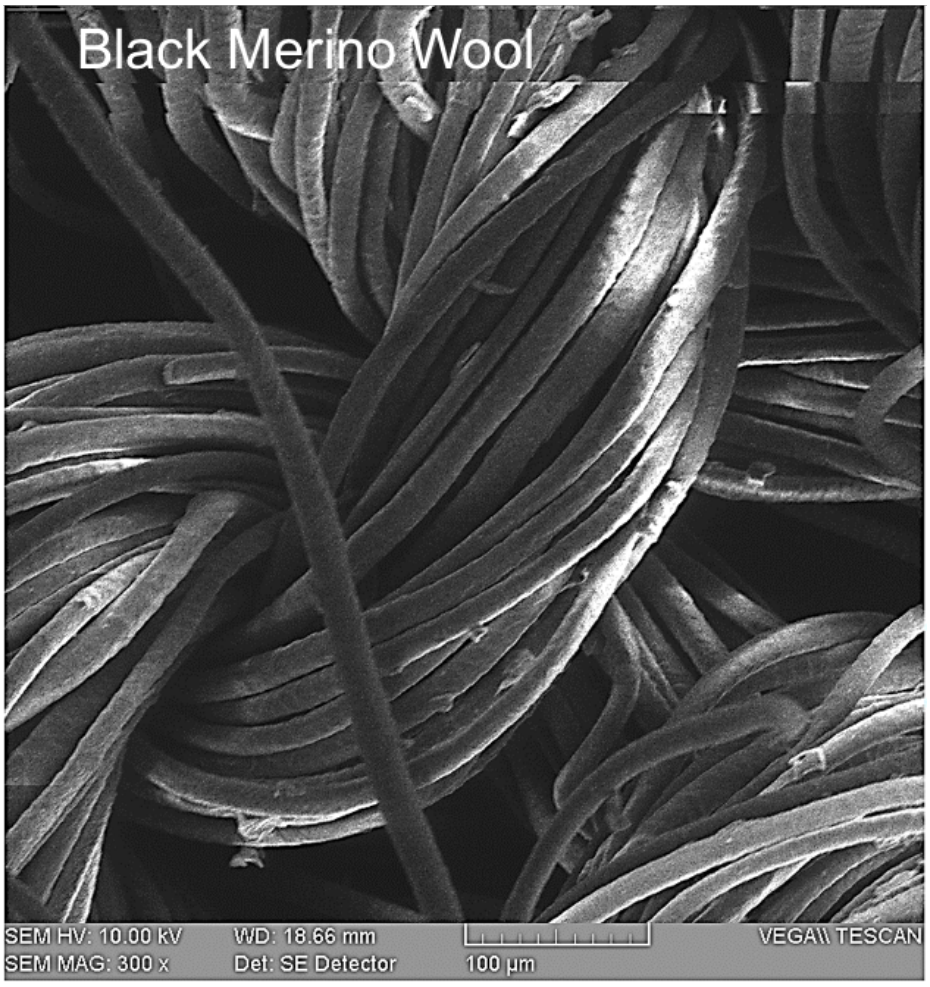

Figure 62: SEM image of a black merino wool fiber bundle. Note that many fibers continue to have a scaly appearance. This is evidence that the plasma has not yet affected the cuticle of the fiber.

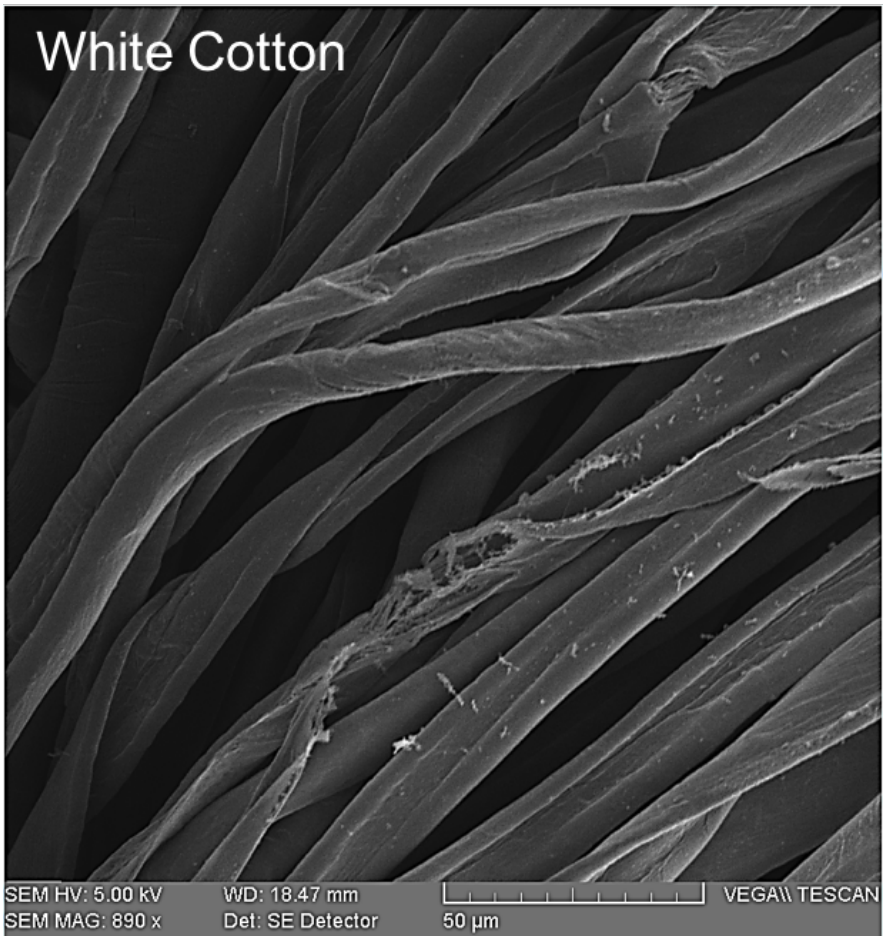

Figure 63: SEM image of a cotton fabric sample after a 10-min 0.85 W/cm2 DBD plasma treatment. The rupture in the center of the image is in stark contrast to the smooth shape of untreated cotton fibers. The fiber slightly above the rupture site has small etches or cracks along the outer wall. Note the smooth walls of the cotton fibers in the background. This is further evidence that DBD plasma treatment does not inflict widespread damage to a fabric sample.

With regards to white cotton, a 10-min DBD treatment at 0.85 W/cm^2 had discernable effects on the structure of a small fraction of cotton fibers. In particular, the center fiber of the SEM image in Figure 63 shows a rupture—as well as associated debris—along the axis of the cotton fiber. In addition, the fiber located slightly above the center of the image no longer has the smooth appearance of an untreated cotton fiber. Instead, there are tiny

cracks, as well as signs of etching, along the contour of that cotton fiber. Still, there are plenty of cotton fibers in this SEM image that show perfectly unharmed cotton fibers.

Figure 64: SEM image of green modacrylic after a 10-min 0.85 W/cm2 DBD plasma treatment. The DBD plasma treatment seemed to only produce linear marks or spots) parallel to the fiber's axis.

The last fabric type was green modacrylic. While the SEM image shown in Figure 64 is the worst-case found during the imaging process, modacrylic seemed to be the most resilient of all fabric types after the 10-min DBD treatment at 0.85 W/cm^2. Instead of ruptures (as seen in cotton) and “poke-a-dots” (as seen in blue and black merino wool),

modacrylic retained its untreated characteristics and only showed signs of minor spotting. This suggests that the DBD plasma only had a surface-level effect on the modacrylic, whereas the same DBD plasma had a more penetrating effect on merino wool and cotton.

4.5.4 Twenty Minute DBD Treatment at 0.85 W/cm^2

All fabrics were also exposed to a 20-min DBD treatment at 0.85 W/cm^2. Blue and black merino wool had readily observable changes in the surface morphology. On some of the blue merino wool fibers in Figure 65, the cuticle is gone and there are several cuts and gashes across the fiber. It is interesting that this treatment did not produce the wax-like substance that the 15-min DBD treatment at 1.27 W/cm^2 produced (see Figure 56). In fact, no wax-like substances were found in any of the 0.85 W/cm^2 treated blue merino wool samples. It is even more interesting that the blue merino wool samples used in both studies (1.27 W/cm^2 and 0.85 W/cm^2) came from the same shirt. Please note that there are several unharmed fibers behind the harshly affected blue merino wool fibers. This shows again that even a 20-minute DBD treatment is far from homogenous.

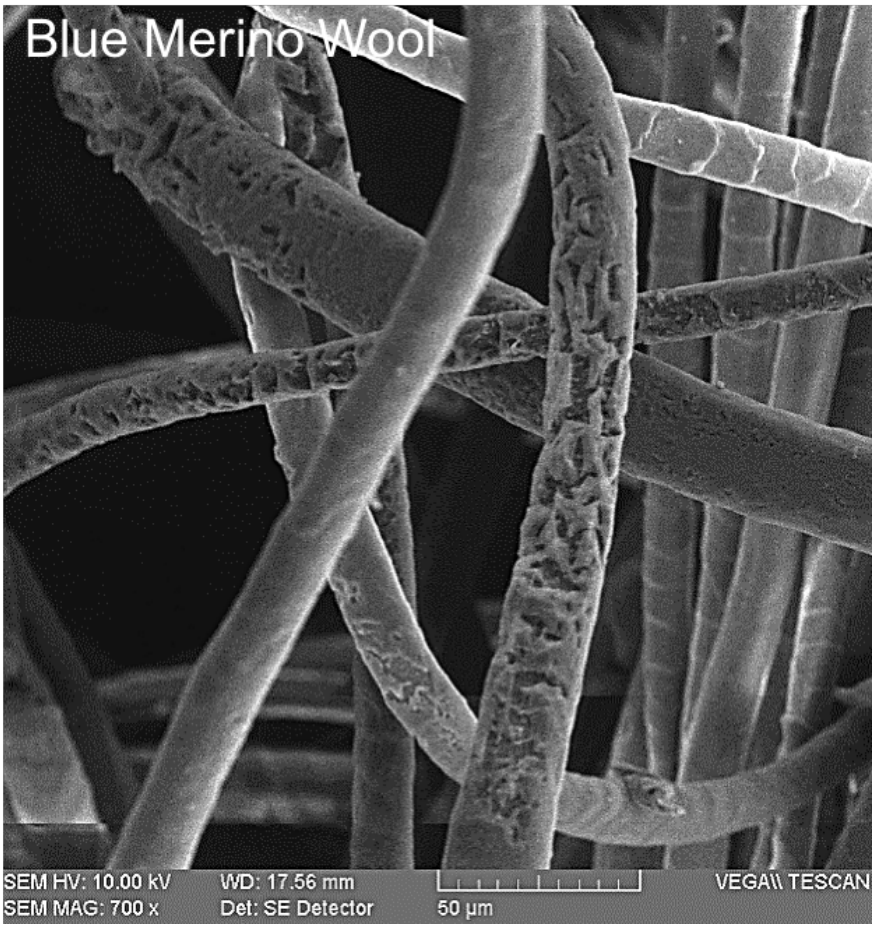

Figure 65: SEM image of blue merino wool after being exposed to a 20-min 0.85 W/cm2 DBD treatment. While the damage to some of the fibers is excessive, there are many fibers in the background that have been unharmed.

The SEM image of the 20-min DBD treated black merino wool shows a widespread effect on the surface structure of the black merino wool fibers. There is substantial cuticle loss across multiple fibers in the field view. With this exception, black merino wool seemed to fair slightly better than blue merino wool under the 20-min DBD treatment. Figure 66 is not only interesting for the spread of plasma-related damage, but also because it shows a single black merino wool fiber (across the top middle of the image with the broken end) with varying damage across it. Towards the bottom end of the fiber, the scaly cuticle is

still visible. As one progresses up this single fiber, the scales gradually disappear as porous etching becomes ever more visible. The exact point at which this happens is hard to pinpoint. It is evident, though, that the plasma degrades the scales by chemical decomposition, instead of removing the scales by disrupting the interface between the cuticle and the cortex. Other fibers within this same SEM image (located on the bottom right) display varying levels of plasma-induced damage.

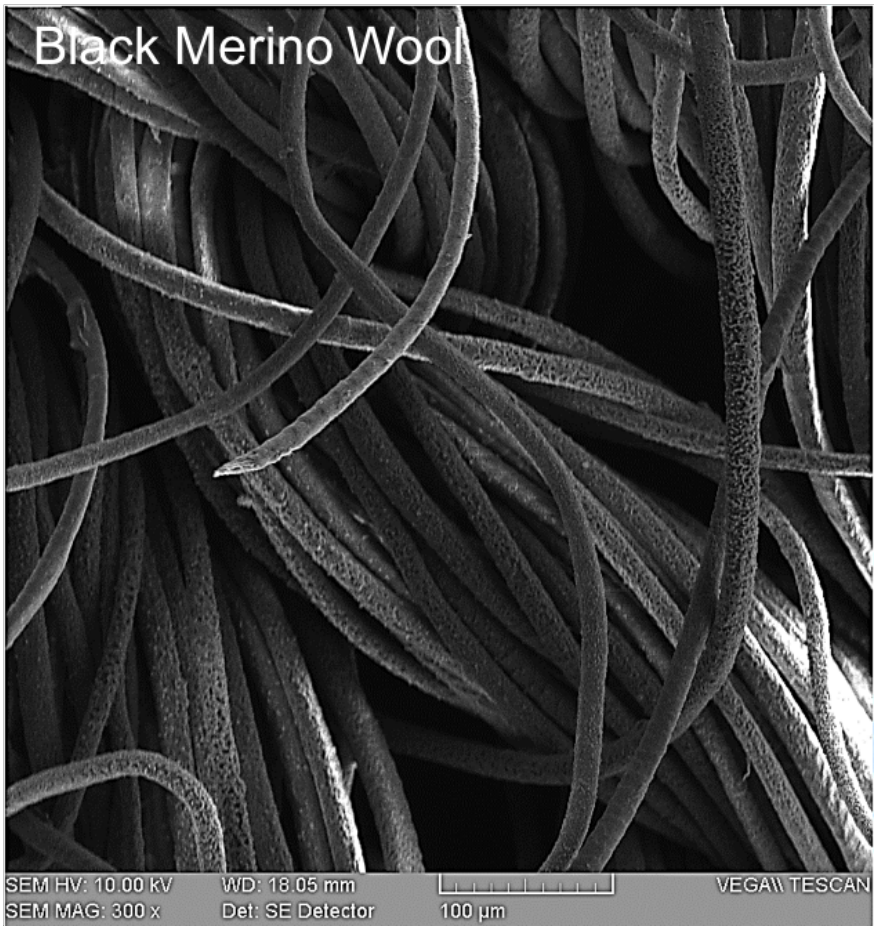

Figure 66: SEM image of black merino wool after exposure to a 20-min 0.85 W/cm2 DBD plasma treatment. At this duration, DBD plasmas are clearly more capable of causing significant harm to merino wool fibers. This suggests that a 20-min DBD plasma treatment at 0.85 W/cm^2 may be near the plasma-compatibility limit.

The SEM image of the 20-min DBD treated white cotton shows similar effects as the 10-min DBD treated white cotton (Figure 67). The major difference is the severity of the plasma etching or rupturing. Again, there is debris around the site of damage—which is characteristic of cotton damage under acidic or basic attack. However, many of the cotton fibers in this "worst-case" SEM image seem unharmed by the 20-min DBD plasma treatment.

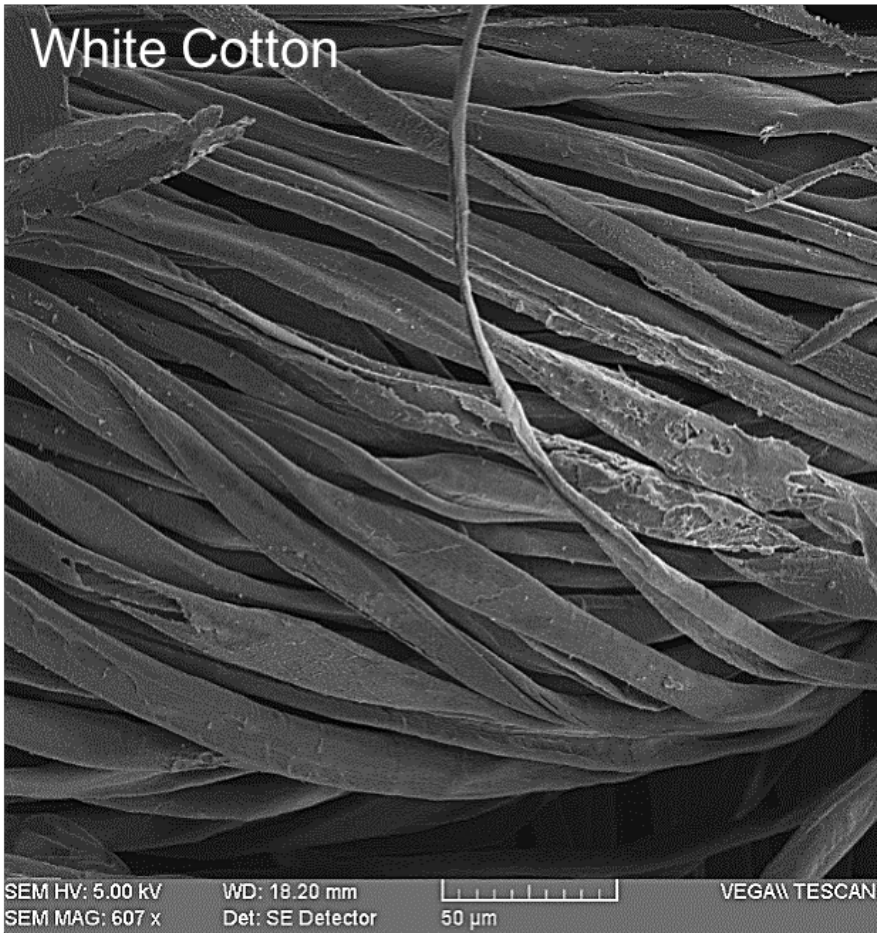

Figure 67: SEM image of white cotton fabric after being exposed to a 20-min 0.85 W/cm^2 DBD treatment. There is an increased degree of etching or rupturing of the cotton fiber.

Figure 68: SEM image of green modacrylic after exposure to a 20-min 0.85 W/cm2 DBD plasma treatment. Unlike other fabrics, modacrylic responded to the plasma treatment by pilling. The surface has become noticeably bumpier, with irregular sized substances covering large stretches of individual fibers.

A 20-min DBD plasma treatment at 0.85 W/cm^2 had distinguishable effects on the surface morphology of modacrylic fibers. Unlike merino wool and cotton, whose cuticles were either decomposed or etched away, modacrylic seems to microscopically pill. All plasma treated modacrylic SEM images, across 1, 2, 5, 10, 20 minute treatment times, lacked any cuts, cracks, or gashes across the fiber. Instead, the surface begins to turn bumpy, spotty, or extrude itself. While the SEM image of Figure 68 seems drastic, there were many other fibers on the scanned modacrylic sample that were largely unharmed by the 20-min DBD treatment at 0.85 W/cm^2. This can be seen in Figure 68.

4.5.5 Fifteen Minute LPPR Treatment at 0.016 W/cm^2

Low pressure plasma treatment at .016 W/cm^2 will not produce any visible morphological changes in blue or black merino wool. Also, no observed changes in the morphology of the fibers were seen with the optical microscope or scanning electron microscope (Figure 69). However, low pressure plasma treatment will cause a curling effect in black merino wool. This was most clearly seen with the 1" x 6" strip of black merino wool that would later be used for tensile testing (Figure 45).

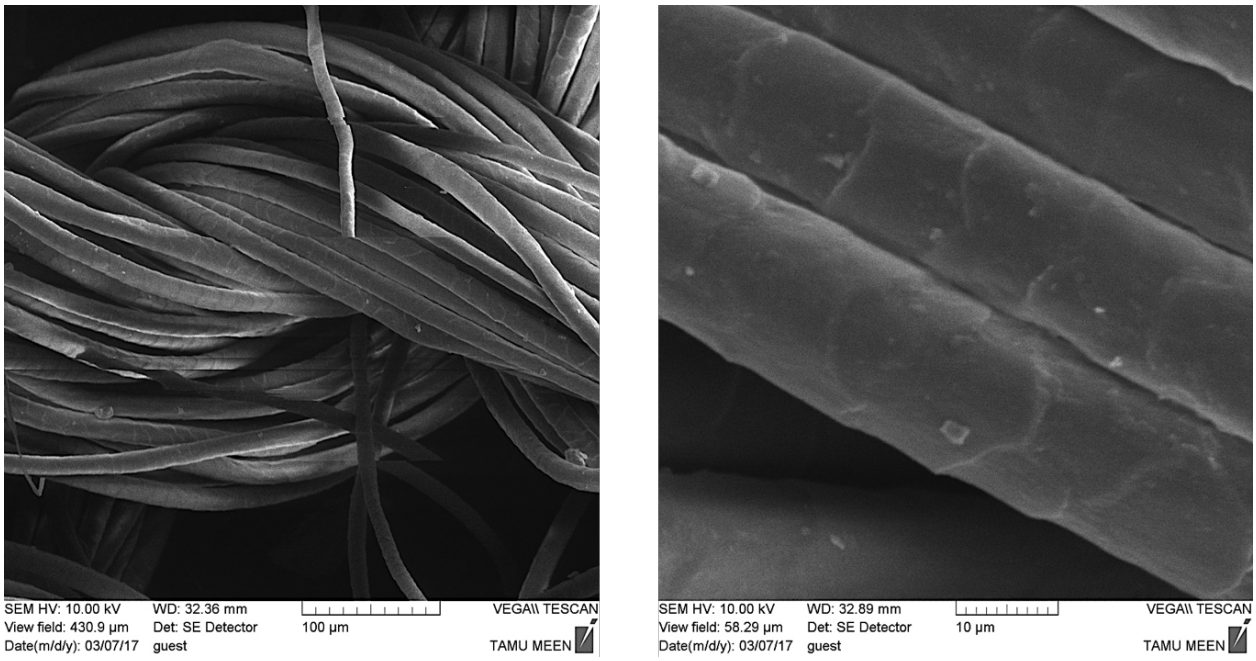

Figure 69: SEM images of blue merino wool after a 15-min 0.016 W/cm^2 LPPR treatment. The presence of the scaly cuticle across the entire view field indicates that LPPR treatment did not cause any changes in the surface morphology of the fibers. Recall from the tensile test results that LPPR-treated blue merino wool had a significantly higher tensile strength than untreated merino wool.

4.5.6 Electron Beam Treatment at 50 kGy

An electron beam treatment of 50 kGy did not produce any noticeable changes in the surface structure of the merino wool. This is clearly seen in the SEM images of E-beam treated blue merino wool shown below (Figure 70). Please note that the SEM images of E-beam treated fabrics are of blue merino wool only. In other words, SEM images were not taken of E-beam treated cotton, modacrylic, or black merino wool.

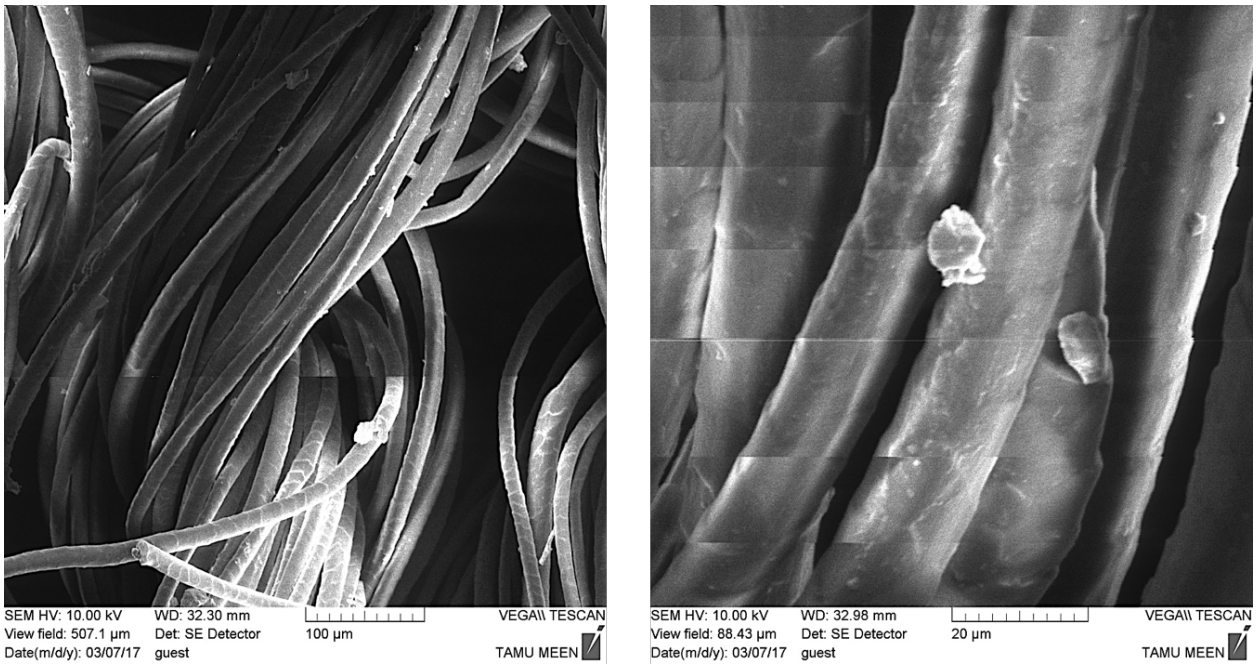

Figure 70: SEM images of blue merino wool after a 50 kGy electron beam treatment. No changes in surface morphology were observed.

4.6 Plasma-Assisted Deodorization of Isovaleric Acid

Approximately 94% of the US population can detect isovaleric acid (IVA). Of those individuals that can, the minimum detection threshold varies 10,000-fold. This variation eliminates the idea of a double-blind human olfactory test of untreated and plasma treated IVA samples. To circumvent this, GC-FID and GC-MS analysis studies were performed on various treated and untreated isovaleric acid samples.

4.6.1 Indirect DBD Treatment of IVA in Water

The first step was to analyze changes in IVA diluted by a carbonless solvent in the GC-FID. A volume of 0.85 mL of H_2O diluted samples of IVA, at a concentration of 4% (v/v), was placed in the teflon liquid sample holder. The 4% (v/v) concentration is close to the maximum solubility of IVA in water, and was chosen to obtain a detectable measurement after the indirect DBD plasma treatment. The 4% (v/v) IVA sample was then placed directly underneath the indirect DBD reactor for a cumulative treatment time of 4 minutes. After every minute of treatment within the 4 minutes of total treatment, the sample was pushed out from underneath the indirect DBD reactor and smelled to subjectively assess changes in odor. After 4 minutes, a subtle change in odor was discerned, and the sample was extracted from the teflon sample holder and placed in a vial for GC-FID analysis. The change in odor can be described collectively as a reduction of the natural pungent odor of IVA and an increased smell of ozone or recently plasma-irradiated substrate. The

results of the control and 4 min indirect DBD treatment of 4% (v/v) of IVA-H2O sample are shown in Figure 71.

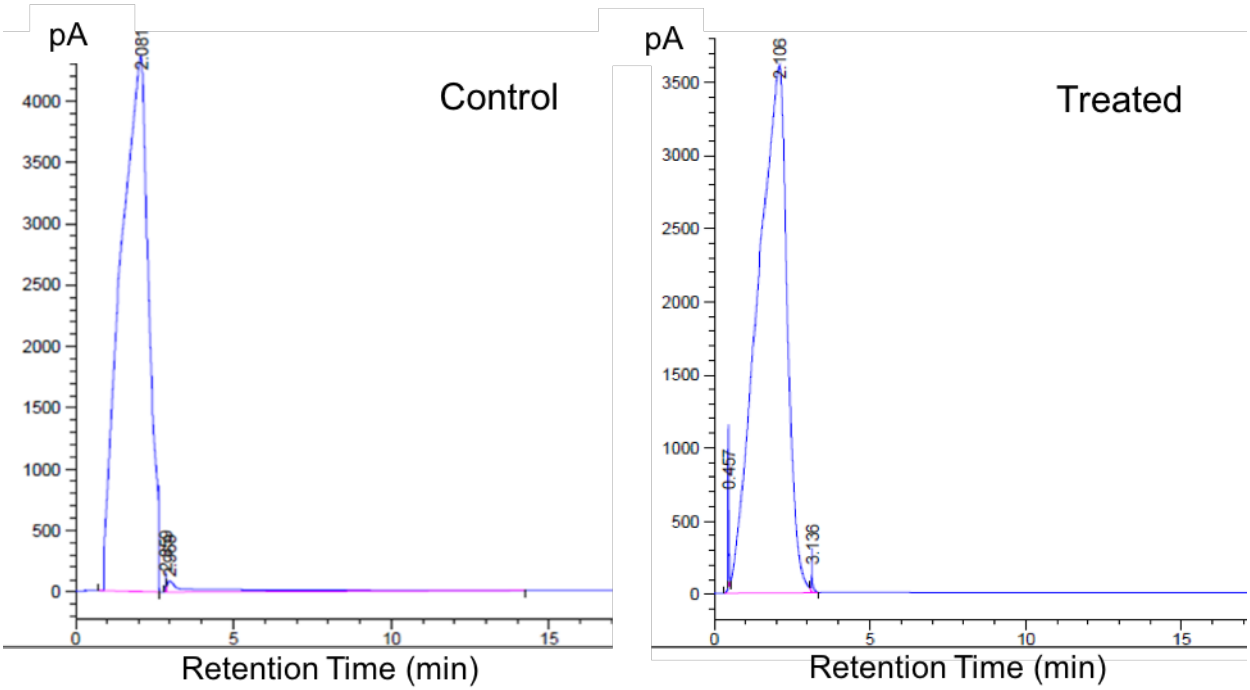

Figure 71: GC-FID chromatogram of isovaleric acid after indirect exposure to a 4-min DBD plasma. The changes between the control and treated isovaleric acid were too small to make any significant analysis.

The results in Figure 71 show that a short, 4 minute indirect DBD treatment may have had a noticeable effect on the peak height of the 4% (v/v) IVA-H_2O solution, as well as the retention time.

The first experiment of the deodorization study provided preliminary evidence that plasma might be able to change IVA solution chemistry. The second experiment in the deodorization study was aimed at determining if a longer treatment of indirect DBD

plasma could eliminate a concentration of IVA closer to the concentration of IVA found in typical sweaty socks. The same experimental methods were followed. The only exceptions were that the starting IVA-H_2O concentration was decreased to 2.51% (v/v), and the indirect DBD reactor treatment times were increased to 10 min and 30 min. Unfortunately, these results proved useless since the higher concentration of water in the solution repeatedly extinguished the flame of the GC-FID. This interfered with a valid collection of results.

4.6.2 Direct DBD Treatment of IVA-Bathed Merino Wool

The third experiment in the deodorization study had the goal of assessing isovaleric acid's compatibility with blue merino wool and analyzing the chemical change of IVA in IVA-wetted blue merino wool after different direct DBD plasma treatments. Direct DBD plasma treatments were performed at different exposure times (from 30 seconds, 1, 2, 4, 8, 16, and 32 min), at a constant power density of 0.85 W/cm^2, 1mm away from the IVA-wetted blue merino wool.

To test various plasma exposure times, 9 circles of blue merino wool were cut from commercially obtained blue merino wool, and completely submerged in a 4% (v/v) IVA-H_2O bath for an entire day (Figure 72). Next, the 9 samples were removed from the 4% (v/v) IVA-H_2O bath and allowed to dry for an entire day inside of a fume hood, over a cleaned, perforated brass rack. At this point, it was observed that the circular samples of

blue merino wool had shrunken and curled significantly. It is unclear if isovaleric acid was the cause of this volume change.

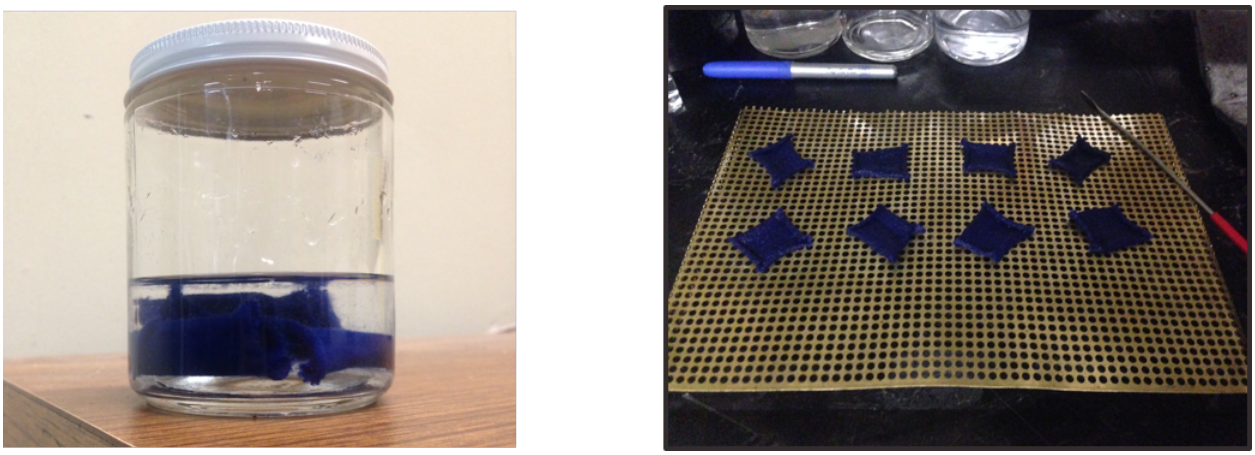

Figure 72: IVA-wetted blue merino wool sample preparation. Left: Nine circular samples of blue merino wool were placed for an entire day inside a 4% (v/v) IVA-H_2O solution. Right: The next day, the merino wool samples were removed from the 4% (v/v) IVA-H_2O bath and placed over a ½" high, perforated brass drying rack. Note the shrinkage and curling that took place inside the IVA-H2O bath.

Due to the volume change of the blue merino wool, a smaller electrode (and smaller fabric holder) had to be used. This unplanned changed reduced the effective plasma treating area from 83% to 36%. With an 83% plasma coverage area, the untreated IVA in the same fabric could be used as a built-in control. However, a 36% plasma treatment area meant that the majority of the IVA in solution would be untreated. Regardless of the plasma treatment area percentages, it would still be possible to simultaneously observe the retention time of untreated and treated IVA for each individual fabric sample across different plasma exposure times. In other words, each blue merino wool sample would provide a control (untreated IVA) and the treatment (treated IVA).

After direct DBD treatment, the merino wool samples were placed in sealed vials containing 10 mL of DCM for an entire day. The 10 mL of DCM used was needed to fully cover the merino wool samples. The samples were left in DCM solution for an entire day to maximize IVA extraction from the blue merino wool (Figure 73).

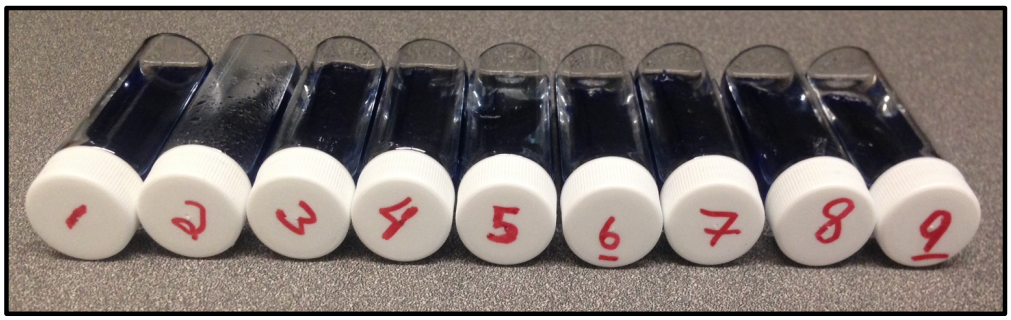

Figure 73: IVA-bathed blue merino wool samples in 10 mL of DCM post DBD treatment. Numbers on caps represent sample numbers. The DBD treated merino wool samples were allowed to rest in these vials for 24 hours to allow DCM to extract the maximum amount of IVA.

Table 4: Sample Composition and Treatment Time

	DCM	IVA	DBD Treatment Time
Sample 1	Yes	No	0 sec
Sample 2	Yes	Yes	0 sec
Sample 3	Yes	Yes	30 sec
Sample 4	Yes	Yes	1 min
Sample 5	Yes	Yes	2 min
Sample 6	Yes	Yes	4 min
Sample 7	Yes	Yes	8 min
Sample 8	Yes	Yes	16 min
Sample 9	Yes	Yes	32 min

The next day, the fabric samples were removed from the glass vials, and stored in separate, empty glass vials. The solution remaining in each of the vials contained small fibers from the merino wool. These were filtered out by using 120mm diameter pre-pleated filter paper that had an average pore size less than 20 um. Interestingly, the color of the filtrate correlated with the amount of DBD exposure (74). This is further evidence that DBD treatment is effective at fading blue dyes.

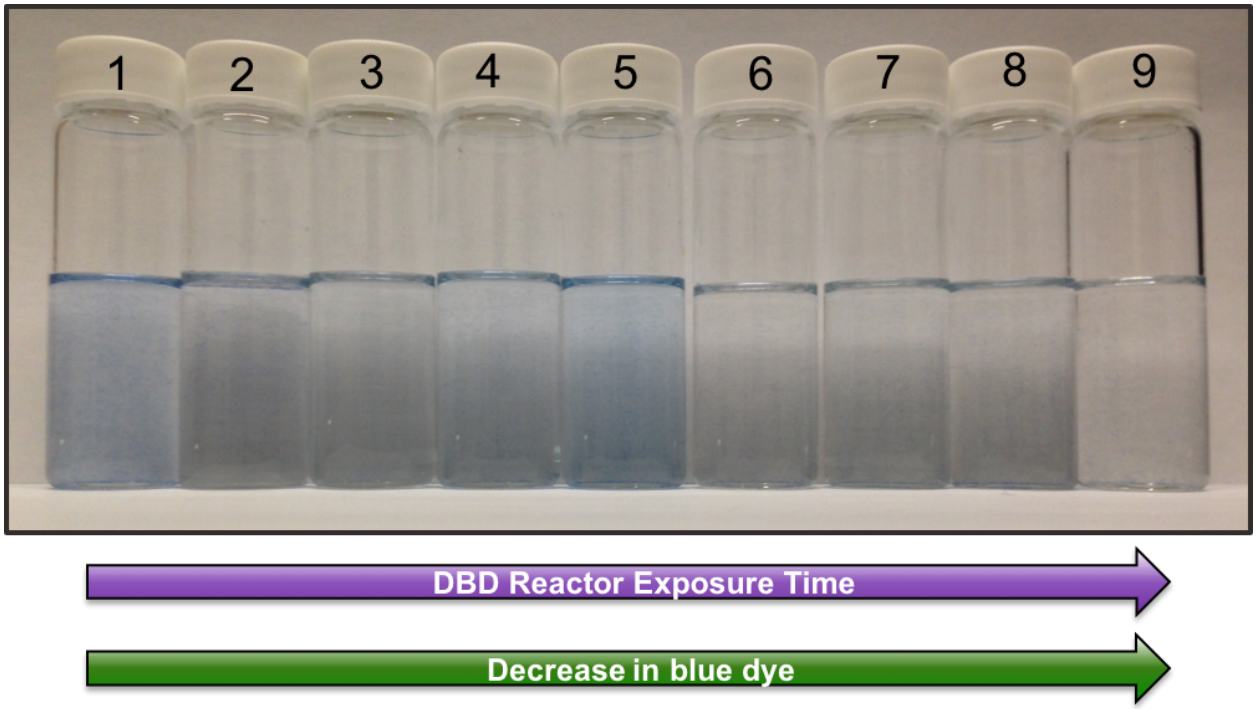

Figure 74: Filtrate from DBD treated blue merino wool after a 24-hour IVA-H2O bath. As the DBD treatment time increased, there was less color in the DCM solvent. As all samples were filtered by the same kind of filter paper, the only explanation is that the DBD plasma treatment increasingly destroyed the blue dye.

The filtrate of each sample was then pipetted into Agilent glass vials and passed through the GC-FID in chronological order. The chromatograms are shown in Figure 75.

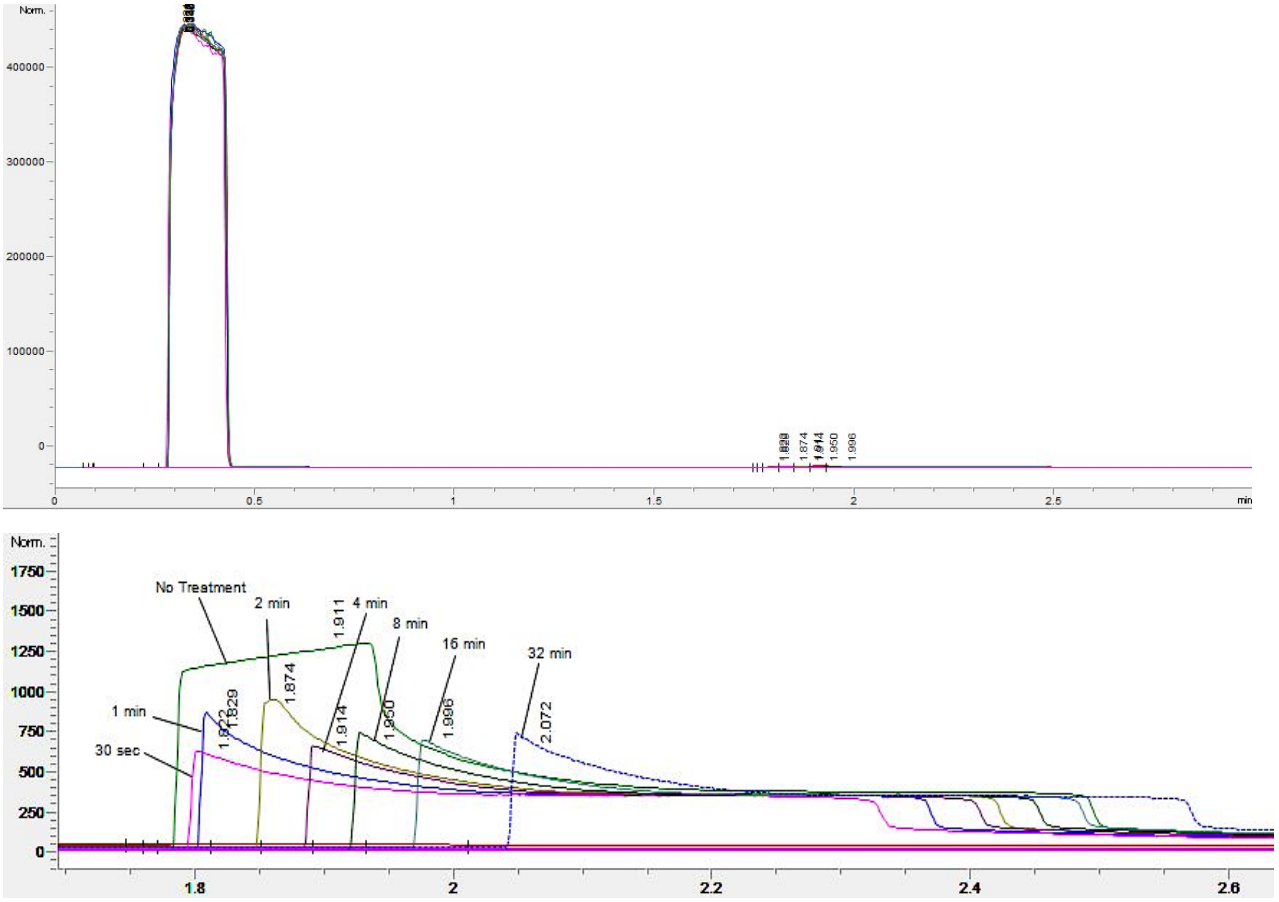

Figure 75: GC-FID chromatogram for DBD treated IVA-stained blue merino wool. Top: Entire chromatogram of experiment. Left peak is the DCM peak with a consistent retention time of .337 min. Bottom: Chromatogram zoomed in to show variation in IVA retention times across 0.85 W/cm^2 DBD treatments of different times. The trend is clear: longer DBD treatment times increased the retention time of the IVA. For both chromatograms, the y-axis units are pA and the x-axis units are retention time in minutes.

In Figure 75, the entire chromatogram of the GC-FID run is shown. On the far left, is the relatively sharp and high DCM peak, eluting at a constant retention time of .337 min. Towards the right of chromatogram are the untreated and treated IVA peaks, which elute

within a retention time range of 1.8 to 2.0 min. The constant retention time of DCM across all treated samples can be used as reference point, which supports the idea that plasma exposure time has a a proportional effect on IVA chemistry.

The close-up of the chromatogram has been annotated with the sample's specific direct DBD treatment time to highlight the direct relationship between DBD treatment time and IVA retention time. These results also show that the control (no treatment) had a broad retention time range, that seemingly encompasses the 30 sec to 8 min treatment samples' retention time. It also appears that a 16 and 32 min direct DBD treatment is required to cause a significant change in retention time—and therefore IVA chemistry. It is curious to note that the treated IVA samples did not produce more than two peaks. It was initially hypothesized that treated samples would produce a peak in between the DCM peak (.337 min) and the untreated IVA peak (1.8 – 2.0 min). The reason being that plasma species would break down the C5 carbon chain of isovaleric acid, produce smaller carbon chains, and yield lower retention times.

The absence of a separate, "treated" peak may be due to 1) a concentration lower than the GC-FID's detection limit, 2) a retention time similar to the DCM peak, and 3) a retention time similar to the untreated IVA peak. Also, the assumption can be made that the shape change between untreated IVA and treated IVA peaks is due to treated IVA molecules having a slightly lower retention time than the untreated IVA. This assumption explains why the treated IVA samples' chromatograms have an asymmetrical, left-shifted

peak, as opposed to the more symmetrical or right-skewed profiles seen in untreated IVA samples.

In summary, treated samples of IVA had a different chromatogram than untreated samples of IVA, which means that direct DBD treatment affected the chemistry of isovaleric acid. Treatment time also appeared to affect IVA chemistry, as judged by the different retention times across different treatment times. Most curious of all, is the finding that an increased plasma exposure time led to higher retention times—which is contrary to the initial hypothesis. To double-check this finding, the experiment was repeated—this time placing samples through the GC-FID in a randomized order. The results of this second run are shown below.

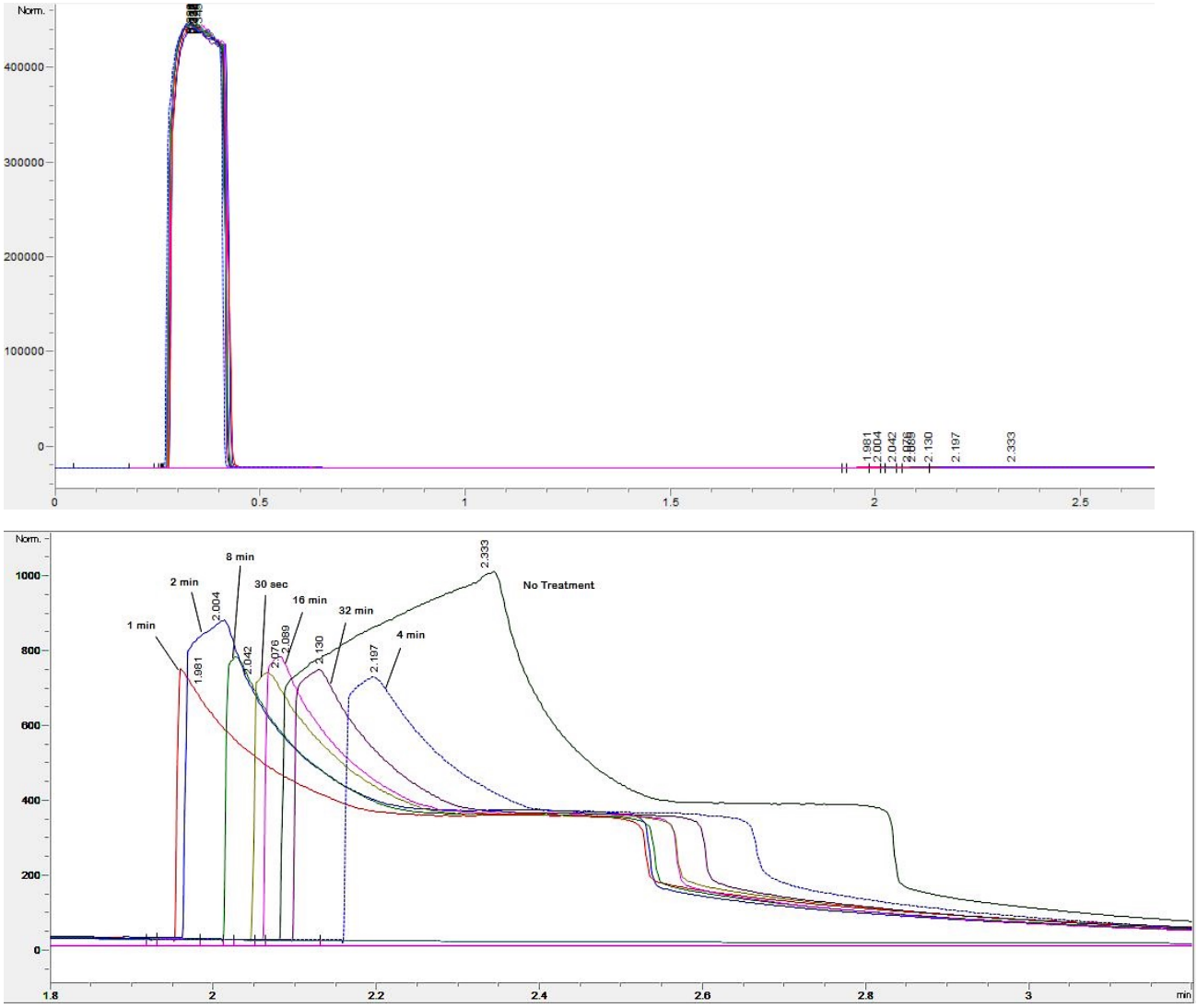

Figure 76: GC-FID chromatogram of duplicated experiment from Figure 75. This time, the samples were loaded in random order to eliminate possibility that fibers in the filtrate were increasingly diminishing the area of the GC-FID column, and via that mechanism, were artificially increasing the retention times of the next loaded sample. While the consistent DCM peaks should already eliminate this possibility, a repeat experiment required little time and resources.

Once again, in Figure 76, we see that DCM had a constant retention time—this time with an average retention time of .350 min. The treated IVA samples had a retention time range of 1.981 – 2.333 min. This time range is higher than the first run's treated IVA time

range, but is of no significance since the focus is on the relative retention times of treated IVA samples.

In the close up of the chromatogram in Figure 76, at times 1.8-4.0 min, we see some differences and similarities between the first and second GC-FID runs. The first difference is that the untreated curve has a different shape than the untreated curve in the first run. The second difference is the untreated curve's relative position on the retention time axis with respect to the rest of the treated samples. In the first run, the untreated curve hovered over the lower plasma exposure time treatments, while the untreated curve in the second run hovers over the higher plasma exposure time treatments.

Despite these differences, a strong similarity is seen between the first two runs. Except for the 30 sec and 4 min DBD plasma treatments, there is definitely a relationship between higher plasma exposure time and higher GC-FID retention times. Even though the samples were randomly sequenced through the GC-FID, a positive relationship between DBD exposure time and GC-FID retention time was observed. The second similarity between the two runs are the shapes of the treated IVA samples. Once again, an asymmetrical, left-skewed distribution is seen in all treated IVA samples, while a more symmetrical, right-skewed distribution is seen in the untreated IVA samples.

Minor differences aside, the same general conclusion can be made of the first two runs of DBD treated IVA samples through the GC-FID: 1) DBD plasma treatment has an

observable effect on the chemistry of IVA as assessed by changes in retention time 2) a positive relationship between DBD exposure time and GC-FID retention time exists as assessed by seeing increased retention times with increased plasma exposure times in two separate studies, and 3) DBD plasma treatment changes a fairly symmetrical, but right-skewed untreated IVA GC-FID distribution to change into a strongly asymmetrical, left-skewed distribution, which was assessed by mere observation. The similarities and differences between the two runs can be more readily seen in Figure 77:

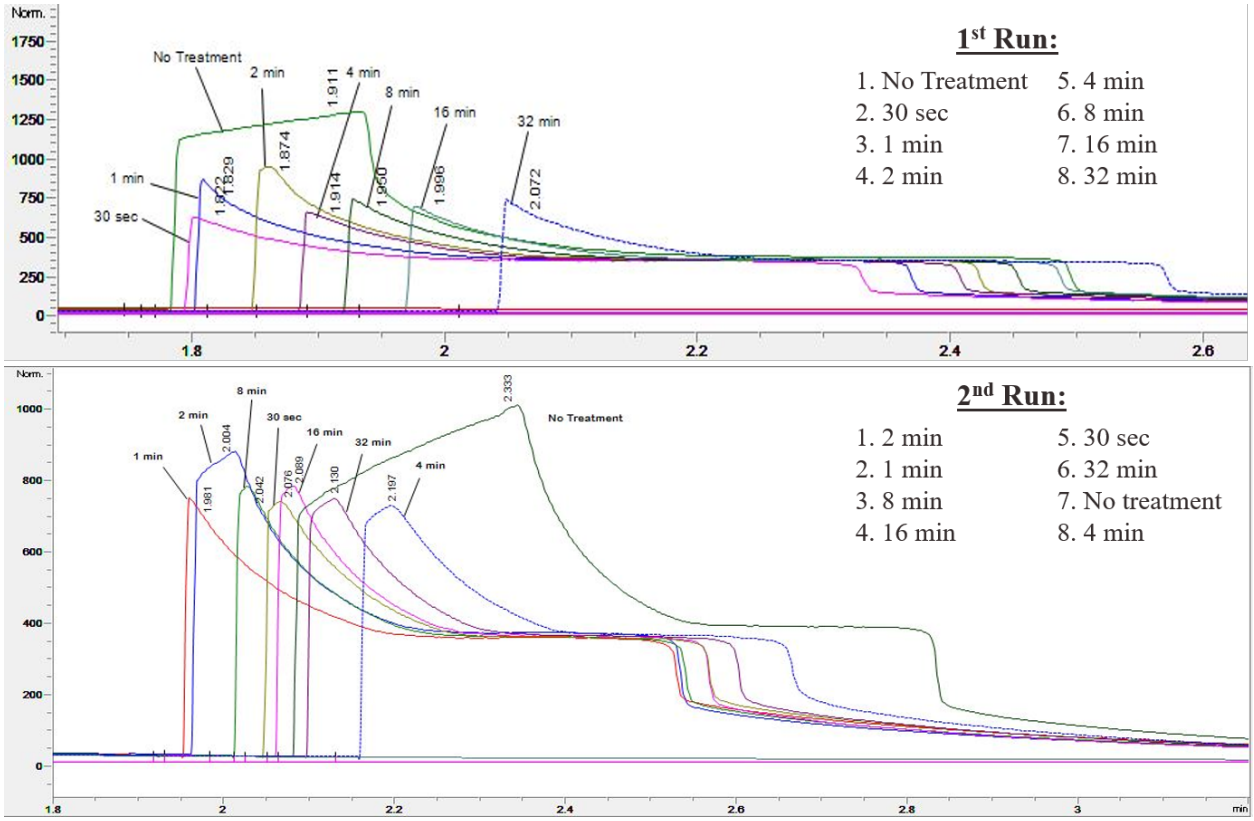

Figure 77: GC-FID chromatogram comparison from both deodorization experiments. Top: GC-FID run of first experiment with samples loaded in chronological order. Bottom: GC-FID run of repeat experiment with samples loaded in randomized order. The sample loading of each experiment is listed on the right side of each chromatogram. With a few exceptions, the overall trend is the same: longer DBD exposure times led to higher IVA retention times.

The second part of the fourth experiment consisted of passing the same samples that were sequenced through the GC-FID, through the GC-MS. In other words, from one DBD treated sample vial, two sets of samples were made. One set of samples went through the GC-FID, while the second set of samples went through the GC-MS. For the GC-MS run, the samples were passed through in a randomized order. The results of the GC-MS run are shown in Figure 78 (gas chromatogram) and Figure 79 (mass spectra) below.

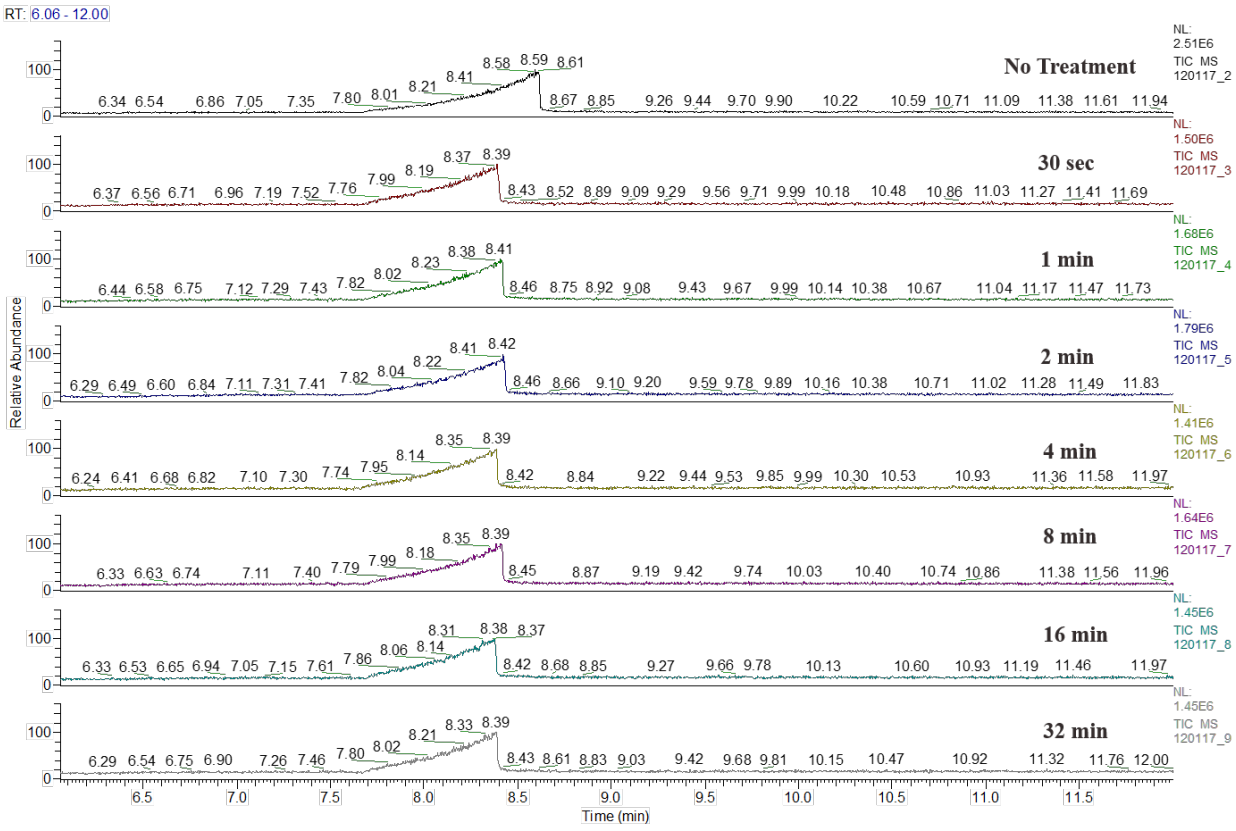

Figure 78: GC-MS Chromatograms of DBD-treated IVA samples. According to these chromatograms, the 0.85 W/cm^2 DBD plasma treatment had zero effect on the retention time of IVA, regardless of treatment time. Treatment times are labeled in black text on the right side of each chromatogram.

In Figure 78, the untreated IVA samples had a longer retention time than all treated IVA samples. Also, it appears that DBD treatment time had an insignificant effect on retention time. These two results directly contradict the earlier finding (with the GC-FID chromatogram) that an increase in DBD treatment time led to higher retention times. Furthermore, all peaks in the gas chromatogram of the GC-MS were strongly asymmetrical and right-skewed. Despite the differences in the chromatograms of the GC-FID and GC-MS, one thing remains constant: direct DBD treatment still appears to have a distinguishable effect on IVA chemistry.

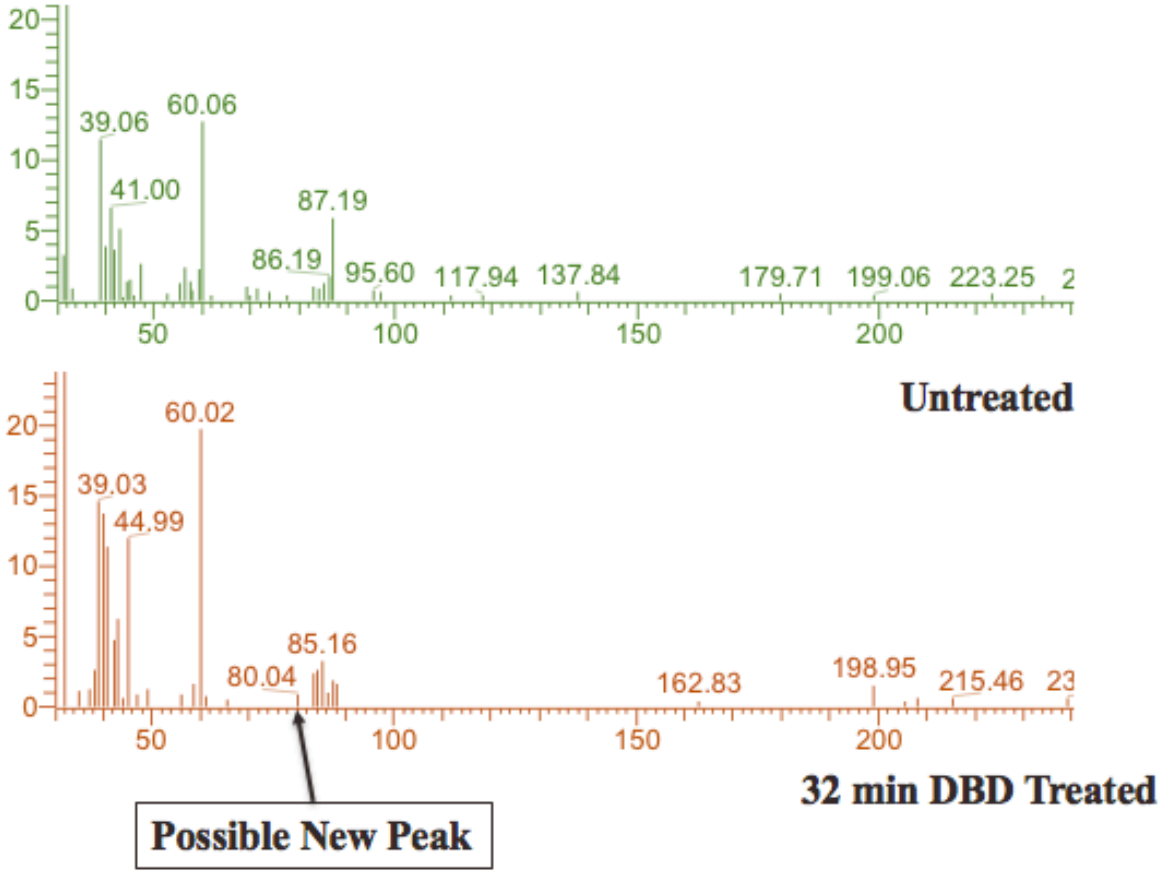

Figure 79: Mass spectrograms of untreated and 32-min, 0.85 W/cm2 DBD treated IVA. A new peak was noticed at 80.04 m/z. Furthermore, the abundance of 60.02 m/z is higher in the treated sample.

Figure 79 shows the mass spectra at the beginning (retention time of 7.7 min) of the peak distributions in the untreated and 32-min treated IVA samples shown in Figure 78. At this retention time, the 32-min treated IVA sample has a new peak at 80.04 m/z, but lacks the peaks at 95.60, 117.94, 137.48 m/z seen in the untreated IVA sample. This missing mass, in the 32-min treated IVA samples, appears to accumulate in the lower m/z side, most notably in the 39.03, 44.99, and 60.02 peaks. This leftward shift in the mass spectra hints at an altered IVA chemical structure. The rest of the peaks, in both mass spectrograms, have been regarded as noise.

Figure 80 shows the mass spectrograms at the end of each of the untreated and 32-min treated IVA samples in Figure 78. Once again, there appears to be a leftward-shift in the mass spectra distribution after a 32-min direct DBD plasma treatment of IVA. For instance, the peaks at 43 and 87 m/z increase by approximately 28% and 54%, respectively. This increase is considerable, and further supports the idea that the plasma species of a low temperature, atmospheric plasma can alter the chemical structure of isovaleric acid. If this is indeed true, then plasma can potentially change or eliminate the cheesy, sweaty smell of isovaleric acid.

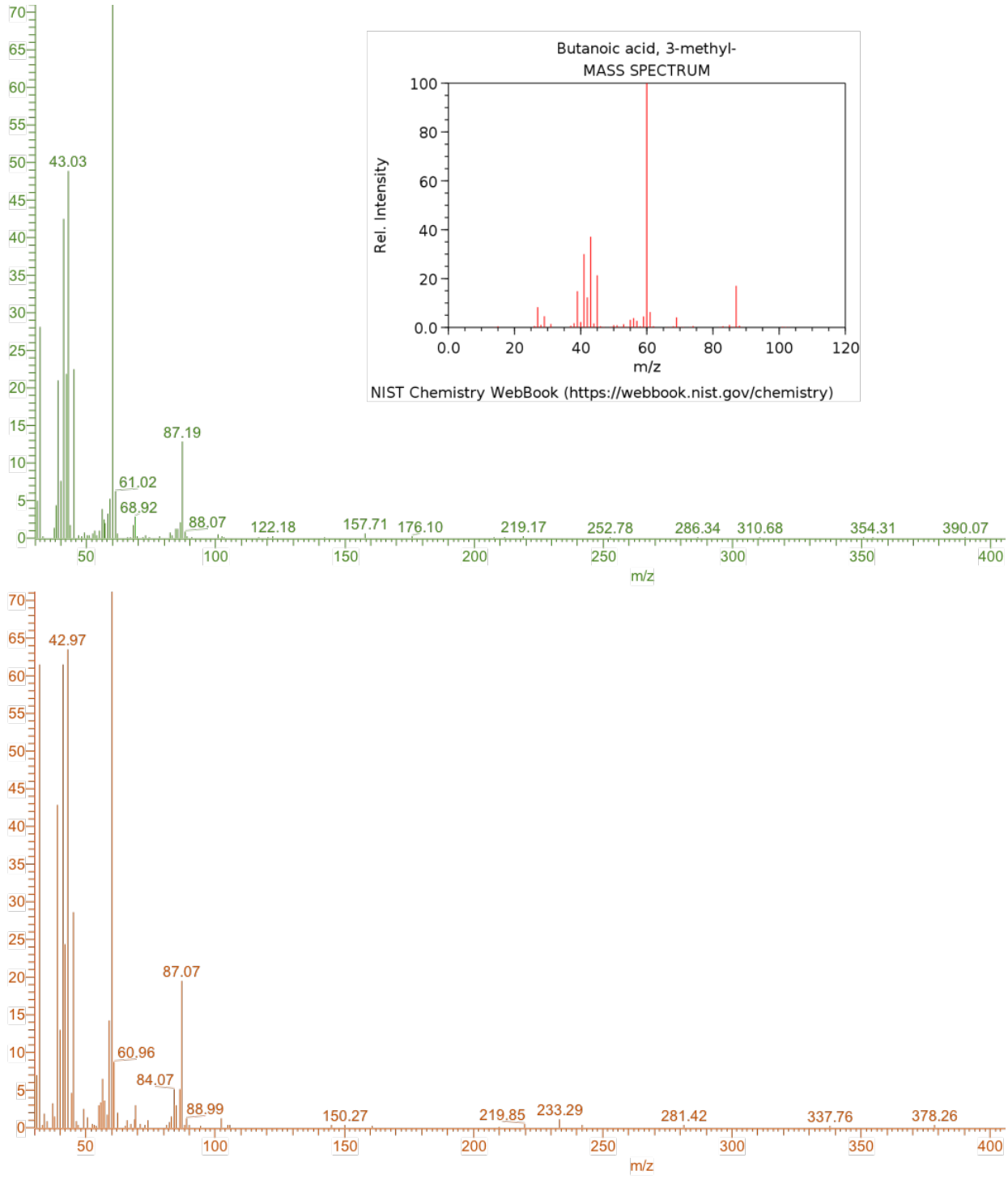

Figure 80: Entire mass spectrogram of untreated and 32-min 0.85 W/cm^2 DBD treated IVA. Green: mass spectrogram of untreated IVA at a retention time of 8.6 minutes. Orange: mass spectrogram of 32-min 0.85 W/cm^2 DBD treated IVA at a retention time of 8.39 minutes. Both spectrograms have a similar peak pattern as the mass spectrum of isovaleric acid (same as 3-methyl butanoic acid) obtained from NIST Chemistry WebBook.

Lastly, Figure 81 shows an overlay of all the treated mass spectrograms at the beginning of their gas-chromatogram profiles (retention time of 7.7 min). This figure is included to highlight that although the gas-chromatograms of treated samples did not change across varying treatment times with the GC-MS, the mass spectrograms did. For example, the 60 m/z peak of the 32-min treated IVA sample is conspicuously higher than the peaks of the remaining treatment times. The same can even be said of the main peak around 38-42 m/z. In conclusion, results from both the GC-FID and GC-MS prove that direct DBD treatment of IVA-wetted merino wool had a discernable chemical effect on the structure of IVA, and that plasma exposure time is an important parameter.

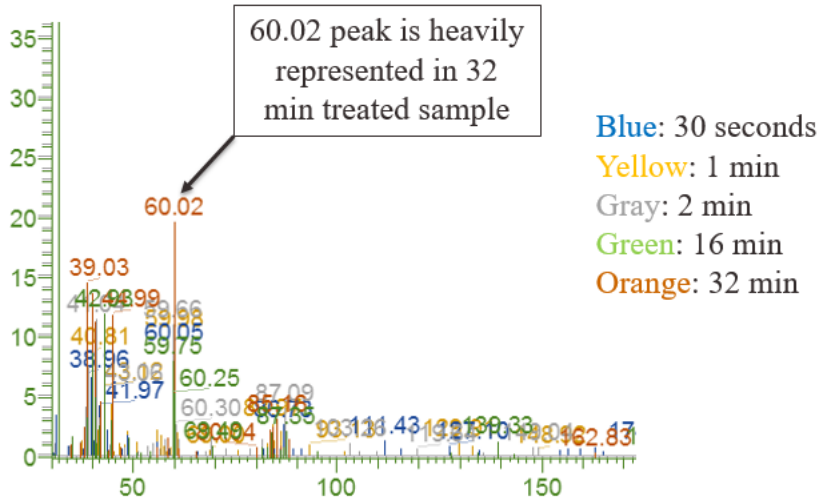

Figure 81: Overlaid mass spectrograms of selected DBD treatment times. The 32-min 0.85 W/cm^2 DBD treatment had a considerably higher peak at 60.02 m/z. This result seems to reestablish the idea that plasma treatment time is an important parameter in changing IVA chemistry. In particular, it shows that a 32-min long DBD treatment was able to create a higher proportion of fragments of 60.02 m/z.

This part of the deodorization study used completely wetted blue merino wool samples for the analysis. The purpose of this was to "see" untreated IVA, alongside the treated IVA, in each of the treated samples' gas chromatograms and mass spectrograms. This

would hypothetically allow each treated sample to have a built-in control group for better analysis. Unfortunately, the change imparted by the DBD plasma treatment was not as drastic as initially assumed, and the profiles or spectra of the untreated and treated IVA seemed to have overlapped.

4.6.3 Direct DBD Treatment of IVA-Spot-Wetted Merino Wool

The fifth experiment of the deodorization study used fabric samples that were spot-wetted with 20 uL of pure isovaleric acid. Additionally, because the effect of power density on IVA deodorization had yet to be explored, the fifth experiment tested samples at higher power densities. In earlier experiments, it was found that cotton did not discolor or burn at higher power densities. This is an important characteristic, as it reduces the possibility of other, unaccounted chemicals distorting or disrupting the effect of a DBD plasma treatment on pure IVA. Since blue merino wool fades and discolors at power densities higher than 30-40%, cotton (from commercially available cotton shirts) will be used as the fabric instead.

In this experiment, white cotton fabric samples were spot wetted with 20 uL of pure isovaleric acid. This was done by first placing the cotton circle over the circular aluminum electrode, sliding the nylon fabric holder over to keep the cotton fabric secure, and dropping two 10uL drops of pure IVA onto the center of the stretched cotton fabric. (The 20 uL volume was chosen because lesser volumes had final concentrations below the

detection limit of the GC-FID). The IVA was placed at the center of the cotton fabric to ensure that all the IVA would be “seen” by the plasma species during the direct DBD treatment. After wetting a single cotton fabric with IVA, it was immediately placed 1mm underneath the DBD reactor, at a specific power density (either 0.85, 1.27, 1.70, 2.13, and 2.55 W/cm^2), for 20 minutes. This was then repeated for all remaining samples.

Directly after the DBD plasma treatment, the fabrics were placed into 4 mL DCM solvent baths. The volume of the bath (4 mL) was chosen for two reasons. The first reason was to keep the solvent volume as small as possible to keep IVA concentrations high. The second reason is to ensure that the solvent (DCM) can fully cover the treated cotton fabric. This last reason is important for extracting as much of the IVA on the treated cotton fabric as possible. After 1 hour of sitting in the DCM solvent bath, the samples were individually passed through a pre-pleated filter paper (pore size < 2um), and randomly sequenced through the GC-FID. To determine the approximate concentration change of IVA in the treated samples, known concentrations of DCM diluted, untreated IVA were also passed through the GC-FID. A control was also included, which had the same concentration as the theoretical maximum concentration of IVA on the yet-to-be-treated cotton fabric. The results of this experiment are shown in Figure 82.

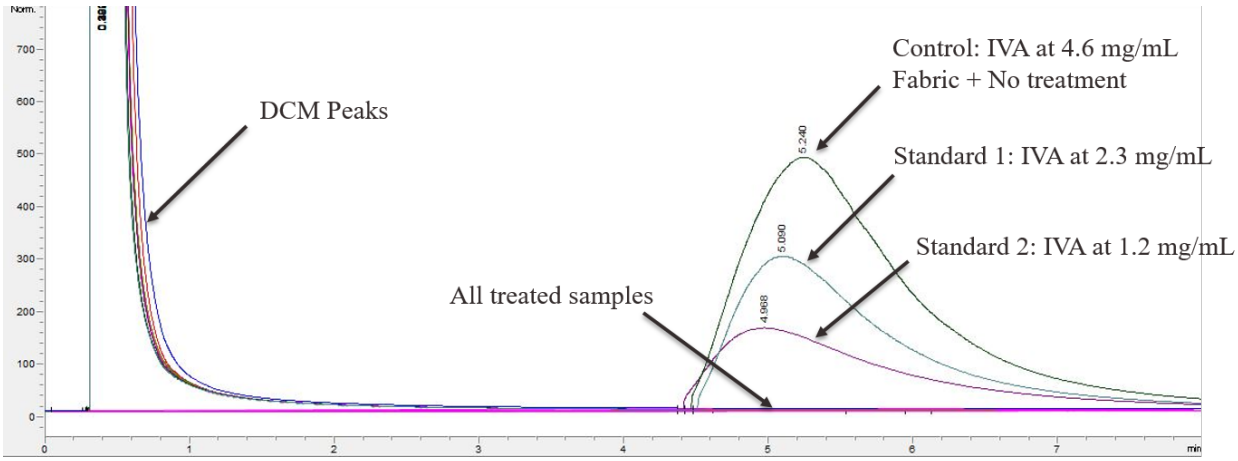

Figure 82: GC-FID chromatogram of IVA spot wetted cotton fabrics. Left peaks are the DCM solvent present in every sample. Towards the right are treated and untreated IVA samples. According to this chromatogram, a 20-min DBD treatment at varying power densities (0.85, 1.27, 1.70, 2.13, and 2.55 W/cm^2) was able to eliminate or substantially reduce the initial concentration of IVA.

In Figure 82, we see the DCM peaks of both treated and untreated samples, as well as the control and two standards. Once again, the DCM peaks have a fairly constant retention time (.399 min), which provides validity to any retention time variation across treatments. As it turns out, however, all plasma treated samples had an IVA concentration below the GC-FID detection limit. This is direct evidence that a direct DBD plasma treatment can eliminate odorous, organic compounds such as isovaleric acid.

Furthermore, it seems as if the critical treatment to eliminate 4.6 mg/mL of isovaleric acid is a DBD plasma treatment that has a 1mm gap distance, a power density of 0.85 W/cm^2, with a total exposure time of 20 minutes. This information was gathered from analyzing the chromatogram of that specific treatment (shown in Figure 83). Unlike other chromatograms which have a declining, asymptotic profile, the .85 W/cm^2, 20 min, 1mm DBD treatment's chromatogram showed signs of a marginal IVA concentration near 5.5-

6.0 minutes in Figure 83. This finding is very important because it shows 1) IVA can be eliminated from fabrics, 2) power density is an important parameter (as is treatment time) in the deodorization of IVA, and 3) specific concentrations of IVA (i.e. 4.6 mg/mL) require specific DBD plasma treatments (.85 W/cm^2, 20 min, 1mm). Most important of all is if soiled socks, and other garments, have a concentration of IVA less than 4.6 mg/mL, then it is very likely that we have found a promising alternative to traditional laundering methods.

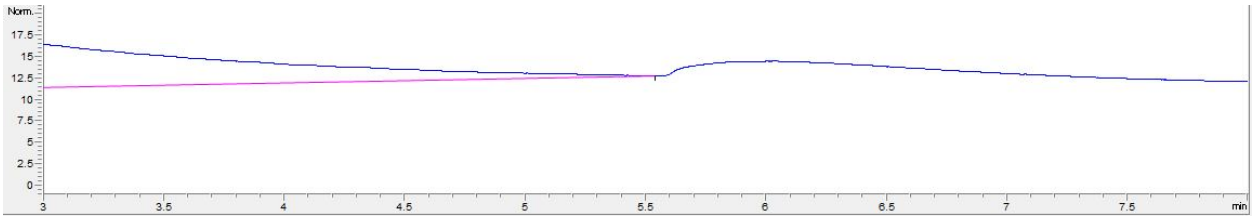

Figure 83: Single GC-FID chromatogram of 4.6 mg/mL IVA treated with a 20-min 0.85 W/cm^2 DBD plasma treatment. The slight bump near retention time of 5.5 min suggests that a 20-min 0.85 W/cm2 DBD treatment may be sufficient to reduce a lower starting concentration of isovaleric acid below the average human threshold detection limit.

To further validate and confirm the results, a new experiment was run. This time, power density was held constant at 0.85 W/cm^2, while blue merino wool samples were treated for 1, 2, 5, 10, 20 minutes. In addition to these five samples, a control and two standards were used. The exact same procedures as the previous study were followed, with some exceptions: standard 1 was made at 4.6 mg/mL of IVA in DCM, while standard 2 was made at 2.3 mg/mL of IVA in DCM. The control was made by placing a blue merino wool sample over the aluminum electrode, and dropping 20 uL of pure IVA. After 1 minute, the control was removed from over the aluminum electrode and placed into a vial containing

4 mL of DCM. Theoretically, the reconstituted concentration of the control would be close to standard 1, but less due to extraction efficiencies.

All eight samples were randomly passed through a GC-MS. The raw data chromatograms are available in the appendix. Figure 84 shows the rate data for the chemical interaction between a 0.85 W/cm^2 DBD plasma and isovaleric acid, as well as the relative IVA concentration with respect to treatment duration. Both plots show that there is a substantial decrease in the concentration of isovaleric acid, and that this elimination process is directly proportional to total DBD exposure time. The left plot shows that the chemical rate constant is 0.083 min^{-1}, with a correlation coefficient of -.98. The right plot of Figure 84 shows that a 10 min, 0.85 W/cm^2 DBD treatment was able to reduce the control IVA concentration (approximately 3.26 mg/mL) by 92%. Furthermore, a 20 min, 0.85 W/cm^2 DBD treatment was able to reduce the starting concentration by 97%.

While it is not known how exactly DBD plasmas eliminate IVA, the importance of this result is that it proves atmospheric, low temperature plasmas can eliminate body odor molecules. These results also indirectly corroborate the previous results (Figure 82 and 83) since the 20-min 0.85 W/cm^2 DBD treatment yielded only a slightly detectable solution of IVA for both the GC-FID and GC-MS analyses.

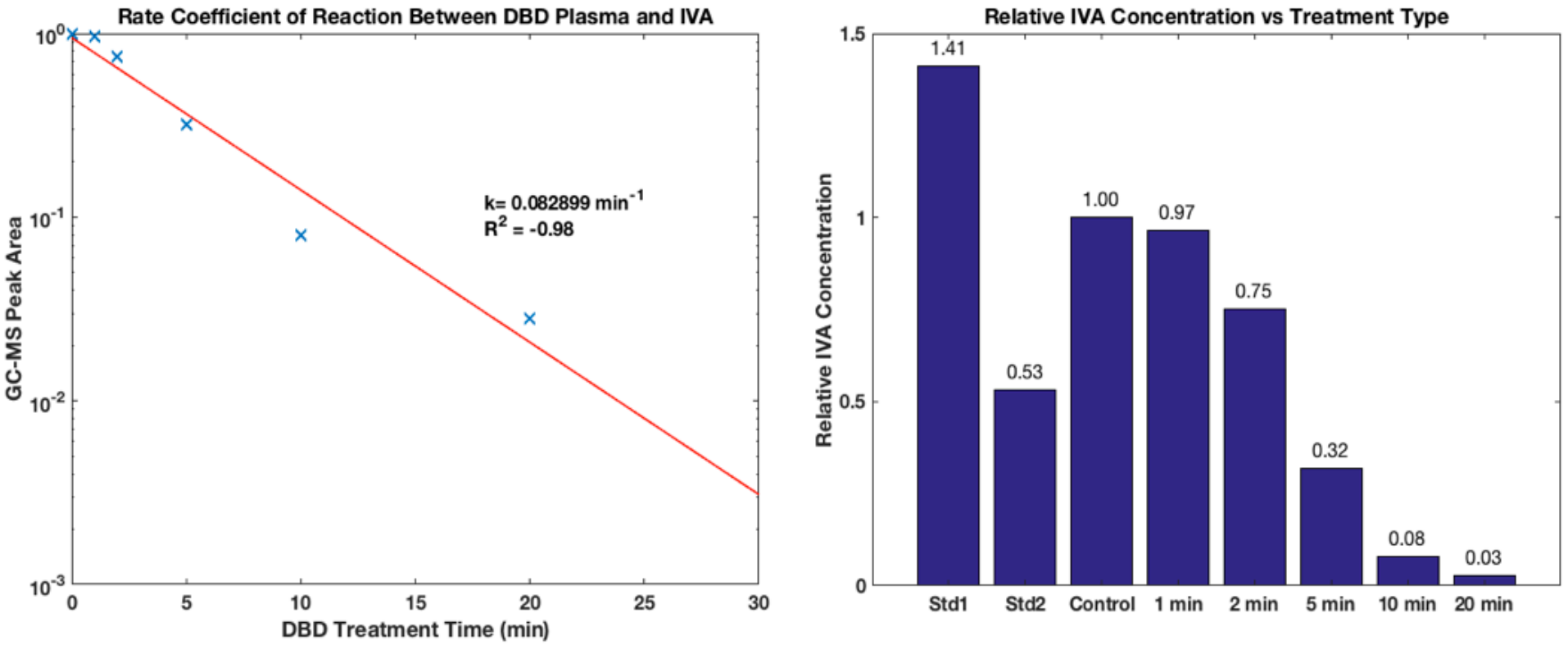

Figure 84: DBD-Isovaleric Acid Reaction Rate Data. These two plots were generated using peak area percentages of GC-MS chromatograms. Left plot shows a linear relationship between the log of peak areas and DBD treatment time. The slope of this line is the rate constant, and was determined to be 0.083 min^{-1}. This appears to be a very accurate determination of the rate constant since the correlation coefficient across 5 different experiments of varying times turned out to be approximately -.98. The plot on the right shows the peak areas of each GC-MS sample with respect to the peak area percentage of IVA. In other words, the relative IVA concentration of the control is 1.00. Standard 1 has a higher relative IVA concentration since it did not suffer from any IVA-fabric extraction efficiencies. The 10-min DBD treated sample had a peak area that was 92% lower than the control peak area.

5. DISCUSSION

This research project began with the question of whether low temperature plasmas could be used to disinfect and deodorize soiled clothing. The first step in tackling this broad question was determining what effect—if any—the low temperature plasmas would have on merino wool. This step would serve to answer if low temperature plasmas were compatible with merino wool. Merino wool was chosen as the first fabric to test since NASA has thought of replacing astronaut's cotton shirts with the superior breathability and odor-resistance of merino wool. While the focus was on merino wool, cotton and modacrylic were briefly studied for comparative study and thoroughness.

To check the compatibility of merino wool with low temperature plasmas, the merino wool was exposed to a 1.27 W/cm^2 DBD plasma for 30 seconds. These parameters were chosen to use DBD plasma settings that were proven successful in fully inactivating a 10^4 CFU/mL culture of *D. radiodurans* [11]. The result was positive. The blue merino wool did not show any visible signs of discoloration or disintegration and showed that an extremophile like *D. radiodurans* could potentially be treated on the surface of merino wool.

This first experiment showed that DBD plasmas could safely disinfect merino wool, but did not address whether this same DBD plasma setting could be used to deodorize a merino wool sample. To answer this question, an important assumption was made to

simplify the experiment: the time needed to fully deodorize a fabric sample should be proportional to the time needed to fully change the wettability of that fabric sample. This thought was based on the fact that deodorization and wettability changes are both surface treatments. This transformed the question of “how much time is needed to deodorize merino wool” to “how much time is needed to make merino wool hydrophilic”.

As the results in Figure 25 show, a 30-sec, 1.27 W/cm^2 DBD plasma treatment was not enough to produce a full wettability change in the merino wool sample. The treatment was only able to slightly reduce the contact angle of the 10uL water droplet. However, increased DBD plasma exposure times correlated with smaller contact angles. It was later found that a full two-minute treatment of a 1.27 W/cm^2 DBD plasma was needed to effect a complete wettability change on the surface of the merino wool closest to the DBD reactor.

At this time, it was unclear if the backside of the merino wool sample (the side closest to the aluminum electrode) was also displaying hydrophilicity after a 2-min 1.27 W/cm^2 DBD plasma treatment. To ensure the wettability changes were distributed on both sides, a backside contact angle test was made. Though the 10 uL water droplet absorption process was different than on the side closest to the DBD reactor, the outcome was the same—complete absorption of the water droplet by the previously hydrophobic merino wool fabric. These tests showed that after two minutes, a DBD plasma was capable of completely changing the wettability of the entire surface (exposed and unexposed) of a merino wool clothing sample. Indirectly, this result suggests that DBD plasmas may be

capable of simultaneously deodorizing the exposed and unexposed surfaces of a fabric sample.

After 2-min, 1.27 W/cm^2 DBD plasmas showed their ability to change the wettability of merino wool and penetrate the thickness of the merino wool, a 50 kGy electron beam and a 0.016 W/cm^2 low pressure plasmas were tested for comparative reasons. The LPPR treatment changed the wettability of the blue merino wool, and was capable of penetrating a stack of six fabric samples after 15 min. Shorter LPPR times (1-2 min) were not able to produce wettability changes in the unexposed surfaces of the fabric as the DBD reactor did. This result was expected since the plasma species density is considerably lower in the LPPR. The 50kGy electron beam treatment did not change the wettability of the merino wool at all, which seems to indicate that electrons within the low temperature plasmas play no role in the wettability changes.

The two-minute requirement to fully change the wettability of the merino wool begged for a closer look into what additional material properties were changing after the DBD plasma treatment. Before investigating other material properties, the lifetime of the wettability change was assessed. It was found that this property change was temporary, with original contact angles being seen 3-4 days after DBD plasma treatment. This observation was not DBD specific. LPPR treated fabrics also showed hydrophobicity days after treatment. The exact mechanism behind the wettability change of merino wool is unknown, but it is believed that plasma-synthesized, hydrophilic species coat the surface of the treated substrate and gradually dissipate over time.

The second material property investigated was plasma-resistance and/or plasma-compatibility. In other words, it was important to understand merino wool's response to an overexposure of low temperature plasma. Understanding this plasma-resistance would help form the borders of a plasma-compatibility envelope. Blue merino wool was exposed to the same DBD plasma (1.27 W/cm^2 at a 1 mm gap distance) for 15 minutes, and noticeable changes were immediately visible after treatment (Figure micrographs, pilling, SEM, overview). Clearly, a 15-min 1.27 W/cm^2 DBD treatment was the upper limit of the plasma-compatibility envelope. The color change from bright blue to dull blue to orange was unexpected. The noticeable pilling was unfortunate as it signified mechanical damage to the merino wool fibers. While certain spots on the merino wool surface showed unpleasant effects (Figure overview), the majority of the merino wool did not show the same degree of severity. This is confirmed in SEM images of the 15-min 1.27 W/cm^2 DBD treated blue merino wool. It was interesting to see that the merino wool did not show any signs of acidic or alkali attack, as is reported in the literature. This suggests that the plasma-induced damage must be occurring in a pH neutral environment.

Surprisingly, the qualitative results obtained for blue merino wool could not be replicated for black merino wool. In fact, the drastic results seen for blue merino wool were also absent in white cotton and green modacrylic after identical DBD treatments. After 15 minutes of a 1.27 W/cm^2 DBD treatment, the only change observed for black merino wool and green modacrylic was a slight-to-moderate degree of pilling. Cotton did not display any visible pilling. These findings suggested that blue merino wool had undergone a dye-

specific reaction with the 15-min 1.27 W/cm^2 DBD plasma, which initially made DBD plasmas seem more harmful than actuality.

Regardless of fabric color, a 15-min 1.27 W/cm^2 DBD plasma caused a macroscopic change (i.e. pilling) in fabric quality. On the microscopic level, this treatment showed significant disintegration of the merino wool's cuticle and the formation of a wax-like substance. These negative changes are sufficient to discourage the treatment of fabrics with 1.27 W/cm^2 DBD plasmas for more than 15 minutes. It may also be safe to assume that 15-min 1.27 W/cm^2 DBD treatments may be plasma exposure limit of most fabrics.

The photos, optical micrographs, and SEM images of the 15-min 1.27 W/cm^2 DBD treated blue merino wool provided significant qualitative evidence that DBD plasmas could impart considerable damage to merino wool if not properly controlled. To provide quantitative data—and to also gather more information on alternative laundering solutions—DBD, LPPR, and E-beam treated fabrics (blue merino wool, black merino wool, white cotton, and green modacrylic) were tensile tested according to ASTM D5035.

The tensile testing provided valuable insight on the importance of the correct plasma washing the correct fabric—similar to the importance of choosing the correct setting on our washing machines to wash our whites, colors, or delicates. For instance, 1.27 W/cm^2 DBD plasmas prevented the tensile testing of blue merino wool, black merino wool, and green modacrylic because the DBD plasmas repeatedly made holes in those fabrics. However, white cotton was able to better withstand the DBD treatment, which allowed the

tensile testing of DBD-treated cotton. Interestingly, the 2-min 1.27 W/cm^2 DBD treatment of cotton imparted approximately the same amount of damage to the fabric as 20 wash cycles. This result is important since one can assume that DBD treatments of lower power density will not cause unacceptable reductions in tensile strength or ductility.

The LPPR treatment had the most wide-ranging effect on fabrics. It strengthened the blue merino wool by +20% (even the median max load increased by an estimated +20%), caused no changes in the strength and ductility of black merino wool, reduced the ductility of cotton by as much as the DBD treatment (-20%), and caused a 23% drop in the tensile strength of green modacrylic. In contrast, E-beam treatment did not affect the strength and ductility of any fabric, with one minor exception: E-beam treated cotton had a 11% reduction in ductility, while experiencing zero changes in its strength. It is apparent by the variability of the mechanical behavior changes of different fabrics to different treatments that the preferred fabric for astronauts will depend on the type of plasma chosen.

While tensile data on DBD treated merino wool is lacking, it can be assumed that DBD treated merino wool would have seen sharper reductions in tensile strength than cotton's 40% drop. This motivated the search for softer plasma treatments. The tensile test data suggested that low pressure plasmas would be an appropriate alternative for merino wool laundering since it provided a strengthening effect to blue merino wool and had zero effect on black merino wool. Immediately after the tensile strength study, the disinfection potential of LPPRs was investigated. It was found that a similar LPPR treatment (as the one used in the tensile test study) could provide a CFU log reduction of up to 1.03 on a

E.coli population. This means that a 4-5 min 0.016 W/cm^2 LPPR treatment is capable of inactivating approximately 90% of the bacteria while not negatively affecting the mechanical properties of merino wool.

Continuing the search for a softer plasma treatment, the power density of the DBD reactor was dialed down by 33% to 0.85 W/cm^2, and most of the experiments that were performed at a DBD power density of 1.27 W/cm^2 were repeated at 0.85 W/cm^2. In doing so, it was learned that longer duration DBD treatments at lower power densities were ultimately better than short duration DBD treatments at higher power densities at potentially laundering fabrics. For instance, a 10-min 0.85 W/cm^2 DBD treatment was able to attain a 2.7 CFU log reduction of E.coli, causes minimal changes to the surface morphology of the fibers of blue merino wool, black merino wool, white cotton, and green modacrylic, and is able to reduce the concentration of isovaleric acid by approximately 92%.

6. CONCLUSION

This research project began with the hypothesis that plasmas could facilitate the disinfection and deodorization of soiled clothing. This hypothesis was based on a collection of research papers that documented the disinfection of various bacteria and the elimination of odorous molecules. The unanswered question within the plasma community was whether non-equilibrium plasmas could disinfect and deodorize clothing, without harming the mechanical properties of the fabric. The experiments provided within this report have shown the first proof-of-concept of a plasma-based laundering system.

In fact, two types of low temperature plasmas have emerged as possible space-laundering agents. A 10-min 0.85 W/cm^2 DBD plasma, for example, can provide an E.coli CFU log reduction of 2.7, can reduce the concentration of an actual body odor molecule by 92%, and can do this while causing minimal damage to the fabric. A 4-5 min 0.016 W/cm^2 LPPR plasma, on the other hand, can provide an *E.coli* CFU log reduction of up to 1.03, and can do so without either negatively affecting the tensile strength or ductility of the treated merino wool or causing any changes to their microstructure.

The implications of these results are far-reaching, as this technology could someday be implemented on spacecraft designed for long-duration space missions and save space agencies a tremendous amount of logistical and financial resources as we begin deep space exploration.

7. FUTURE WORK

The research presented answered many questions related to plasma's ability to launder soiled clothing. However, many questions still remain before an actual plasma laundering system can be implemented on spacecraft. These questions are related to five major areas: (1) plasma-fabric compatibility, (2) plasma disinfection, (3) plasma-assisted deodorization, (4) design and engineering, and (5) synthetic fiber research.

Regarding plasma-compatibility, it is worth exploring if indirect DBDs can provide a larger operating envelope than direct DBDs, while still appreciably disinfecting and deodorizing soiled fabrics. It is also important to answer how many "plasma wash cycles" each fabric can sustain from each plasma type (i.e. direct DBD, indirect DBD, low pressure plasma discharge). Also, it would be useful to know whether certain fabric preparation processes make textiles more or less susceptible to plasma species.

Plasma's ability to disinfect is well understood, but it would be useful to attain a 2.7 CFU log reduction (as was achieved with the direct DBD) with the indirect DBD and LPPR—obviously allowing for greater reaction times. In this way, equivalent reaction times can be prescribed for each plasma type to provide greater flexibility in the selection of plasma type onboard the spacecraft.

While the elimination of isovaleric acid was observed after direct DBD treatment, human body odor is a cocktail of small carboxylic acids. This means that low temperature plasmas need to pass the test with other body odor molecules (i.e. propionic acid and methyl hexenoic acid). This includes assessing the capability of indirect DBDs and the LPPR to eliminate isovaleric acid and other odorous molecules. Finally, it is very important to answer the following two questions: (1) can low temperature plasmas deodorize real human body odor and (2) what are the final products of the chemical reaction between the plasma species and human body odor molecules. Hopefully, the products of the reaction are something that the spacecraft's ventilation system will be able to handle. After answering all of the aforementioned, it will then become important to design, build, and operationally qualify an actual plasma laundering prototype.

In the end, the solution to the space laundry problem may require a three-prong approach: the first being the sterilization of the clothes with electron beams pre-launch to reduce the amount of odor-causing bacteria; the second being an effective plasma-based laundry device to disinfect and deodorize; the third being a precisely engineered synthetic fabric that is plasma resistant, which will increase the maximum plasma wash cycles allowed (MPWCA) rating.

8. REFERENCES

[1] Space Wear. Updated April 2, 2003. Retrieved from https://www.spaceflight.nasa.gov/living/spacewear/index.html

[2] Astronauts' Dirty Laundry. Updated June 14, 2003. Retrieved from https://www.nasa.gov/audience/forstudents/k-4/home/wear_feature.html

[3] Dunbar, B. (n.d.). Mars Program Planning Frequently Asked Questions. Retrieved February 23, 2017, from https://www.nasa.gov/offices/marsplanning/faqs/

[4] Escobedo, V. M., Jr. (Ed.). (2016, November 22). Intravehicular Activity Clothing Study (IVA Clothing Study). Retrieved February 23, 2017, from https://www.nasa.gov/mission_pages/station/research/experiments/1084.html

[5] Mosher, Sarah Kramer and Dave. "Here's how much money it actually costs to launch stuff into space." *Business Insider*. Business Insider, 20 July 2016. Web. 22 Feb. 2017.

[6] Kosswig, K. 2000. Surfactants. Ullmann's Encyclopedia of Industrial Chemistry

[7] Eduard Smulders, Wolfgang Rybinski, Eric Sung, Wilfried Rähse, Josef Steber, Frederike Wiebel, Anette Nordskog, "Laundry Detergents" in Ullmann's Encyclopedia of Industrial Chemistry 2002, Wiley-VCH, Weinheim.

[8] Klausing, S. L., Maloney, J, Easter, E., "Evaluating Dimensional Change in Home Laundry.", AATCC Review, 2012, Vol. 12 (6), pp. 51-57;

[9] Buisson, Y. L., Rajasekaran, K., French A. D., Conrad D.C., Roy P.S., "Qualitative and Quantitative Evaluation of Cotton Fabric Damage by Tumble Drying". Textile Research Journal, 2000, Vol. 70 (8), pp. 739-743

[10] Cooper M, G Fridman, and D Staack. “Decontamination of surfaces from extremophile organisms using nonthermal atmospheric-pressure plasmas.” *IEEE Trans. Plasma Sci*, vol. 37, no.6, pp. 866-871, 2009

[11] Kelly-Wintenberg K, TC Montie, C Brickman, and JR Roth. “Room temperature sterilization of surfaces and fabrics with a one atmosphere uniform glow discharge plasma.” *J Ind Microbiol Biotechnol*, vol. 20, pp. 69-74, 1998

[12] M. Laroussi, “Low temperature plasma-based sterilization: Overview and state-of-the-art,” Plasma Processes Polym., vol. 2, no. 5, pp. 391–400, 2005.

[13] Kogelschatz, U. “Dielectric-barrier Discharges: Their History, Discharge Physics, and Inudustrial Applications.” Plasma Chemistry and Plasma Processing, Vol. 23, No. 1, March 2003.

[14] Borcia G, Anderson C, and Brown N. “Surface treatment of natural and synthetic textiles using a dielectric barrier discharge”. Surface & Coatings Technology 201 (2006) 3074-3081.

[15] Kan C, Lam Y, Yuen C. “Microscopic study of cotton fibre subjected to different functional treatments”. Current microscopy contributions to advances in science and technology. (A. Mendez-Vilas, Ed). Formatex 2012. 1130-1136

[16] “Human Body Odor—Etiology, Treatment, and Related Factors”. Inaba M, Inaba Y. 1992.

[17] Ensminger, M. E.; R. O. Parker (1986). Sheep and Goat Science, Fifth Edition. Danville, Illinois: The Interstate Printers and Publishers Inc.

[18] Fippon, J.A. (1992) The Structure of Wool; Chapter 1, In: Wool Dyeing, Lewis, D.M. (Ed.), Bradford (UK): Society of Dyers and Colourists

[19] The Chemical Technology of Textile Fibres: Their Origin, Structure, Preparation, Washing, Bleaching, Dyeing, Printing and Dressing. Von Georgievics, Georg. 2012.

[20] Rippon, J.A. et al, (2003) Wool, in Encylcopedia of Polymer Science and Technology, New York : Interscience Publishers.

[21] Leeder, J.D. (1984) Wool – nature's wonder fibre, Ocean Grove, Vic.: Australasian Textile Publishers, Morton, W.E. and Hearle, J.W.S., [1993] Physical Properties of Textile Fibres, 3rd Ed., Macnhester, UK: The Textile Institute.

[22] Focus on Fabrics, Dorothy Siegert Lyle. Published by National Institute of DryCleaning; Revised edition 1964.

[23] Nonwoven Technical Guide. Cotton Incorporated. Retrieved February 23, 2018, from http://www.cottoninc.com/product/NonWovens/Nonwoven-Technical-Guide

[24] Brissette R. "The Use of Synthetic Modacrylic Fibers". Bulletin of the N.Y. Academy of Medicine. Vol. 43, No.8, August 1967

[25] Tanaka T, Terakado, O, and Hirasawa, M. "Flame retardancy in fabric consisiting of cellulosic fiber and modacrylic fiber containing fine-grained MoO3 particles." Fire Mater. vol. 40, pp. 612-621, 2016

[26] E.P.G. Gohl, L.D. Vilensky, Textile science, Longman Cheshire Pty Limited, 1980

[27] Gas Discharge Physics. Razier, Yuri. P. 1991.

[28] Wang C, Liu Y, Xu H, et al., "Influence of atmospheric pressure plasma treatment time on penetration depth of surface modification into fabric". Applied Surface Science 254 (2008) 2499-2505.

[29] Wang C and Qiu Y. "Two sided medication of wool fabrics by atmospheric pressure plasma jet: Influence of processing parameters on plasma penetration". Surface & Coatings Technology 201 (2007) 6273-6277.

8. APPENDIX

A. Tensile Test Box Plots

A1. Blue Merino Wool

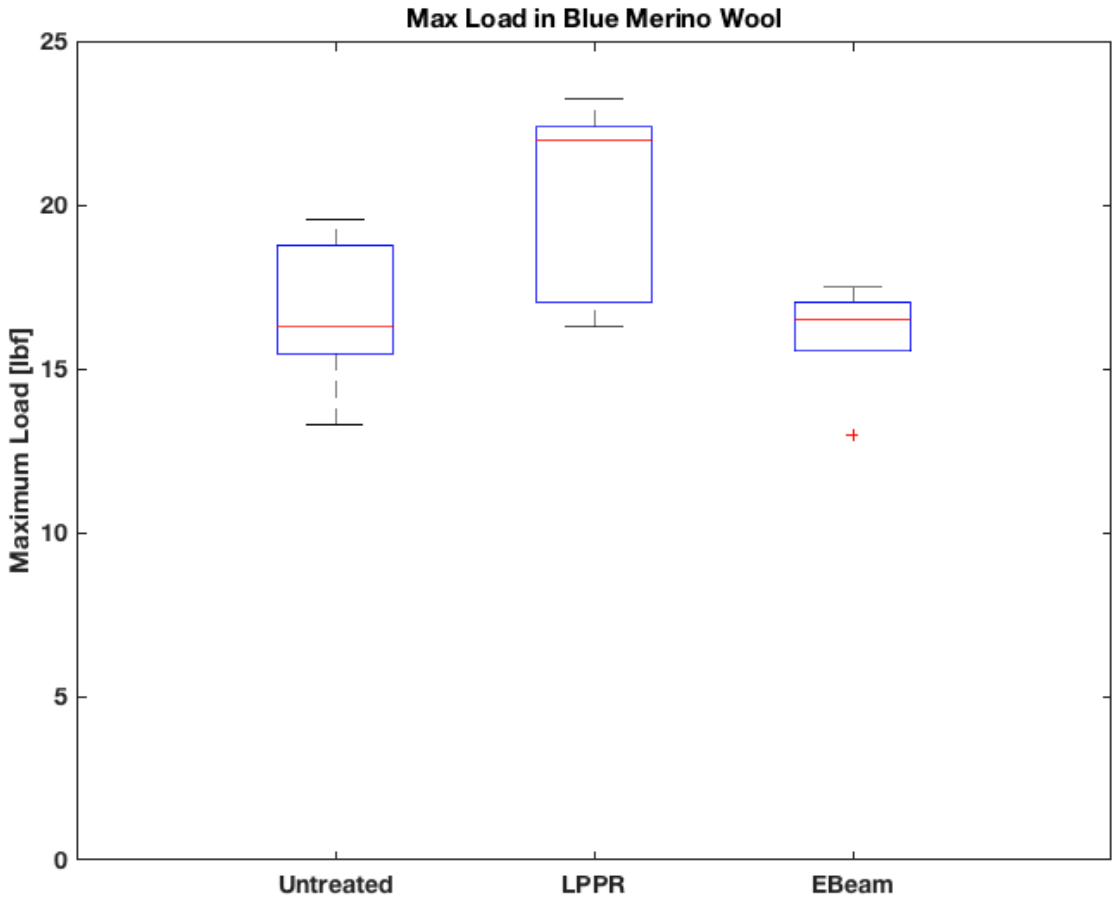

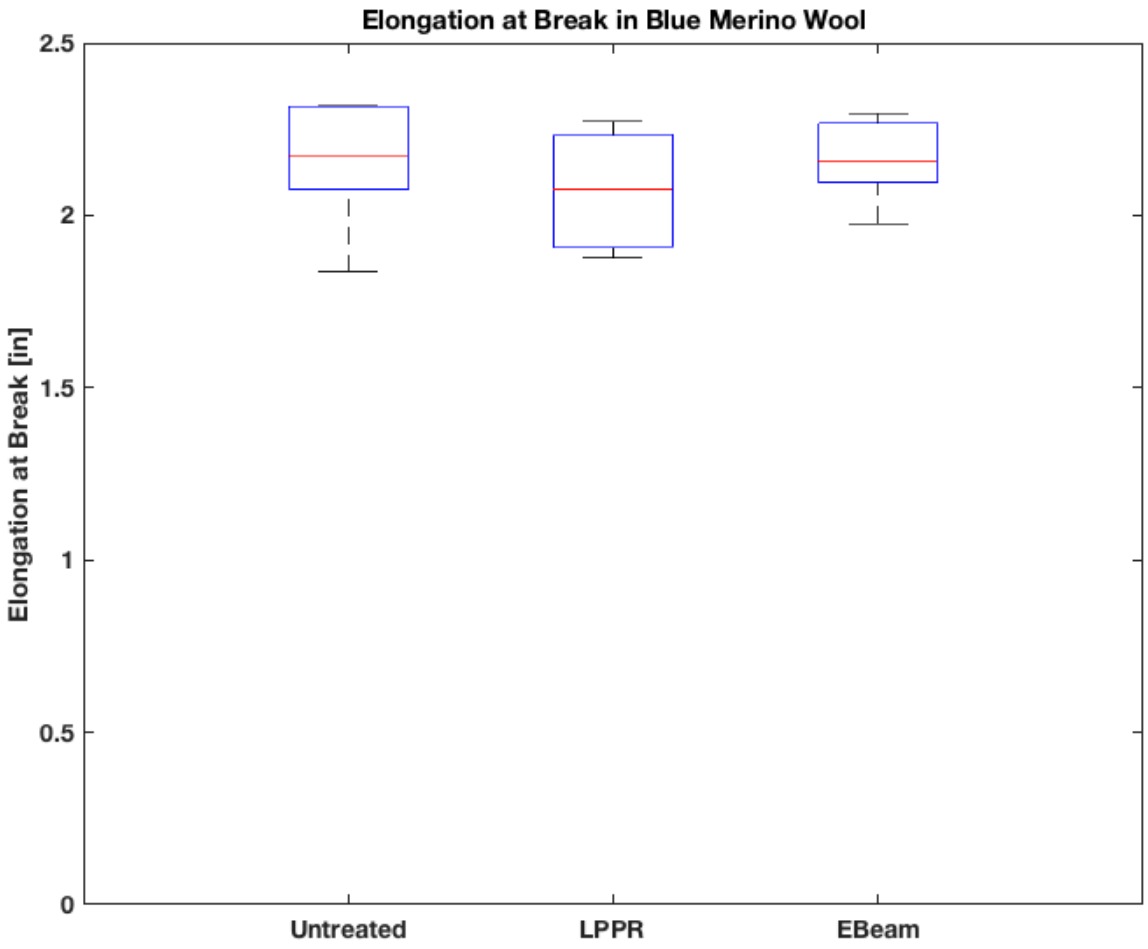
Elongation at Break in Blue Merino Wool
Elongation at Break [in]
2.5
2
1.5
1
0.5
0
Untreated
LPPR
EBeam

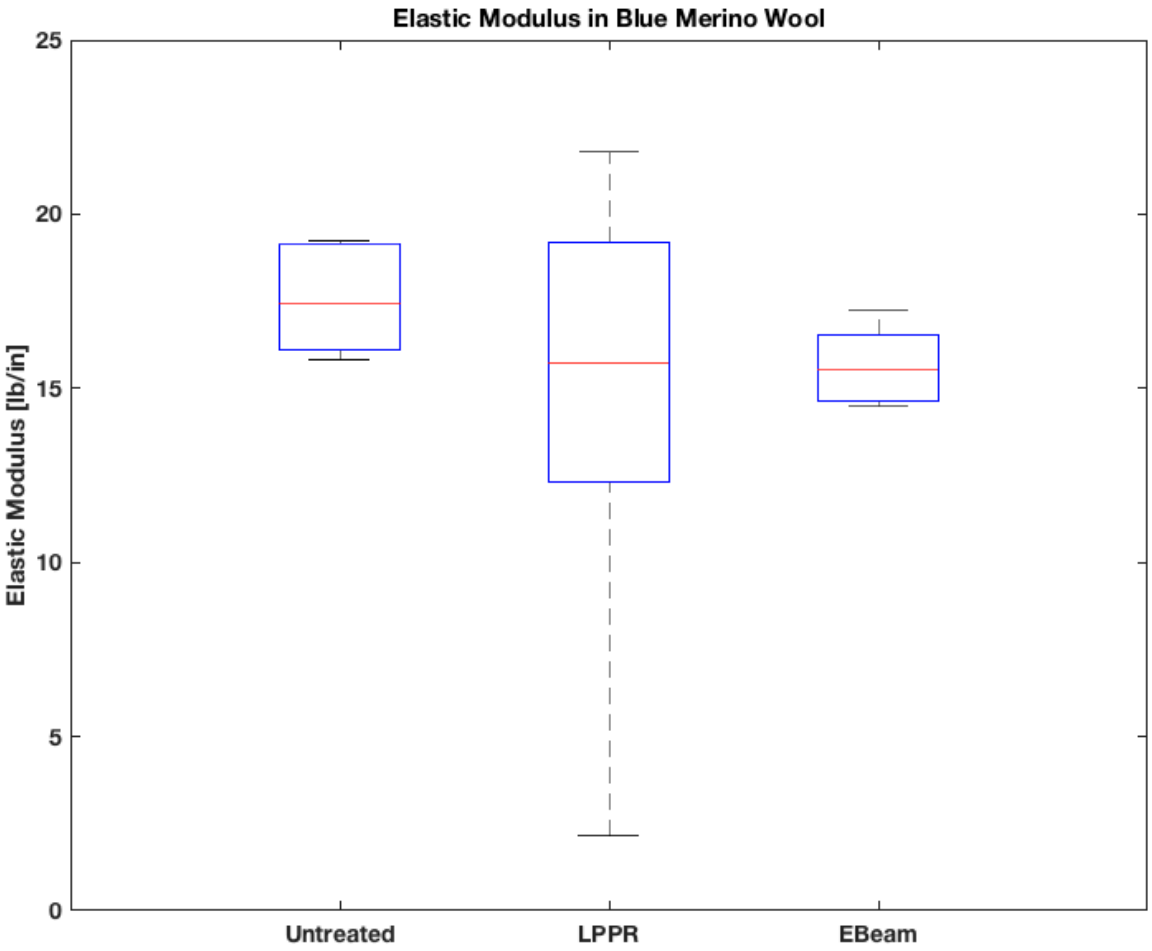
Elastic Modulus in Blue Merino Wool
Elastic Modulus [lb/in]
25
20
15
10
5
0
Untreated
LPPR
EBeam

A2. Black Merino Wool

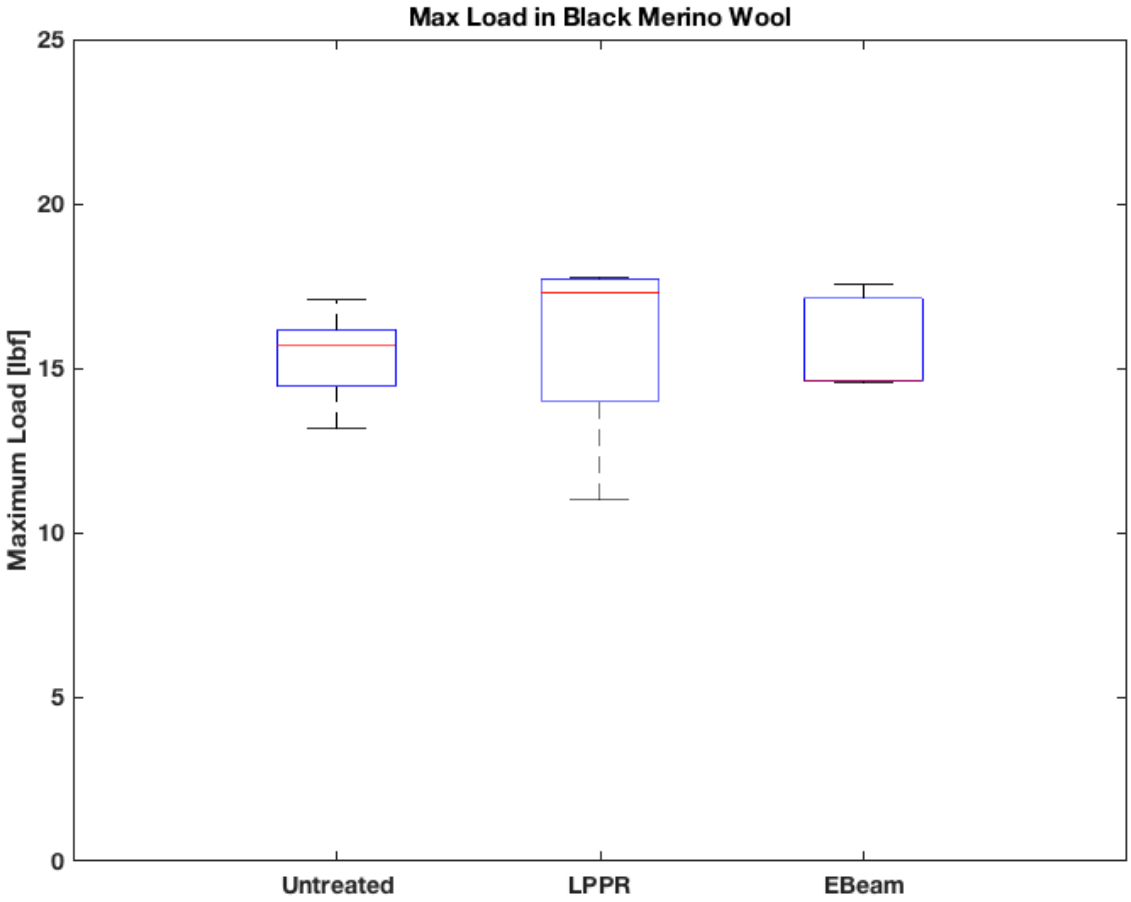

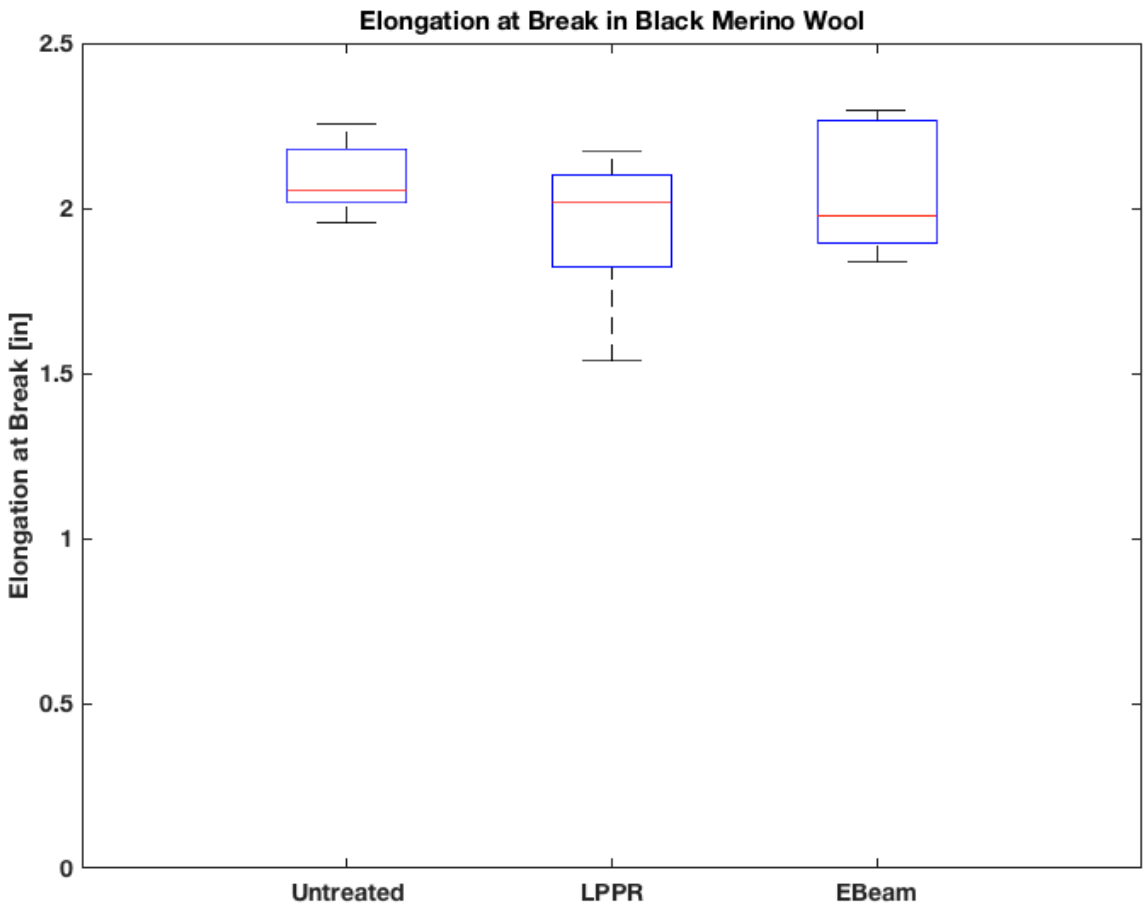
Elongation at Break in Black Merino Wool
Elongation at Break [in]
2.5
2
1.5
1
0.5
0
Untreated
LPPR
EBeam

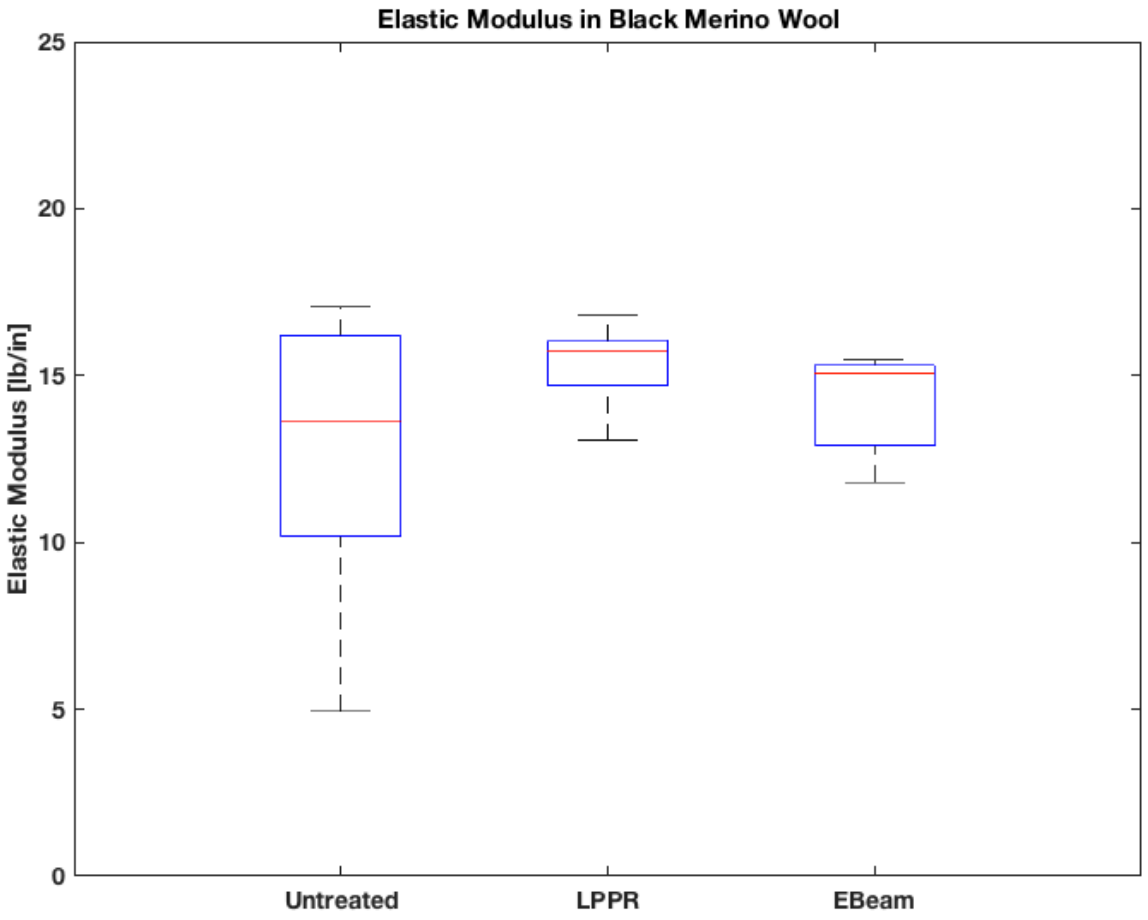
Elastic Modulus in Black Merino Wool
Elastic Modulus [lb/in]
25
20
15
10
5
0
Untreated
LPPR
EBeam

A3. White Cotton

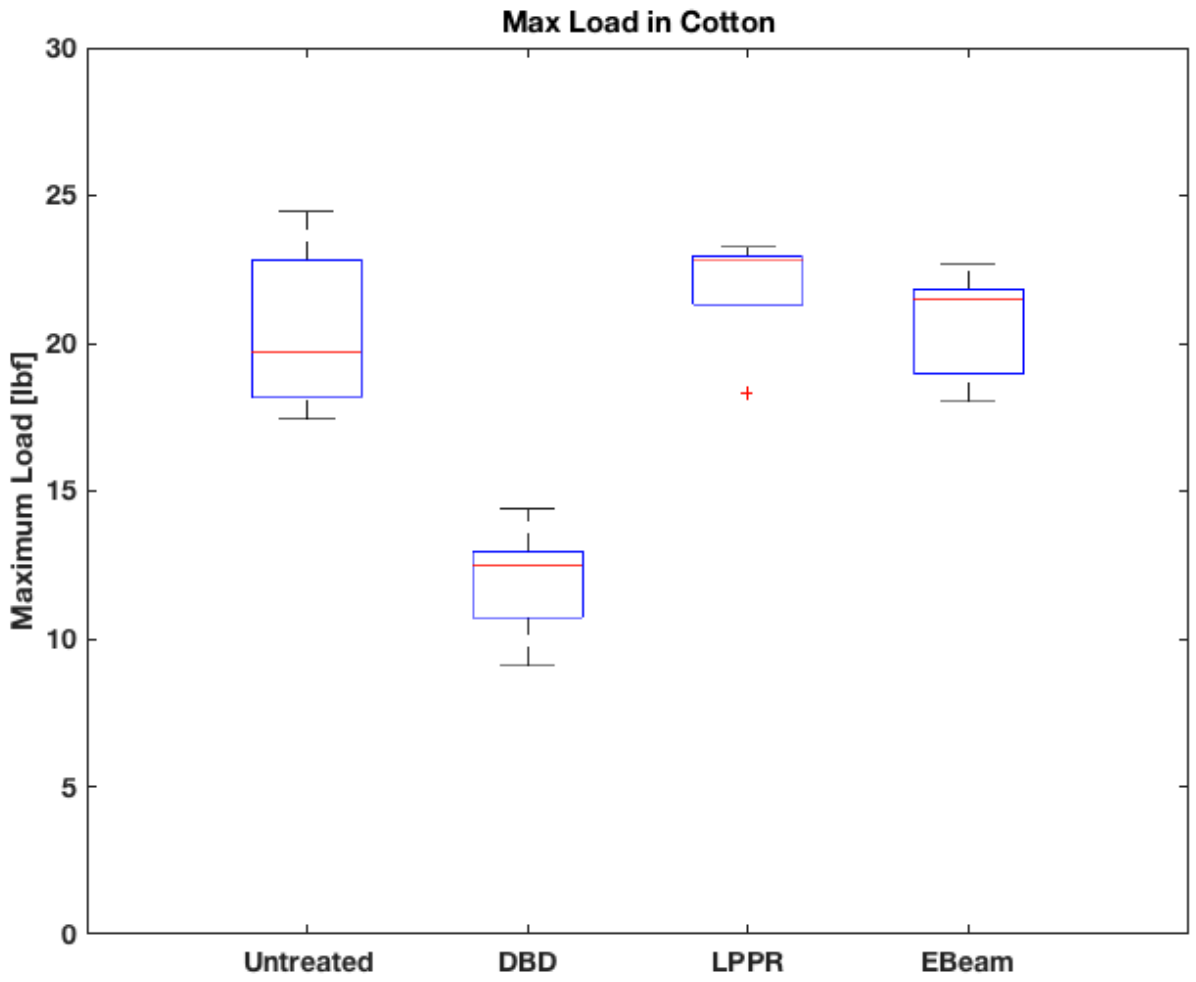

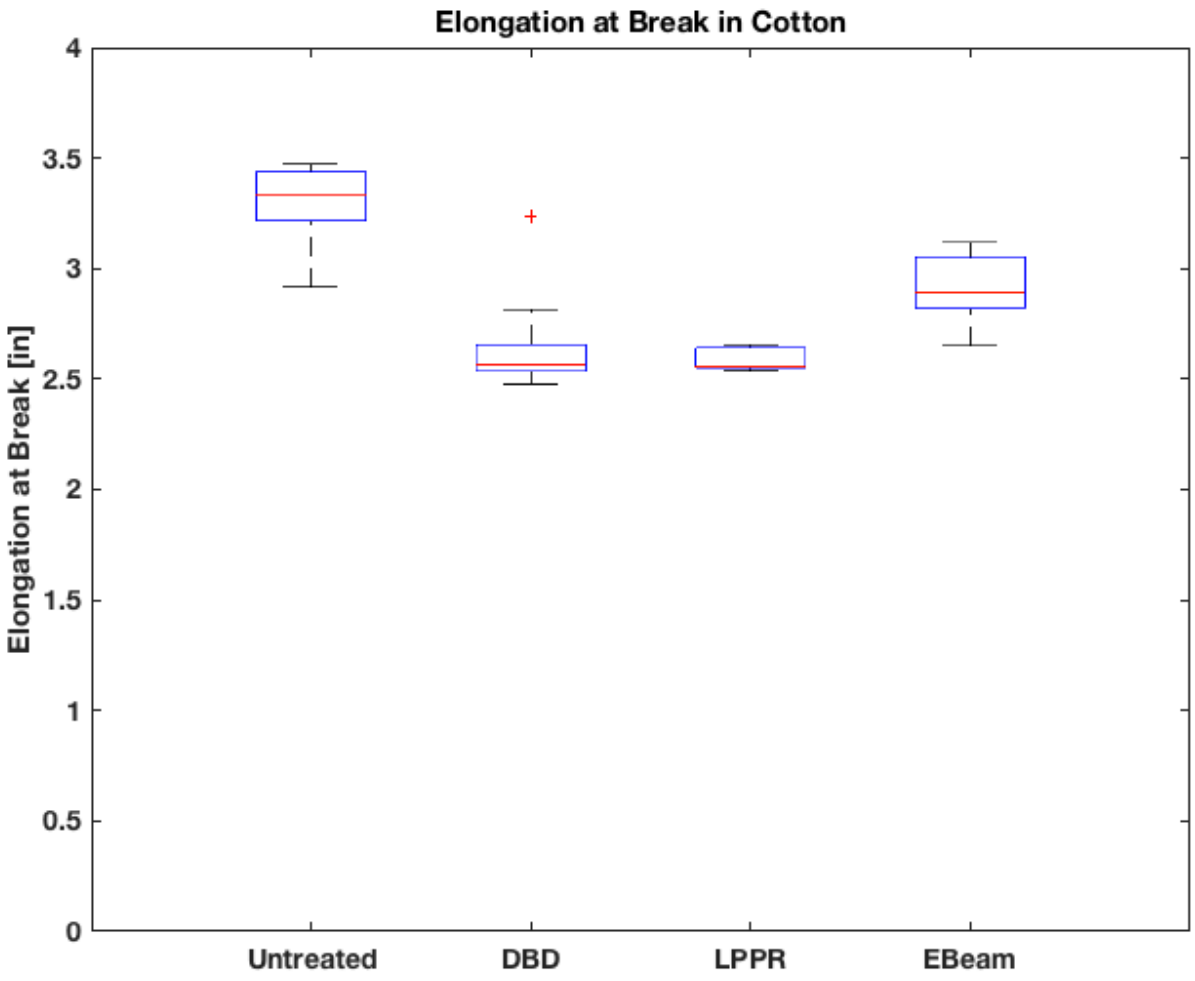
Elongation at Break in Cotton
Elongation at Break [in]
4
3.5
3
2.5
2
1.5
1
0.5
0
Untreated
DBD
LPPR
EBeam

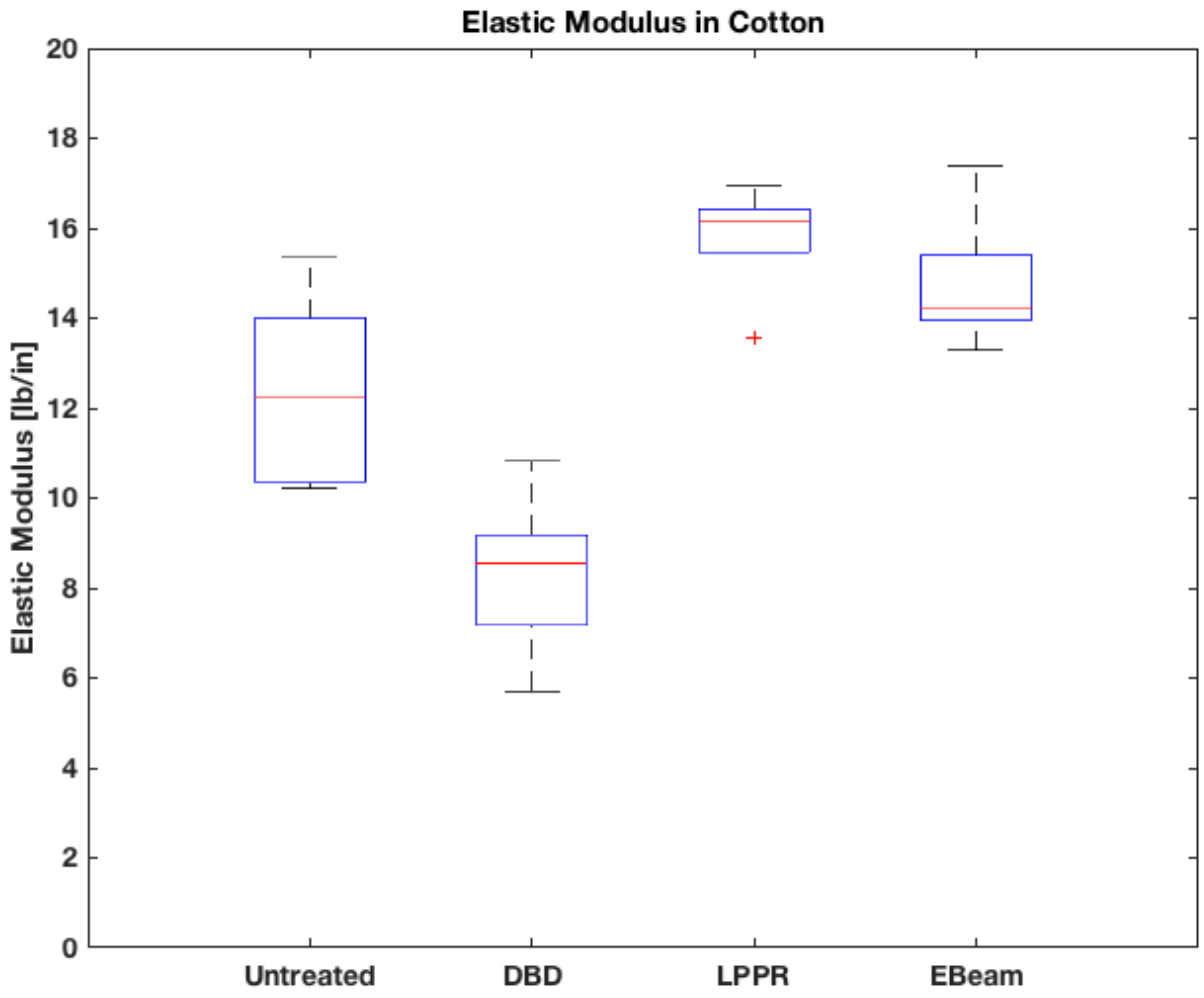
Elastic Modulus in Cotton
Elastic Modulus [lb/in]
20
18
16
14
12
10
8
6
4
2
0
Untreated
DBD
LPPR
EBeam

A4. Green Modacrylic

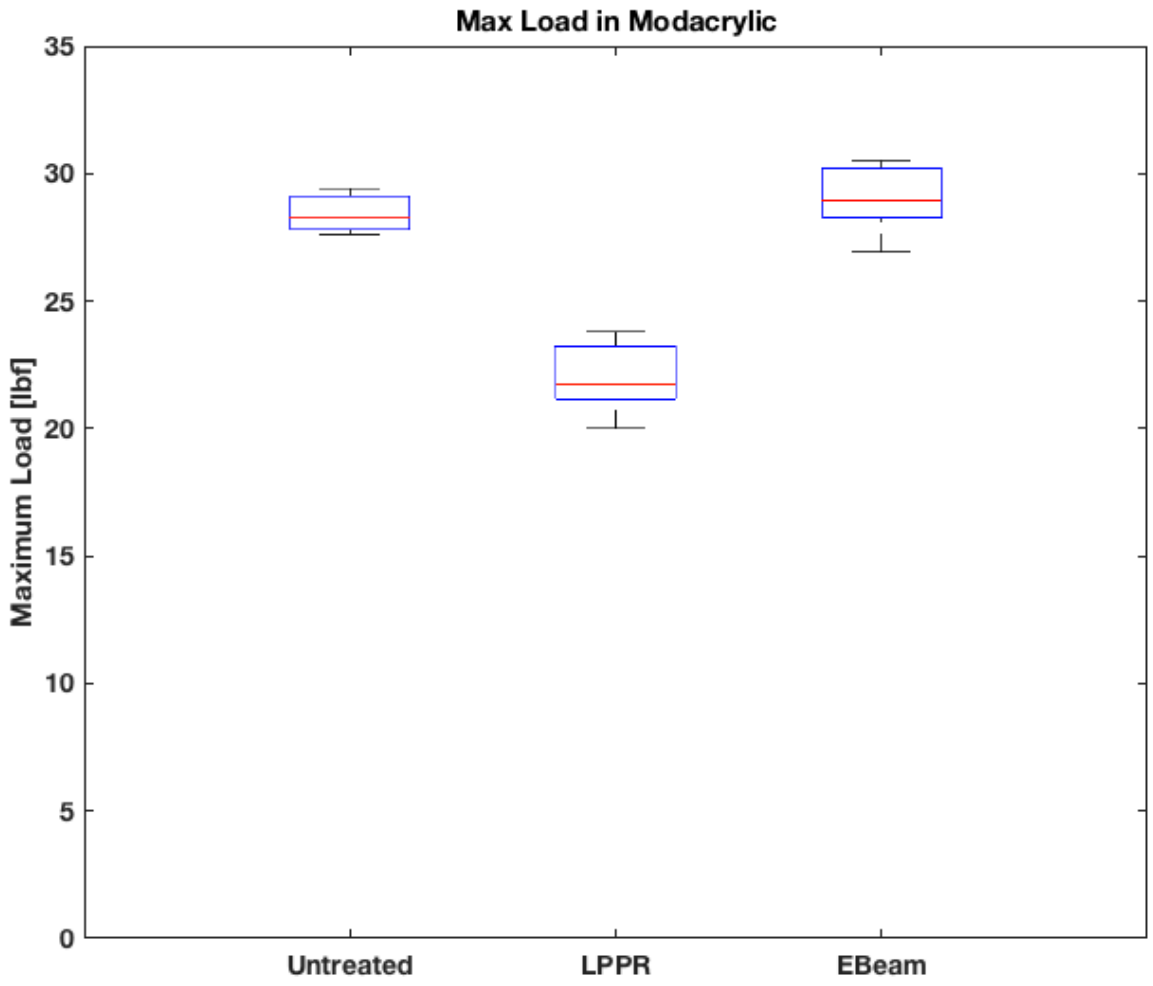

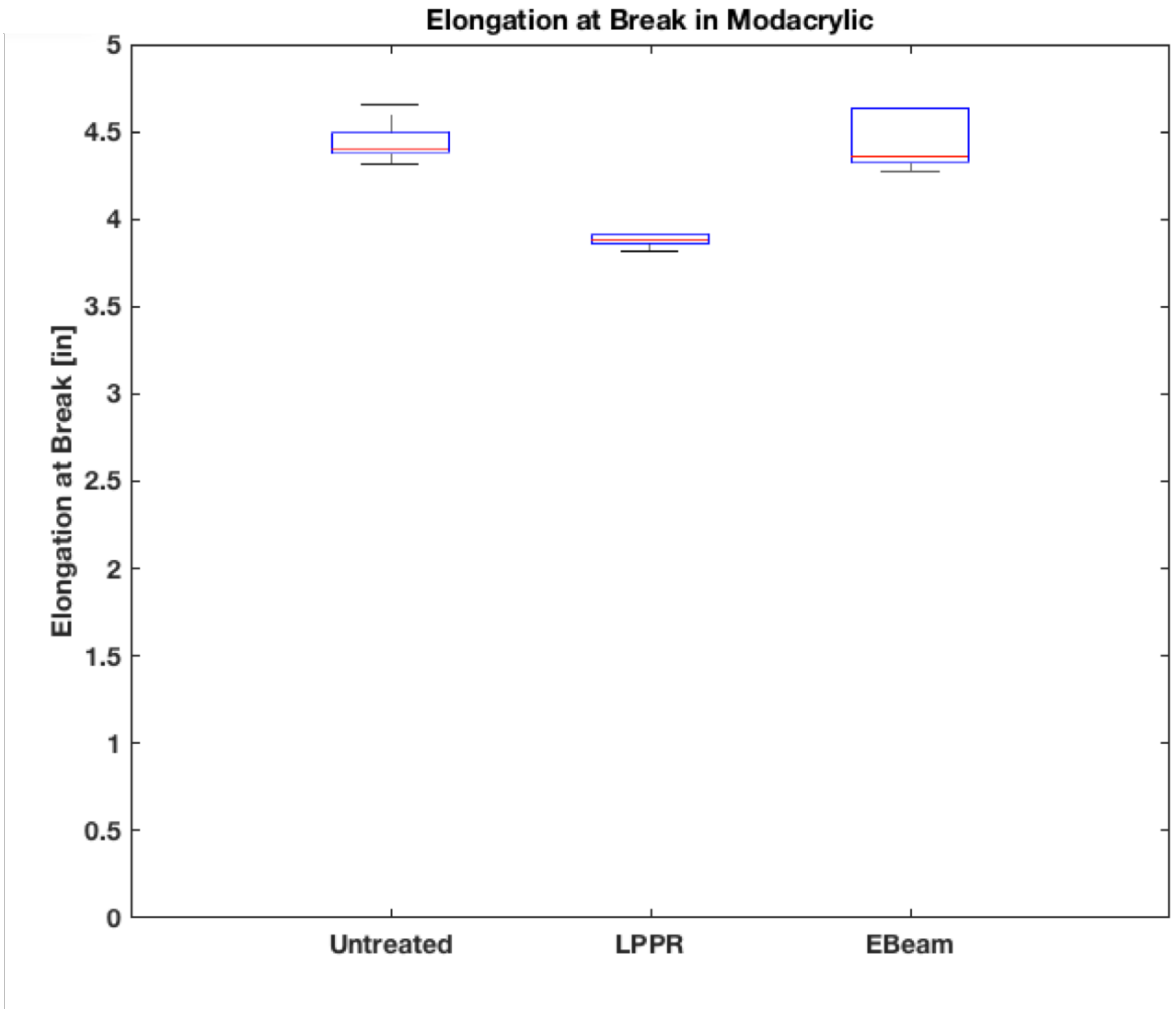
Elongation at Break in Modacrylic
Elongation at Break [in]
5
4.5
4
3.5
3
2.5
2
1.5
1
0.5
0
Untreated
LPPR
EBeam

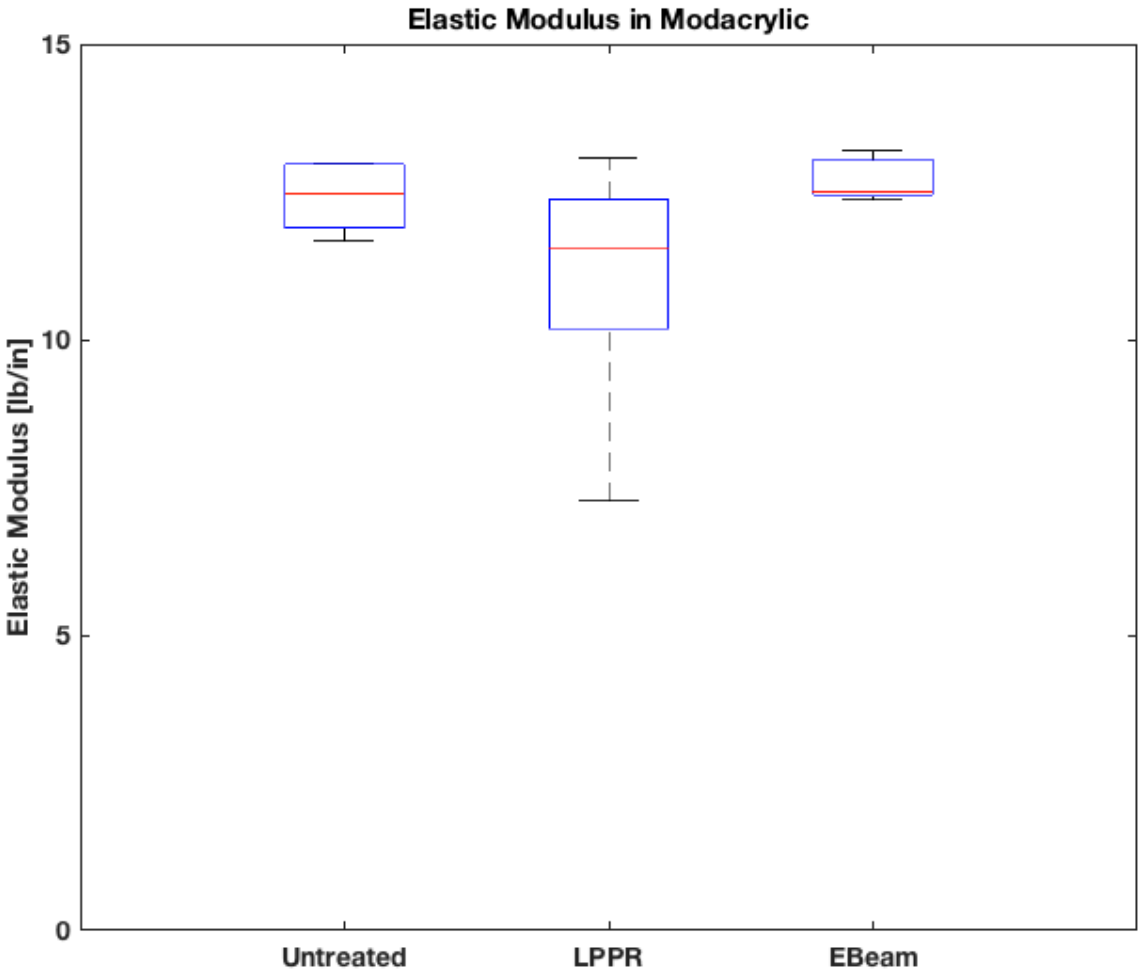
Elastic Modulus in Modacrylic
Elastic Modulus [lb/in]
15
10
5
0
Untreated
LPPR
EBeam

B. Pilling Effect on Black Merino Wool and Green Modacrylic

B2. Black Merino Wool

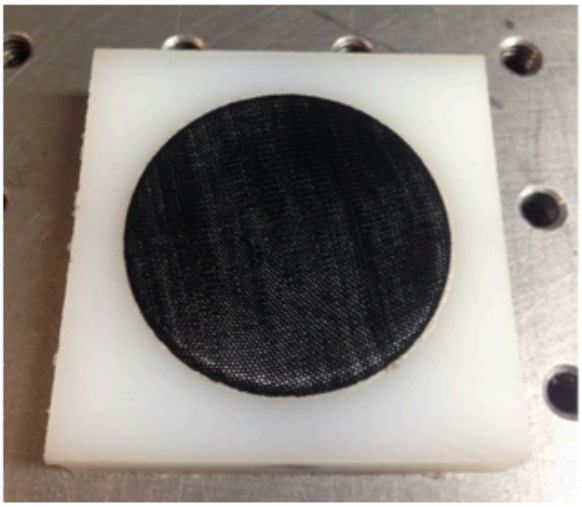

Before DBD Treatment

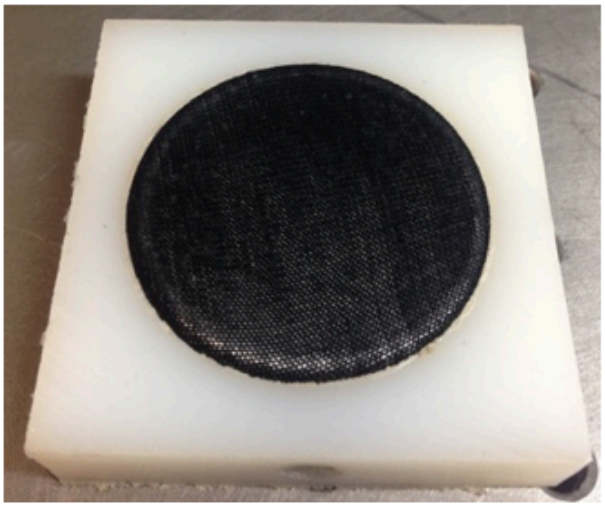

After 15 min of 1.27 W/cm^2 DBD Treatment

B3. Modacrylic

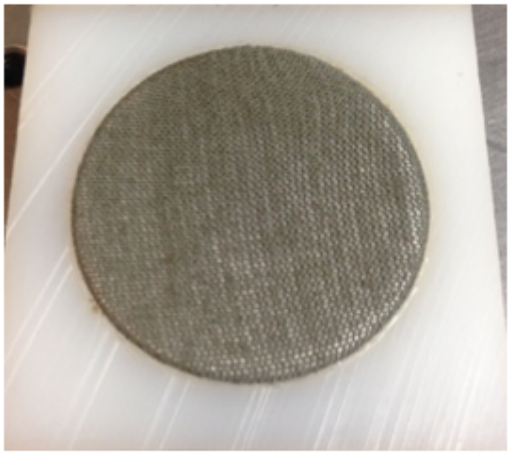

Before DBD Treatment

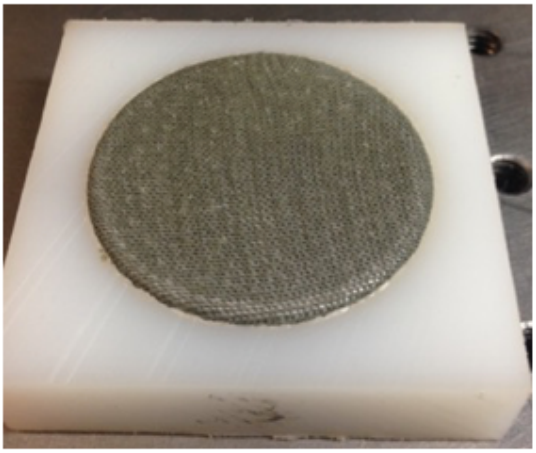

After 15 min of 1.27 W/cm^2 DBD Treatment

C. GC-MS Chromatograms